SLAC-587
UC-404
(SSRL-M)

PSEUDOGAPS AND IMPURITY EFFECTS IN HIGH TEMPERATURE SUPERCONDUCTORS*

Paul Johnathan White

Stanford Synchrotron Radiation Laboratory
Stanford Linear Accelerator Center
Stanford University, Stanford, California 94309

SLAC-Report-587
March 2000

Prepared for the Department of Energy
under contract number DE-AC03-76SF00515

Printed in the United States of America. Available from the National Technical Information Service, U.S. Department of Commerce, 5285 Port Royal Road, Springfield, VA 22161

* Ph.D. thesis, Stanford University, Stanford, CA 94309.

PSEUDOGAPS AND IMPURITY EFFECTS IN HIGH TEMPERATURE SUPERCONDUCTORS

A DISSERTATION
SUBMITTED TO THE DEPARTMENT OF APPLIED PHYSICS
AND THE COMMITTEE ON GRADUATE STUDIES
OF STANFORD UNIVERSITY
IN PARTIAL FULFILLMENT OF THE REQUIREMENTS
FOR THE DEGREE OF
DOCTOR OF PHILOSOPHY

By
Paul Johnathan White
March 2000

I certify that I have read this dissertation and that in my opinion it is fully adequate, in scope and quality, as a dissertation for the degree of Doctor of Philosophy.

Zhi-Xun Shen
(Applied Physics)
(Principal Adviser)

I certify that I have read this dissertation and that in my opinion it is fully adequate, in scope and quality, as a dissertation for the degree of Doctor of Philosophy.

Sebastian Doniach
(Applied Physics)

I certify that I have read this dissertation and that in my opinion it is fully adequate, in scope and quality, as a dissertation for the degree of Doctor of Philosophy.

Shoucheng Zhang
(Physics)

Approved for the University Committee on Graduate Studies:

Abstract

In science the questions found are almost as important as the answers. High temperature (high T_c) superconductivity is a phenomenon that has made researchers question accepted notions of solids in many aspects. Many ideas need revision such as BCS superconductivity and the quasiparticle notion. Clearly, these are large issues and this body of work seeks only to add some insight into these things.

This work contains angle resolved photoemission data from BSCCO (Bi_2 Sr_2 Ca Cu_2 $O_{8+\delta}$), a high T_c material chosen for convenience with respect to the experimental technique. In particular, the studies included O doped BSCCO, single plane BSCCO, and Zn doped BSCCO. O doping, a common tool for altering the carrier concentration, helped to establish the origin of T_c as being limited by either phase fluctuations or the superconductor pairing strength. While reestablishing the agreement of the data with *d*-wave pairing, the data also demonstrated the relevant energy scales of interest across the doping regime. In studying single plane BSCCO as a function of carrier concentration, *d*-wave pairing again was reinforced and the limiting factors of T_c in the single layered compound proved to be quite similar to that of the bilayer compound. The results for Zn doped BSCCO are presented in a more phenomenological flavor. Significant changes occurred in the spectra such as the suppression of the superconducting dip and the spectral peak along ΓY. While a unique microscopic theory does not readily present itself, these are dramatic changes to key portions of BSCCO spectra. Also, an anomalous change of spectral weight appeared in this material.

Acknowledgments

It is with pleasure and pride that I am blessed to thank such a warm and caring family as mine. Their presence in my life gave me the strength and conviction to go forward. This thesis is not the culmination of my own life's work, but the culmination of the hard work and love of those before me. It is to their sacrifices to which I am indebted, and it is to them that I owe my love and respect.

To my friends throughout the years, I can only say that the fortune of knowing you all was mine. Life presents us with so few opportunities to call a stranger "brother" or "sister". It is with sincere sentiment that I thank you all. My life and my soul are the better for knowing you.

A great deal of thanks to Arthur Walker and Walter Lowe for responding to various distress calls. Much gratitude to Milo Lewis, Mark Gibson, Kent Robinson, Stephanie Carlson, Mike Nalls, Diana Viera, and Ray for their presence and reminder of 'grace under pressure'.

To my educators through the years, I thank you all. First, I would thank Mrs. Eve Fenton. Without my knowing, she influenced me at quite an early age, a fact which I have never really appreciated in full. Next, Robert Waters introduced me to a world beyond my senses; my world became a much larger place because of it. Finally, of Dr. Robert M. Williams I can only say thank you for giving me the heart of a natural philosopher. My appreciation for nature and the world has grown because of it.

I would like to thank Zhi-Xun Shen for being my advisor during these years and allowing me the freedom to tend to my responsibilities. My gratitude is also extended to Bill Spicer for his years of wisdom and compassion. I also thank my reading

committee for their careful perusal of this work. I thank the Shen group (past and present) for their cooperation and work. Special thanks go to Anne Y. Matsuura, Changyoung Kim, Jeff Harris, and Donglai Feng. Paula Perron and Marcia Keating have guided me administratively and with uncommon patience. Marilyn Gordon and Gloria Barnes have been very capable administrative assistants. To all my friends at SSRL, warm regards.

Financial support has been provided by NDSEG (Grant DAAH04-93-G-0276), Associated Western Universities, and the DOE.

For Morris and Paulette

Contents

List of Tables

List of Figures

Chapter 1

Introduction

1.1 Scientific Context

In 1911 Kamerlingh Onnes, the first man to liquefy Helium (4°K), discovered superconductivity in mercury. Superconductors not only exhibit zero *DC* electrical resistivity but also the Meissner-Oschenfeld effect, *i.e.*, the expulsion of **B** field lines from its interior. They were truly novel materials. The following years produced landmark experiments, such as the isotope effect and flux quantization, and sundry superconducting materials. These early superconducting materials resembled elemental metals or simple alloys. At the time, the normal state of these materials was regarded as within the bounds of band theory, and, therefore, knowable to some significant extent. Therefore, an effort was made to develop a microscopic theory for this exotic effect below T_c. Later, such a theory was put forth by Bardeen, Cooper, and Schrieffer. The microscopic theory (known as BCS theory) explained many of the effects seen by experimentalists. Wonderfully elegant equations came out of this such as the relationship between the superconducting gap and the critical temperature ($\Delta(0) = 1.7kT_c$).

Usually, technology lags some years behind scientific theory, but even in the 1970's-80's, there was no really practical use of this exotic phenomenon called super conductivity (with the exception of MRI, of course). The reasons for this stem mostly from

the temperature required for most materials to go superconducting, which was typically less than 20°K. The necessity of large amounts of liquid helium made practical application cost prohibitive. This severely limited the appeal of this novel effect.

However, in 1986, Bednorz and Muller at IBM-Zurich found the La-Ba-Cu-O system, the first high T_c compound, which superconducted at about 30°K. Very soon it was realized that there was something special about the CuO_2 plane. The race began to find similar compounds of slightly different stoichiometry to achieve truly high T_c. The goal, of course, was to find something higher than liquid nitrogen temperature, 77°K, so one could exploit the relatively large abundance and inexpensive aspect of this coolant. The race is exemplified in Fig. 1.1, where we see a plot of T_c versus year of discovery for a few superconductors. The dramatic slope over the past ten years demonstrates how rapid the pursuit has been.

However from a technological and engineering standpoint, these materials have been wanting in several regards. Quite evident is the complexity of their manufacture; these are are transition metal oxides, *i.e.*, ceramics, whose growth is difficult. The ceramic nature presents problems as they are not malleable and cannot be drawn into fine wires unlike their earlier metallic counterparts. Also, through the years it was found that these materials are truly not well understood. Therefore designer engineering of these systems seemed less and less likely.

The worth of these systems come in the challenges they present in their understanding. Since their discovery, the foundations of solid state physics have been challenged and re-evaluated. In that sense, their worth has been immeasurable because they have shown us where our framework is not stable. It is this which is the challenge, not the fanciful levitating trains or the lossless power conduits. Although, these things may very well follow if we unlock the mystery. Nevertheless, the aim of this work is only to shed some light on this monumental problem.

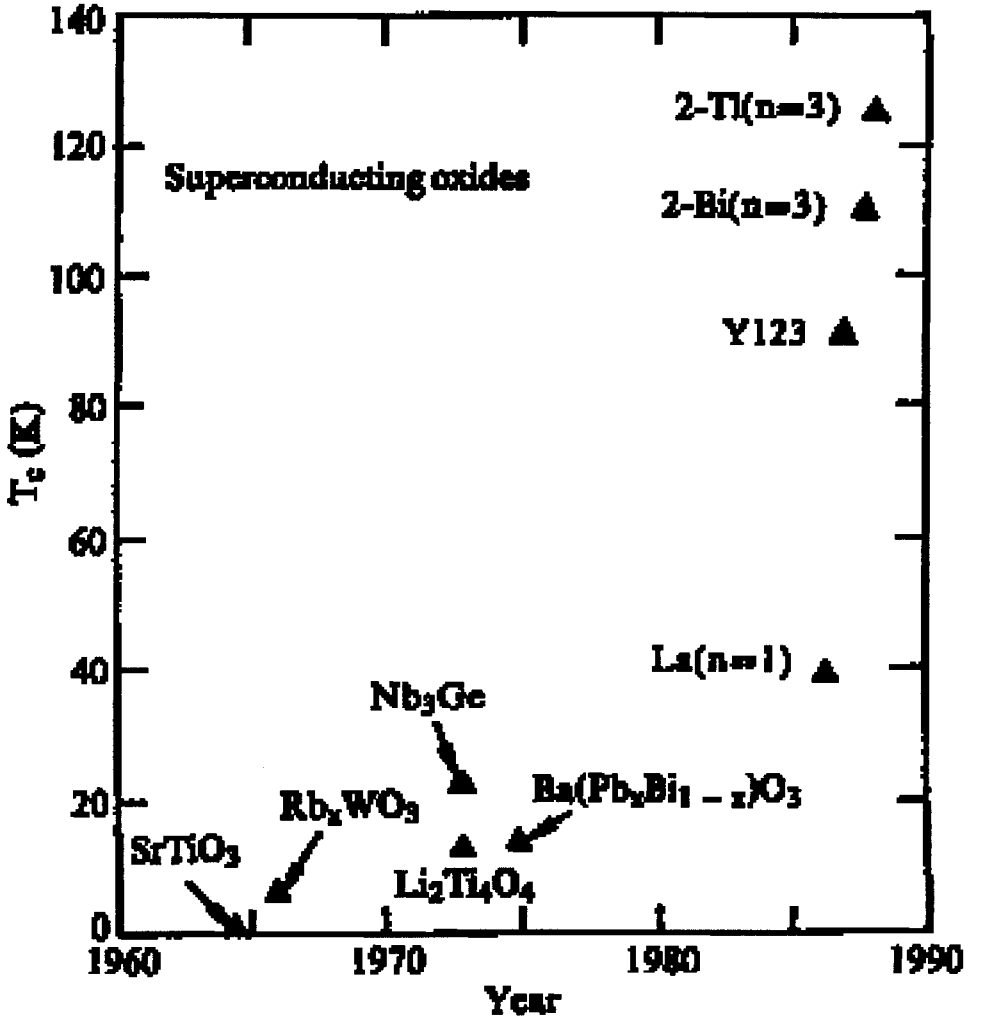

Figure 1.1: T_c versus the year of discovery of superconductivity in a few of the oxide supercunductors. n is the number of immediately adjacent Cu-O planes. Figure taken from Ref. 1.

1.2 References

1. Gerald Burns, *High Temperature Superconductivity*, Academic Press, Inc., Boston 1992

Chapter 2

Experimental Details

2.1 Historical background

Hertz observed the phenomenon of photoemission in 1887. Using a relatively crude apparatus by today's standards, he studied the photoelectric effect, a phrase later coined by Einstein and given to the phenomenon. Light was generated by an arc, d, as seen in Fig. 2.1. A secondary arc, f, was observed. Hertz systematically varied the material, p, between the arcs in an attempt to study the effect more. It wasn't until Einstein proposed the photoelectric effect as a possible explanation for the phenomenon that it was understood well. Einstein noticed that electrons weren't emitted until a characteristic energy, ω, was reached such that $E_{kin,max} = \hbar\omega - \phi$ - E_B where the left hand side is the maximum kinetic energy of the photoexcited electrons, ω is the angular frequency of the light, and E_B is a quantity known as the binding energy. The quantity, ϕ, was found to be material dependent; it became known as the work function and is typically 3-4eV. The workfunction is the threshold energy for photoemission, below which, the light does not have enough energy to emit a photon in a classical sense.

Photoemission was later understood in terms of the *three step* model (see Fig. 2.2) put forth by Spicer and Berglund [3]. The model assumes three separate processes in the interaction of light with a valence band electron in a solid. Basically, the first one involves photoabsorption by the electron to some excited state. Next, the electron

finds its way to the surface via a diffusion process. Lastly, the electron escapes the solid altogether and is detected in the experiment. Under some assumptions, this picture of the photoemission process describes the effect very well.

The whole aim of this was to better understand the density of states within a solid. The density of states give the number of states for the electron a given energy. It is this quantity that acts as a fingerprint for a given solid. It is our ability (or inability) to predict this that determines how well solids are truly understood. Given the density of states, we can develop a good idea of conduction (or lack of conduction) in a material. Also, a rough idea of the carrier density, thermal properties, *etc.* can be made. Knowing the individual contribution of various bands to the density of states provides one with even more information about various things as well. In short, there is a wealth of information in the density of states and even more in knowing the actual band structure.

2.2 Band Theory Interpretation

Band theory is one of the cornerstones of our paradigm for electron transport within a solid. Succinctly, it is the graph of E vs. $\mathbf{k}$ for an electron in a solid. Conventionally, angle resolved photoemission is used to find the band structure of a solid. It involves not only detection of an electron of a given energy but also the direction whence it was ejected from the solid. There is a one to one correlation of the parallel component of the electron's momentum in the solid to the parallel component out of the solid. We have the following equation

$$\frac{\mid \mathbf{p}_{\parallel} \mid}{\hbar} = \mid \mathbf{K}_{\parallel} \mid = \sqrt{\frac{2m}{\hbar^2} E_{kin}} \sin\theta \tag{2.1}$$

where $\mathbf{K}$ is the wavevector of the photoexcited electron inside the crystal, $\frac{\mathbf{p}}{\hbar}$ is the wavevector of the photoexcited electron in vacuum, and all other constants have the usual meaning. (The advanced reader will now note that $\mathbf{K}_{\parallel} = \mathbf{k}_{\parallel} + \mathbf{G}_{\parallel}$.) The preceding description works well for samples that are optically flat,*i.e.*, samples where there is a 'good' definition of the parallel component; otherwise, this mapping analysis breaks down. It is also worth noting that absolute $\mathbf{K}$ determination is most practical

in the case of a sample with strong 2D characteristics. Since $\mathbf{k}_{||}$ is only conserved, $\mathbf{k}_{\perp}$ varies due to lack of knowledge of the work function and 'inner potential', two spurious quantities which warrant further discussion themselves but not in this work.

The other aspect of photoemission is that electrons at this energy tend to escape from only $10\mathring{A}$ below the surface. This is due to the 'electron escape depth profile' seen in Fig. 2.5. This necessitates a very clean surface; to this end, most samples are cleaved *in situ* at very low pressures of $2x5e^{-11}$Torr to reveal a fresh, unoxidized surface.

2.3 Quasiparticles

A brief word on quasiparticles is in order. Typically, ARPES data is interpretted as band structure information in the majority of the community. It is a fact that the photocurrent, I, (under certain approximations, *e.g.* the sudden approximation and others) is exemplified by this equation

$$I \propto \sum_{f,i} |< \phi_{f,E_{kin}} \mid r \mid \phi_{i,\mathbf{k}} >|^2 \, A(\mathbf{k}, E) \tag{2.2}$$

where f and i stand for initial and final states respectively, which, when coupled with r and squared, make up the matrix element, and A($\mathbf{k}$, E) is the *spectral function* defined in terms of the Green's function, G, by

$$A(\mathbf{k}, E) = \pi^{-1} Im[G(\mathbf{k}, E)] \tag{2.3}$$

Defining the unperturbed system with '0' and the system with correlations with '1'(*i.e.*, $E^1_{\mathbf{k}}$ - $E^0_{\mathbf{k}}$ -$\Sigma(\mathbf{k},E^1_{\mathbf{k}}) = 0$), one has an expression for the spectral function in photoemission

$$A(\mathbf{k}, E) = \frac{1}{\pi} \frac{Z_{\mathbf{k}} Im[E^1_{\mathbf{k}}]}{(E - Re[E^1_{\mathbf{k}}])^2 + (Im[E^1_{\mathbf{k}}])^2} + A_{inc} \tag{2.4}$$

The poles of A($\mathbf{k}$, E) determine the quasiparticles positions in energy. $Z_{\mathbf{k}}$ is a number less than one called the renormalization factor. The *lifetime* of the quasiparticles is determined by the Im[Σ]. Having a long lifetime is important to be able to meaningfully describe quasiparticles. The above is a terse discussion on an elaborate subject. The reader is referred to Ref. 1 from which this discussion was borrowed.

2.4 Instruments

Angle resolved photoemission experiment were carried out in three different ARPES systems for all types of samples giving consistent results. In one case the photon source is unpolarized 21.2eV photons and a total energy resolution of 20meV FWHM, while in the other case 22.4eV linearly polarized photons were used with a resolution of 35meV FWHM. The analyzer acceptance angle was $\pm 1°$ corresponding to a **k**-space window of radius $0.045\frac{\pi}{a}$ or $0.037\mathring{A}^{-1}$. Base pressures of the vacuum system were $4x10^{-11}$ torr, and Fermi energies were determined from a reference Au film. Other ARPES spectra were recorded with a Scienta analyzer attached to beamline 10 of the Advanced Light Source. The total energy resolution was typically 15meV and the angular resolution was $\pm 0.15°$ with the spectrometer operating in angle mode. The nominal chamber pressure was $6x10^{-11}$ torr and the photon energy used was 25eV. Low energy electron diffraction (LEED) measurements confirms the quality of the UHV-cleaved surfaces and show a Bi-O plane superstructure that is well known in the Bi-based cuprates.

2.5 References

1. Stephan Hufner, *Photoelectron Spectroscopy*, Springer-Verlag, Berlin 1995

2. Barry Wells, *private communication*

3. C.N. Berglund and W.E. Spicer, *Phys. Rev. A* **136**, 1030 and 1044 (1964)

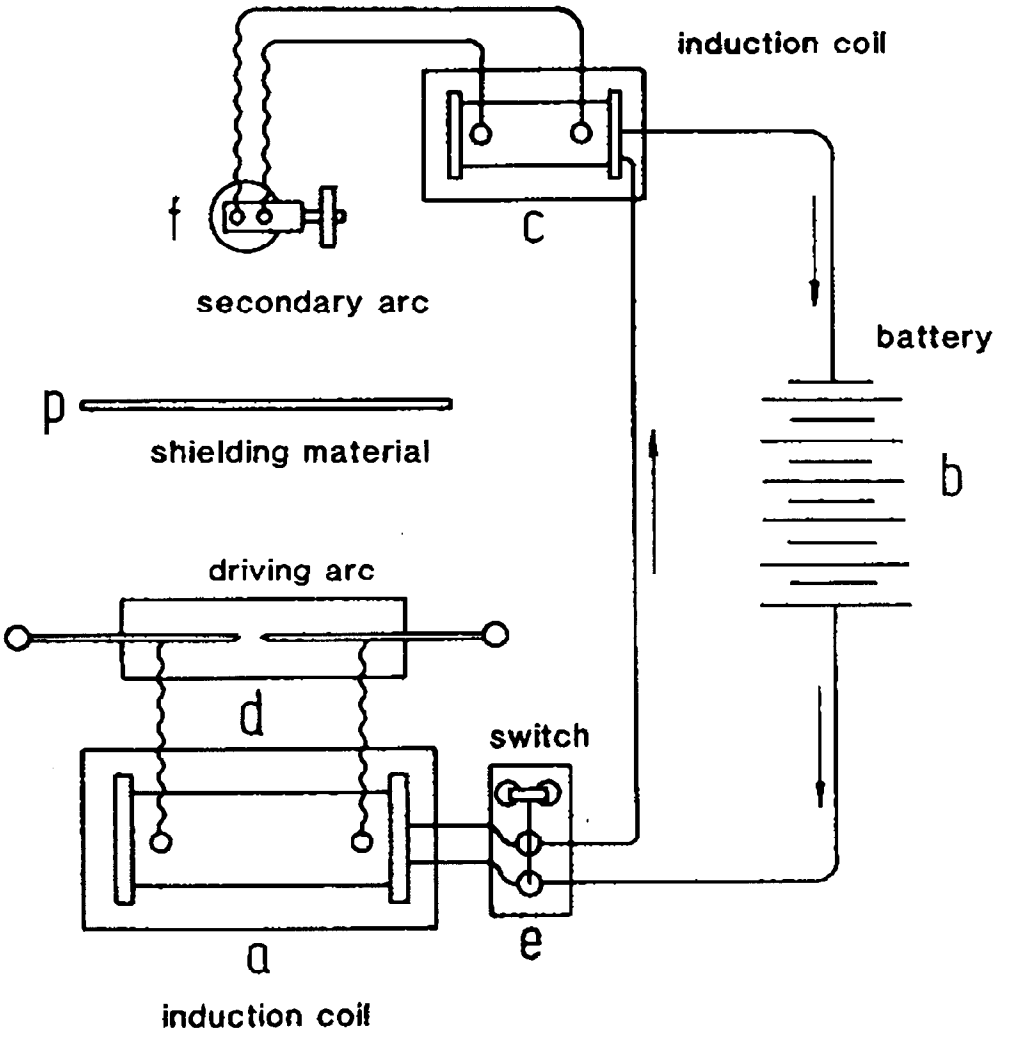

Figure 2.1: An early photoemission experiment. Figure taken from Ref. 1.

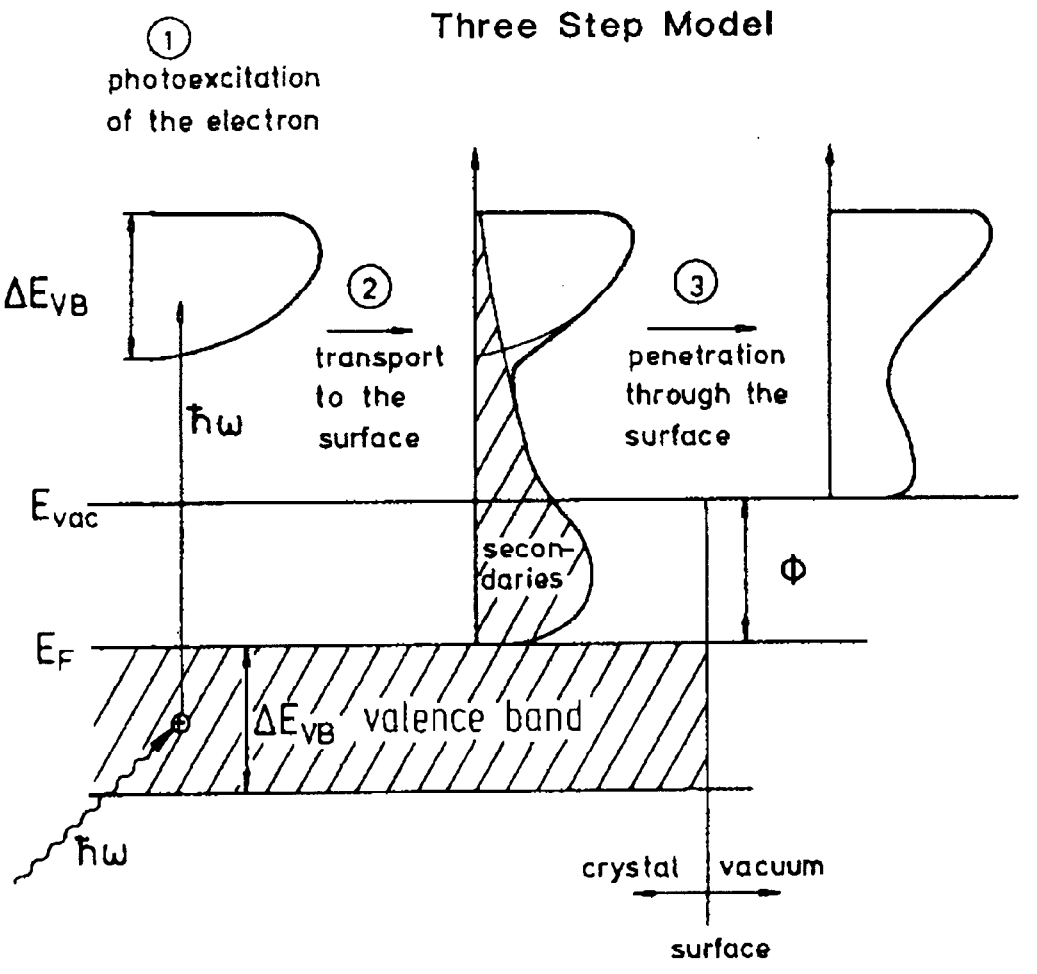

Figure 2.2: Pictorial representation of the *three step* model from Spicer and Berglund [3]. Figure taken from Ref. 1.

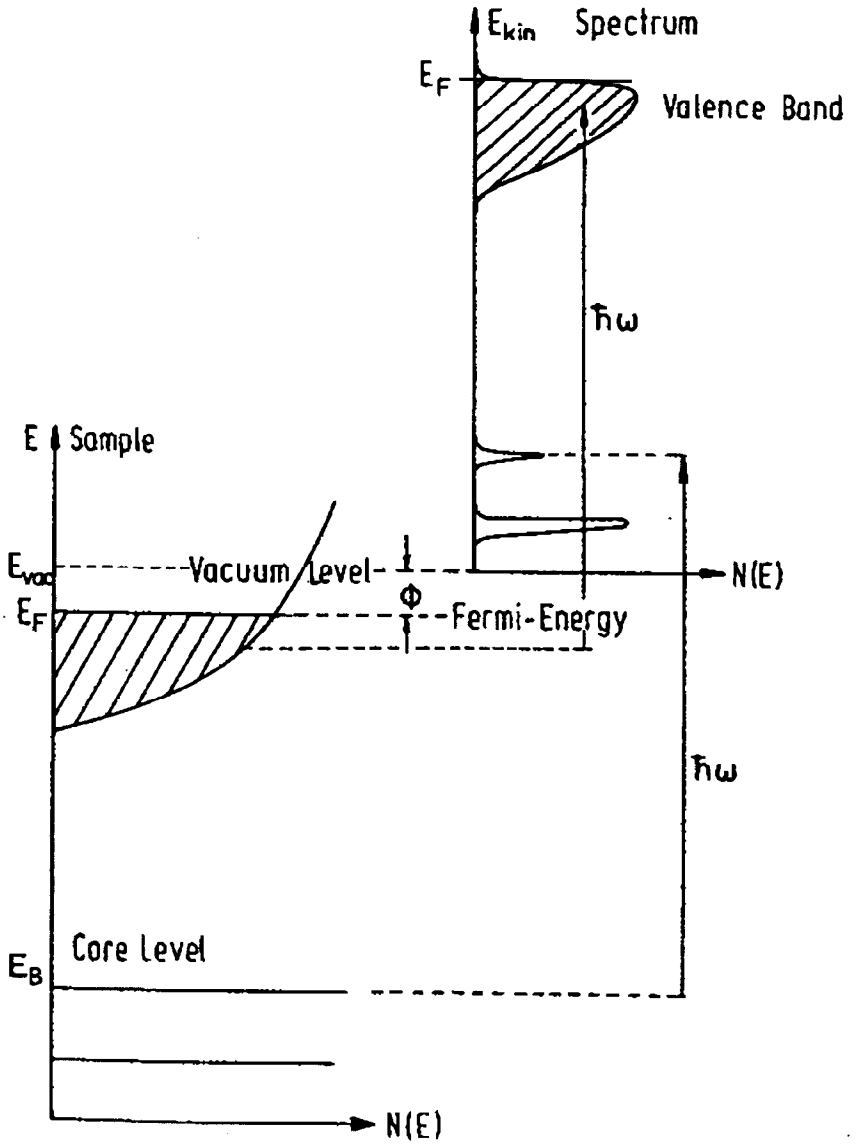

Figure 2.3: Diagram relating the density of states including core levels to an angle integrated photoemission experiment. Figure taken from Ref. 1.

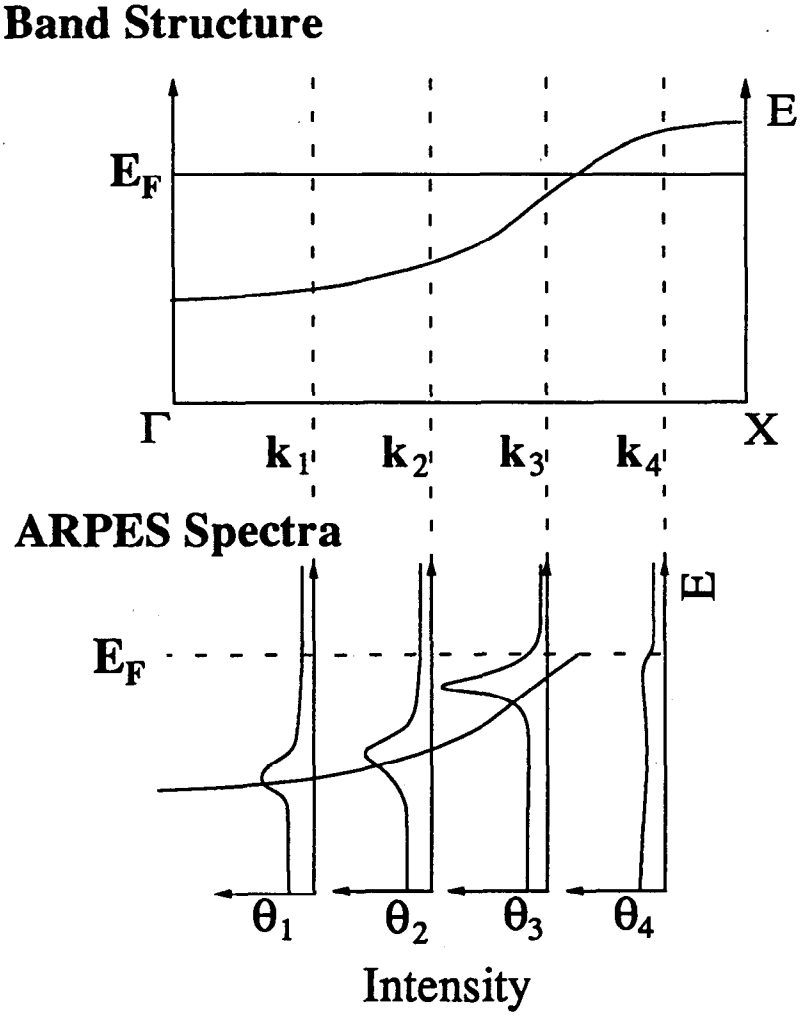

Figure 2.4: Diagram illustrating the dispersion of a band to angle resolved photoemission data. Figure taken from Ref. 2.

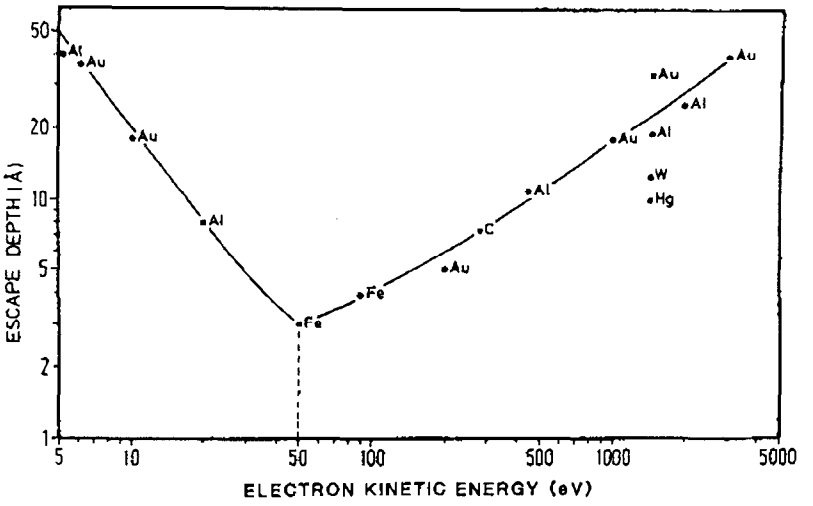

Figure 2.5: Diagram illustrating the electron escape depth as a function of kinetic energy. Figure taken from Ref. 1.

Chapter 3

Superconductivity and BSCCO

$Bi_2Sr_2CaCu_2O_{8+\delta}$ (BSCCO or Bi2212) is a layered high temperature superconductor with a $T_c \approx$70-91K depending on the hole doping and impurity concentration. High T_c compounds are layered transition metal oxides (*e.g.*, CuO_2) with varying numbers of CuO_2 planes per unit cell and sundry interlayer materials. Doping is usually achieved with the addition of holes (NdCeCuO is a notable exception) through the addition of oxygen or altering the ratio of cations to ions. The structure is given in Fig. 3.1. Because of the number of cations and ions, the growth of the ideal compound is more difficult than that of other superconductors, say LSCO for example. BSCCO is also notorious for its superstructure, the effect of which is demonstrated by back-scattered X-ray (Laue) diffraction in Fig. 3.2.

The phase diagram for HTSC is shown in Fig. 3.3. While BSCCO itself does not cover the whole range via oxygen doping alone, the general shape is still characteristic of it as well as that of other compounds such as YBCO and LSCO. We generally speak of BSCCO as being either underdoped, optimally doped, or overdoped. These names are just delineation of areas on the phase diagram to the left of, precisely at, or to the right of $T_{c,max}$. A more complete phase diagram would include a third orthogonal axis indicating impurity concentration in the plane (as will be shown spectroscopically in later chapters). However, impurities in BSCCO are hard to quantify due to the presence of so many other elements in the compound. In general, we travel across the phase diagram via oxygen doping (done in an annealing furnace at 400-500°).

Oxygen sits in the Bi-O layer, not in the Cu-O layer, and the Bi-O layer serves as a charge reservoir. $T_{c,max,BSCCO} \approx 91°K$ with the boundary scaling appropriately on both sides. The inset of Fig. 3.3 provides characteristic ρ vs. T plots in the different regions. Since we operate normally in the SC region, we turn our attention to plots of that sort for different Ni and Zn concentrations.

Fig. 3.4 and Fig. 3.5 show in-plane resistivity curves for various dopings of BSCCO. It is noted that Ni and Zn substitute for Cu in the CuO_2 planes, *i.e.*, intraplanar vs. interplanar impurities. As can be expected the residual resistivity, which is obtained by extrapolating the linear part down to 0°K, increases monotonically with doping increase. T_c also follows this trend of decreasing monotionically with increased impurity concentration. Also, the small upturn in the maximum doping is indicative of extra inhomogeneity, which is expected at the solubility limit. These limits are very small; about a percent for Zn and 2.5% for Ni. Of course, varying oxygen will produce a reduced T_c but will not have the same, dramatic effect on $\rho(0)$.

Fig. 3.6 depicts the band structure of BSCCO. It is included to demonstrate the complexity of bands in the valence band. In principle, ARPES could generate a mapping of this sort, but, due to the 'spaghetti' nature of the electronic structure, it becomes unpractical. In fact, we are only concerned with bands that cross the Fermi level as those are the important ones for transport. As the figure illustrates, that is a less dense space in the band structure.

3.1 References

1. Barry Wells, private communication

2. B. Battlog, *Phys. Today* **44(6)**, 44 (1991)

3. D.-S. Jeon *et al.*, *Physica C* **253**, 102 (1995); R. Yoshizaki *et al.*, *Jrnl. of Low Temp. Phys.* **105**, 927 (1996)

4. S. Massidda *et al.*, *Physica C* **176**, 159 (1991)

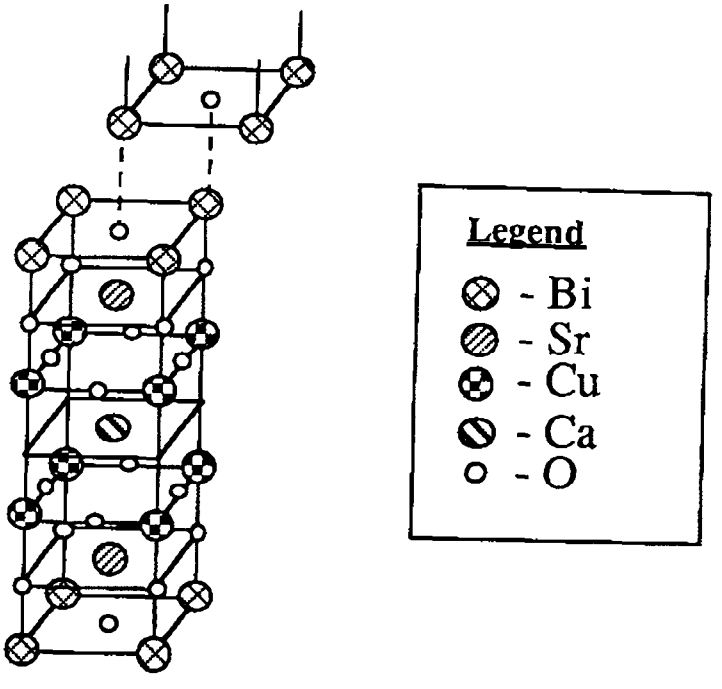

Figure 3.1: Ideal structure of BSCCO. Oxygen in the original compound resides the Bi-O layer. Taken from Ref. 1.

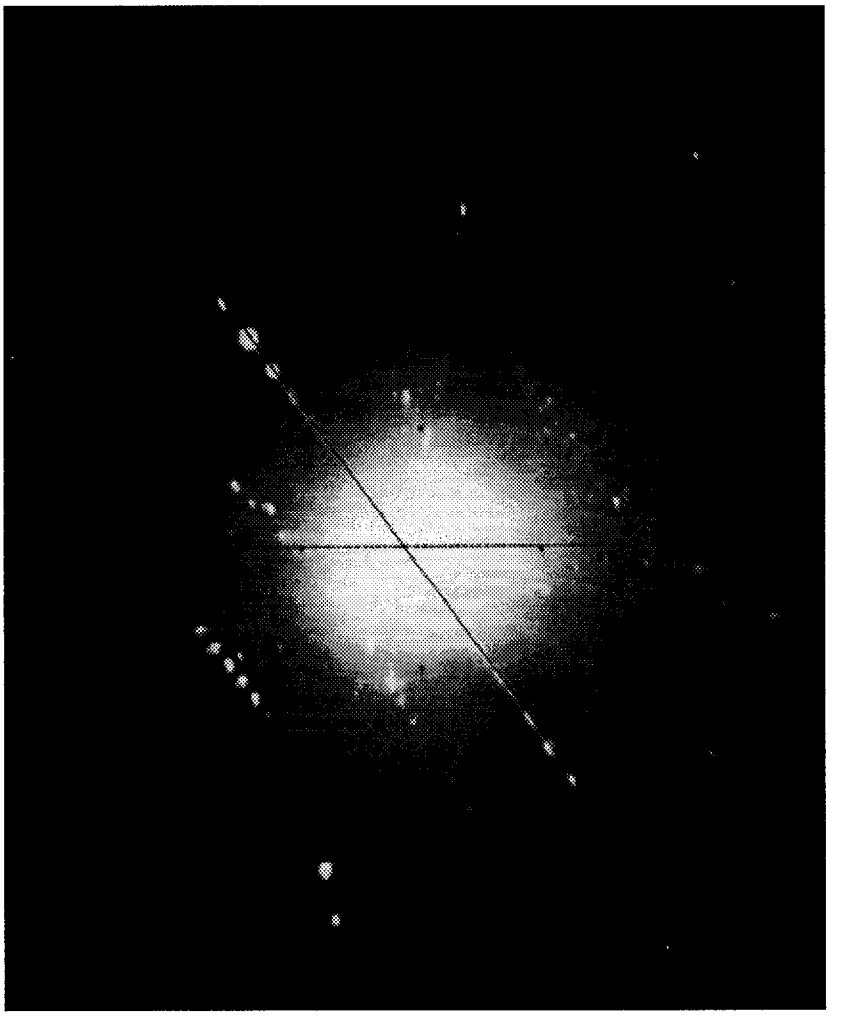

Figure 3.2: Laue photograph of BSCCO sample.

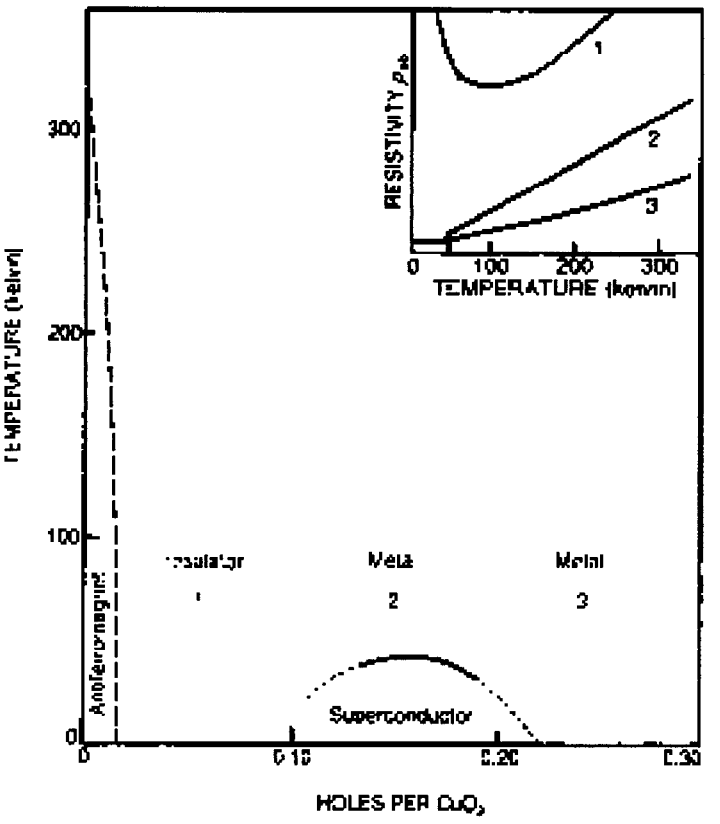

Figure 3.3: Phase diagram for high temperature superconductors. Temperature is vertical and hole concentration is horizontal. The exact details of the range vary from material to material, but the topology remains constant. Taken from Ref. 2.

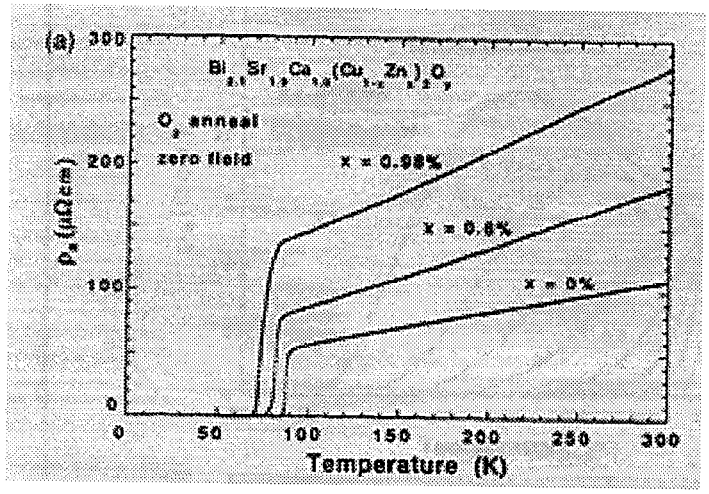

Figure 3.4: Diagram illustrating the in-plane resistivity curves for various amounts of Zn. Figure taken from Ref. 3.

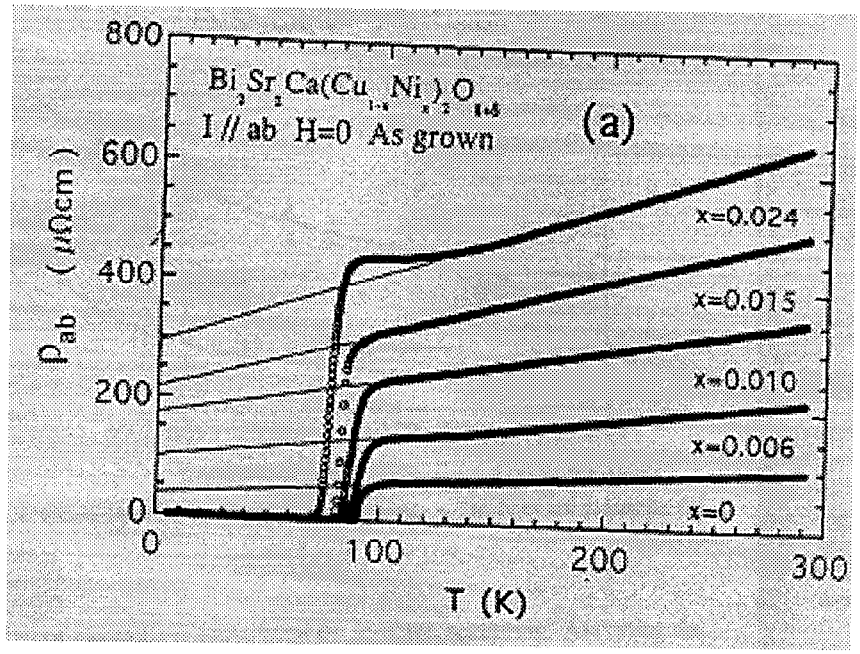

Figure 3.5: Diagram illustrating the in-plane resistivity curves for various amounts of Ni. Figure taken from Ref. 3.

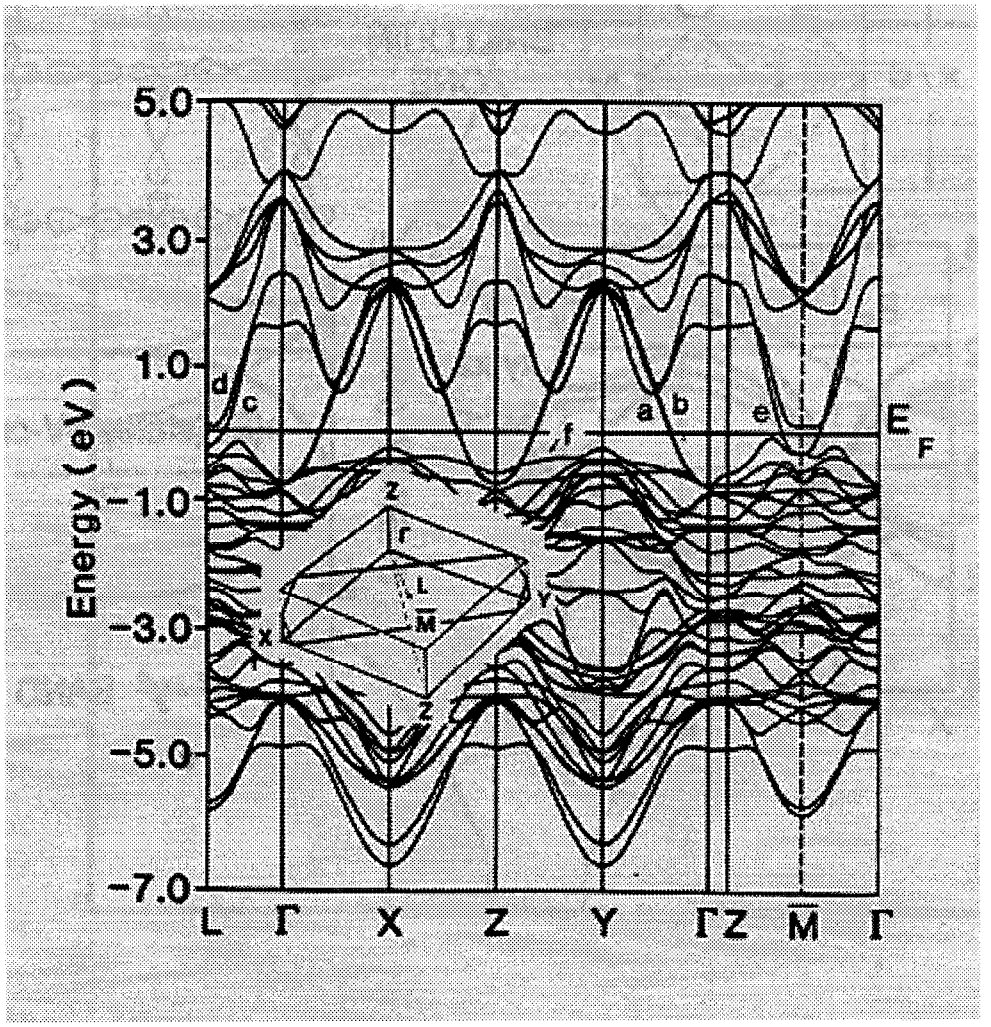

Figure 3.6: Band structure of Bi2212. Brillouin zone is included for clarity. Figure taken from Ref. 4.

Chapter 4

The SC Gap in OD Regime

4.1 Data and Discussion

Exciting advancement towards the understanding of high T_c superconductors has come with the observation of the normal state excitation gap in underdoped (UD) materials [1]. The gap and other unusual behaviors have been observed or inferred in many experiments, including NMR [2, 3], neutron [4], optical [5, 6], transport [7, 8, 9], and thermal measurements [10, 11]. Recently, this gap was observed in single-particle excitation spectra measured by angle-resolved photoemission spectroscopy (ARPES) [12, 13, 14]. These experiments shed light on the problem by providing momentum-resolved information on the gap. The energy gap, when characterized by the leading edge position of the spectra, is found to be highly anisotropic. Furthermore, the anisotropy is very similar to the $d_{x^2-y^2}$ superconducting gap [13, 14]. The anisotropic nature of the gap was subsequently reported [15]. The later experiments yielded more detailed information of the leading edge as a function of angle and temperature, providing additional evidence that the normal state gap (NG) is of the same origin as the $d_{x^2-y^2}$ superconducting gap (SG) [15, 16]. Furthermore, it has been found that the NG (Ref. 15) and the SG (Ref. 16) do not decrease with very significant T_c reduction in the UD regime.

These findings are consistent with the theoretical ideas [17, 18, 19, 20, 21, 22, 23, 24, 25] which postulate that the superconducting transition temperature (T_c)

in the UD regime is not the temperature when pairs start to form, as in the case of BCS theory. Instead, T_c is the temperature when pairs, which form above T_c, become phase coherent. A similar conclusion has also been deduced from muon spin resonance experiments [26]. In this picture, T_c suppression in the UD regime is caused by a reduction in the carrier density which decreases the phase coherence temperature, but the T_c suppression in the overdoped (OD) regime is caused by a decrease in the pairing strength. Since the pairing strength is scaled by the SG size, it is natural to further test the theory by measuring the SG size in the OD regime. Experimental results for the SG in the OD regime are currently controversial [27, 28, 29]. Optical measurements indicate that the SG is independent of doping [27]. Two Raman-scattering experiments suggest a significant SG reduction in the OD regime [28, 29], but they differ from each other by reporting an s-wave gap in one case [28] and a d-wave gap in another [29].

Presented here are ARPES data suggesting a rapid suppression of the SG in OD $Bi_2Sr_2CaCu_2O_{8+\delta}$ (Bi2212). Compared with that of samples near optimal doping, the SG of the OD samples is about 35% smaller while the T_c is only 10% lower. The rapid decrease of the SG with T_c in the overdoped regime contrasts sharply with the fact that the SG does not seem to decrease with T_c in the underdoped regime [16]. At the same time, the SG remains highly anisotropic with the anisotropy being consistent with the $d_{x^2-y^2}$ pairing symmetry. In addition to the rapid suppression of the SG, we report a correlated collapse of the NG and a change in the electronic structure near $(\pi, 0)$ at a much higher energy scale. Our single crystals were grown by directional solidification and their T_c's were measure by superconducting quantum interference device magnetometry [30]. Four very slightly UD Bi2212 samples with a nominal T_c of 88K were selected. Two of them were further annealed in one atmosphere oxygen in order to be overdoped with T_c's of 78K each.

Fig. 4.1 presents normal and superconducting spectra for the two sets of samples at the Fermi surface near $(\pi, 0.23\pi)$ where the $d_{x^2-y^2}$ gap reaches a maximum. The normal-state spectra of the 78K OD samples are sharper and their leading edges reach E_f. Due to the opening of the SG below T_c, the leading edges move to higher binding energies with a simultaneous growth of resolution limited peaks at the gap edges.

By contrast, the normal-state spectra of the 88K UD samples are broader and their leading edges never reach the Fermi level, reproducing the NG [12-16]. Below T_c, the leading edges move slightly while sharp but smaller peaks develop. We characterize in Fig. 4.1 the SG and the NG size by the midpoint leading edge position [31]. Although the midpoint does not have rigorous meaning and one may get different gap values with a fitting ansatz [32], this experimental quantity suffices to reflect the systematic trend of the gap size vs. doping. In all four samples, we see no evidence for a gap along (0, 0) to (π, π) direction within our experimental uncertainty, consistent with the gap being of $d_{x^2-y^2}$ symmetry [31]. This finding differs from the study by Kendziora *et al.* whose analysis of the symmetry independent Raman-scattering peak position led to a conclusion of s-wave pairing in the OD regime [28]. It is presently unclear whether this difference is caused by the fact that Kendziora *et al.* studied a more overdoped sample (T_c of 57K instead of 78K in the present case). On the other hand, our finding is consistent with the conclusion by Hackl *et al.* whose analysis of the low energy power law of the frequency dependence of the electronic Raman signal suggests an OD sample with T_c ~55K has a d-wave symmetry [29]. The different conclusions between the two Raman experiments are not caused by doping difference in the samples since the transition temperatures are very similar. Our results also contradict an earlier ARPES study of an OD sample with similar T_c (83K) that reported a significant decrease of the SG anisotropy leading to an anisotropic s-wave gap in the OD regime [33]. The discrepancy here is probably caused by the fact that the earlier study chose to measure the gap minimum along the ΓX direction where the extrinsic effects due to the BiO superstructure are the strongest. We have measured the gap minimum along the ΓY direction. Values in Fig. 4.1 show that the SG in the OD sample is about 35% smaller than that of very slightly UD samples, although T_c is only about 10% lower. At the same time, the NG collapses almost completely [13, 14]. The rapid SG suppression is consistent with Raman experiments [28, 29] but differs from optical experiments [27]. It would be interesting to investigate why the gap obtained by the c-axis optical conductivity [27] should differ from the Raman and photoemission experiments which measure the quantity in the a-b plane. In contrast to the SG reduction, the intensity of the sharp peak near the gap edge below T_c

increases by at least a factor of 2. The simultaneous increase of this peak intensity and the gap suppression in the OD regime contrasts sharply with earlier results from the UD samples where the peak decreases with T_c suppression while the gap does not [16]. This suggest that T_c reduction in the OD samples has a different origin and is related to a decrease in pairing energy. This finding provides additional support for the theoretical ideas discussed earlier [17-25].

Accompanying the suppression of the SG and the NG is a significant change in the electronic structure at a much higher energy scale near $(\pi, 0)$, while the electronic structure along the (0,0) to (π, π) line remains very insensitive to doping [12-14]. Fig. 4.2 shows spectra along $(\pi, 0)$ to (π, π) line for two kinds of samples. For the 88K sample, there is a very broad feature centered around -150 to -200meV at $(\pi, 0)$. The centroid of this feature disperses rapidly from $(\pi, 0)$ to (π, π) and disappears after crossing the Fermi surface. [34]. Note that the low binding energy portions of the spectra are cut off by something different from the Fermi function convoluted with the instrument resolutions, as indicated by the energy position of the leading edge in the spectra. That is the NG discussed above. In the 78K sample, however, the feature at $(\pi, 0)$ moves much closer to the Fermi level ($\sim$50meV) and the NG is nearly zero. Further, it becomes sharper with significantly smaller dispersion, reproducing the flat band reported earlier [35].

Fig. 4.3 summarizes our findings in a phase diagram. The empirical T_c versus doping curve for Bi2212 (Ref. 36) is plotted with the vertical scale to the right. The trend of the NG and the SG in the UD regime is inferred from previous works where both the NG and the SG (Ref. 16) or just the NG (Ref. 15) are measured in a wide range of doping. The data highlight the rapid suppression of energy scales in the OD regime. Since the SG size decreases much faster than T_c suppression and the $\frac{SG}{T_c}$ ratio should not be smaller than the mean field value even in the OD regime, the T_c of the nearly optimally doped sample must have been suppressed by phase fluctuations as well. The shaded area at higher energy depicts the evolution of the electronic structure near $(\pi, 0)$. The data make clear that the suppression of the superconducting gap size is closely correlated with a rapid change of the electronic structure near $(\pi, 0)$.

There are several reasons why the empirical connection between the SG suppression and the electronic structure change at $(\pi, 0)$ may be very important. First is the large energy scale involved. As one goes from underdoped to overdoped cases, the energy scale of the $(\pi, 0)$ feature drops from -150 to -200meV to about -50meV. This change is much larger than the SG size of about 25meV. On the other hand, the energy scale of the broad maximum near -150meV to -200meV at $(\pi, 0)$ does not change much in the UD regime. Second, there is a significant difference in the spectral lineshape in the two cases. The broadness of the spectra from the UD sample is not due to poor sample quality, as evidenced by the resolution limited sharp peak below T_c [13, 15, 16]. The spectra from the 88K sample are somewhat sharper than that of further UD samples [12-16], consistent with the trend in Fig. 4.2. The lineshape change reveals a key essence of the paradox in the data: bad "quasiparticle" characteristics are actually good for superconductivity as far as the pairing strength is concerned. In this sense, there may be two aspects of the energy gap in the normal state. The leading edge NG has similar magnitude to that of the SG and is likely of the same origin. The 'energy gap' reflected in the centroid of the feature near $(\pi, 0)$ is empirically related to the leading edge NG but of much higher energy scale. Since the energy scale involved is similar to J, one may wonder whether this change is related to the antiferromagnetic interactions known to be important in UD materials [25]. Whatever its origin may be, the feature near $(\pi, 0)$ may underscore the novelty of the underlying electronic structure upon which high T_c superconductivity occurs.

sample / K space	Overdoped 78K		Overdoped 78K		Underdoped 88K		Underdoped 88K	
	NG	SG	NG	SG	NG	SG	NG	SG
(π, 0.23π)	3.5 (5)	15.5 (4)	3.5 (5)	18 (4)	24 (5.5)	26 (4)	27 (5)	26 (4)

Table 4.1: Superconducting gap (SG) and normal state gap (NG) size at $(\pi, 0.23\pi)$ for the four samples defined by the leading edge midpoint in meV. Parentheses indicate error bars.

4.2 References

1. B.G. Levi, *Phys. Today* **49**, 7 (1996)
2. H. Yasuoka *et al.*, in *Strong Correlation and Superconductivity*, edited by H. Fukuyama, S. Maekawa, and A.P. Malozemoff (Springer-Verlag, New York, 1989), p.254
3. M. Takigawa *et al.*, *Phys. Rev. B* **43**, 247 (1991)
4. J. Rossat-Migno *et al.*, *Physica B* **169**, 58 (1991)
5. J. Orenstein *et al.*, *Phys. Rev. B* **42**, 6342 (1990)
6. C.C. Homes *et al.*, *Phys. Rev. Lett.* **71**, 1645 (1993)
7. Y.F. Yan *et al.*, *Phys. Rev. B* **52**, R751 (1995)
8. B. Batlogg *et al.*, *Physica C* **235-240**, 130 (1994)
9. T. Ito, K. Takenaka, and S. Uchida, *Phys. Rev. Lett.* **70**, 3995 (1993)
10. J.W. Loram *et al.*, *Phys. Rev. Lett.* **71**, 1740 (1994)

11. J.L. Tallon *et al.*, *Phys. Rev. Lett.* **75**, 4114 (1995)

12. D.S. Marshall *et al.*, *Phys. Rev. Lett.* **76**, 4841 (1996)

13. A.G. Loeser *et al.*, *Science* **273**, 325 (1996)

14. A.G. Loeser *et al.*, *Physica C* **263**, 208 (1996)

15. H. Ding *et al.*, *Nature* **382**, 51 (1996)

16. J. M. Harris *et al.*, *Phys. Rev. B* **54**, 15665 (1996)

17. S. Doniach and M. Inui, *Phys. Rev. B* **41**, 6668 (1990)

18. S. Kivelson and V. Emery, *Nature* **374**, 434 (1995)

19. N. Trivedi and M. Randeria, *Phys. Rev. Lett.* **75**, 312 (1995)

20. G. Kotlair and J. Liu, *Phys. Rev. B* **38**, 5142 (1988)

21. W.G. Wen and P.A. Lee, *Phys. Rev. Lett.* **76**, 503 (1996)

22. Y. Suzumura *et al.*, *J. Phys. Soc. Jpn.* **57**, 2768 (1988)

23. B.L. Altschuler, L.B. Ioffe, and A.J. Millis, *Phys. Rev. B* **53**, 415 (1996)

24. P.W. Anderson, private communication

25. R.B. Laughlin, *J. Phys. Chem. Solids* **56**, 1627 (1995)

26. Y.J. Uemura in *Proceedings of the CCAST Symposium on High T_c Superconductivity and C_{60} Family*, Beijing, 1994, edited by S. Feng and H.C. Ren (Gordon and Breach, New York, 1994), pp. 113-142

27. S. Uchida, private communication

28. C. Kendziora, R.J. Kelly, and M. Onellion, *Phys. Rev. Lett.* **77**, 727 (1996)

29. R. Hackl *et al.* in *Spectroscopies Studies of Superconductors* edited by I Bozovic and D. van der Marel SPIE, Bellingham

30. D.M. Mitzi *et al.*, *Phys. Rev. B* **41**, 6564 (1990)

31. Z.-X. Shen *et al.*, *Phys. Rev. Lett.* **70**, 1553 (1993)

32. H. Ding *et al.*, *Phys. Rev. Lett.* **74**, 2784 (1995)

33. R.J. Kelly *et al.*, *Science* **271**, 1255 (1996)

34. The feature is very broad, but it still disperses and loses intensity after the expected Fermi surface.

35. D.S. Dessau *et al.*, *Phys. Rev. Lett.* **71**, 2781 (1993)

36. W.A. Groen, D.M. DeLeeuw, and L.F. Feiner, *Physica C* **165**, 55 (1990)

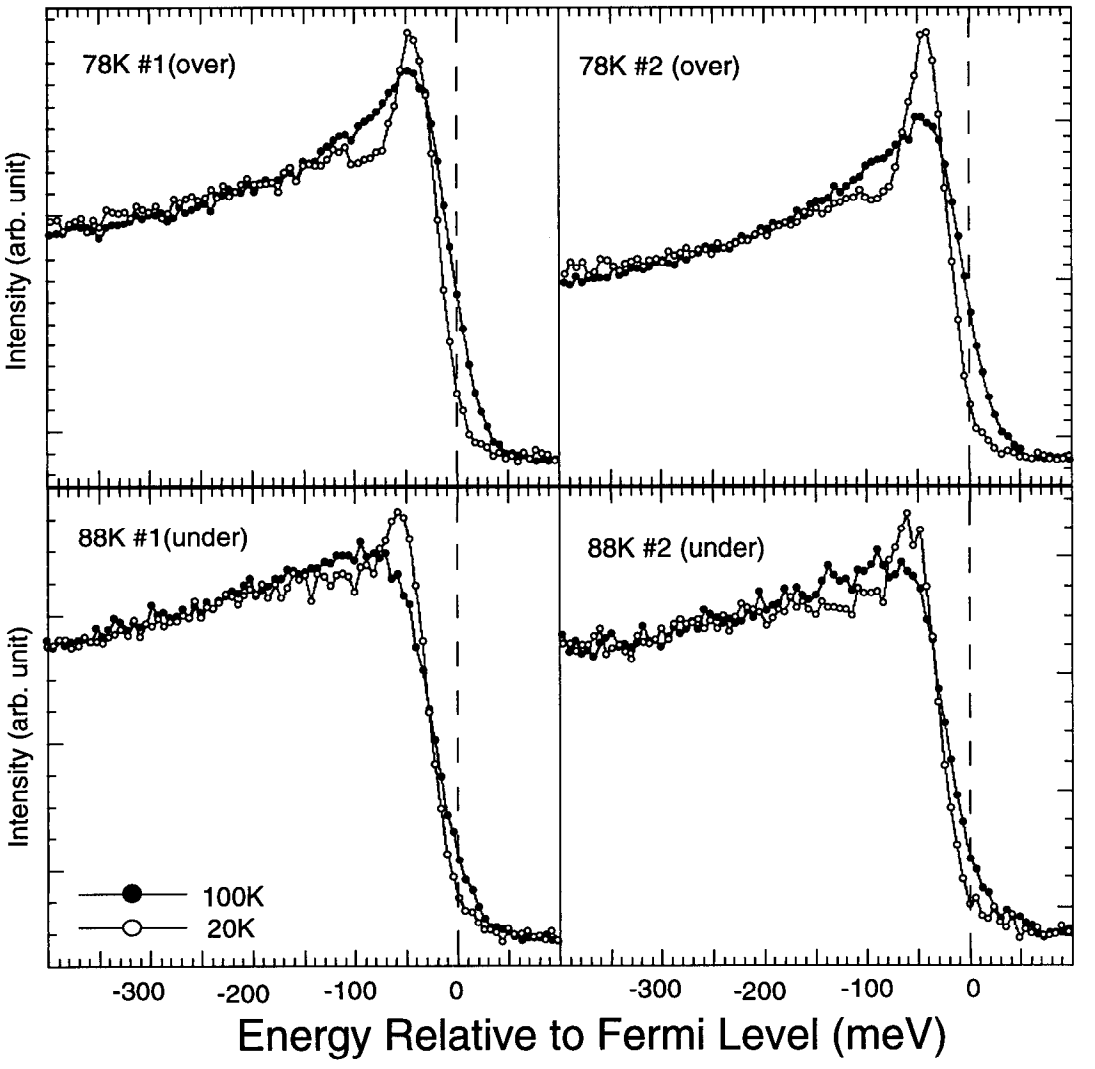

Figure 4.1: Angle resolved photoemission data recorded above and below T_c at $(\pi, 0.23\pi)$ where the $d_{x^2-y^2}$ gap exhibits a maximum. The 78K samples have no normal state gap (NG) and a much smaller superconducting state gap (SG). The 88K samples have larger NG and SG. The 78K samples have significantly larger peaks at gap edge below T_c.

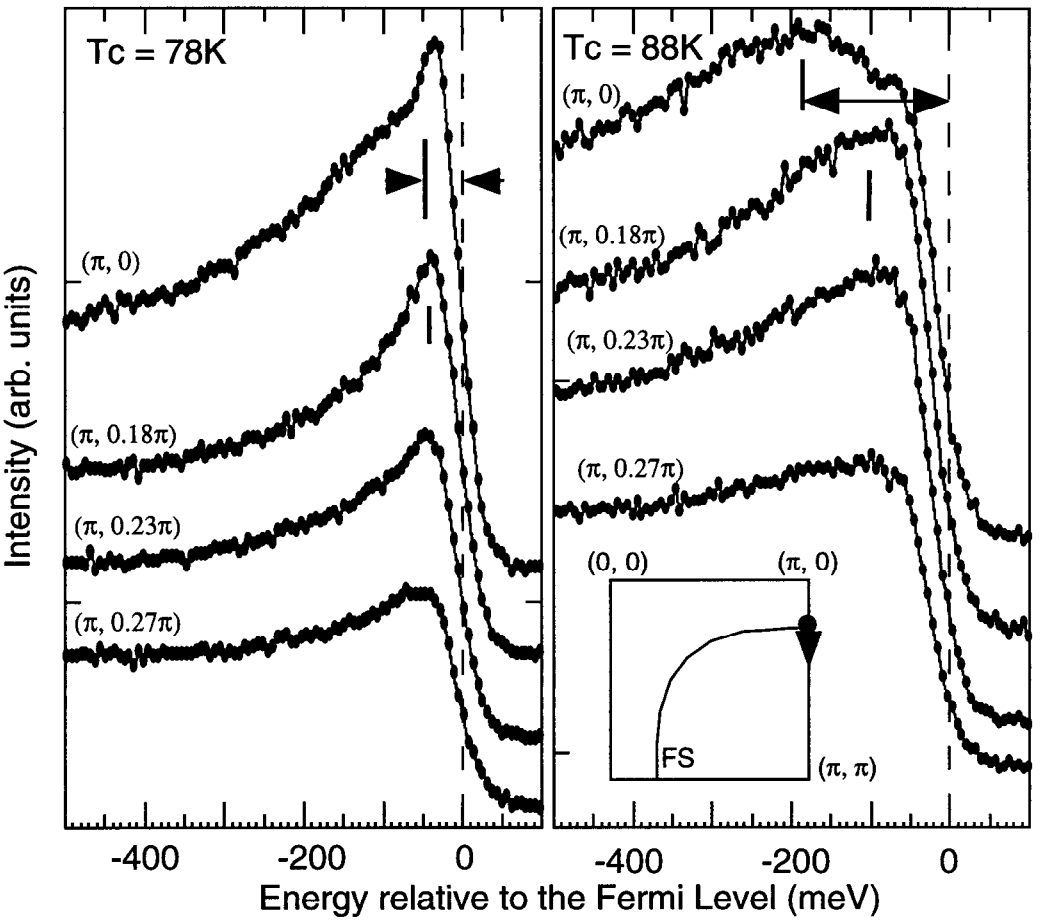

Figure 4.2: Electronic structure near $(\pi, 0)$ for the two samples reveals a striking difference. The arrows highlight the energy scale difference. The 88K UD sample has a broad feature near -200meV at $(\pi, 0)$. This feature becomes sharper and moves to -50meV in the 78K OD sample with much less dispersion.

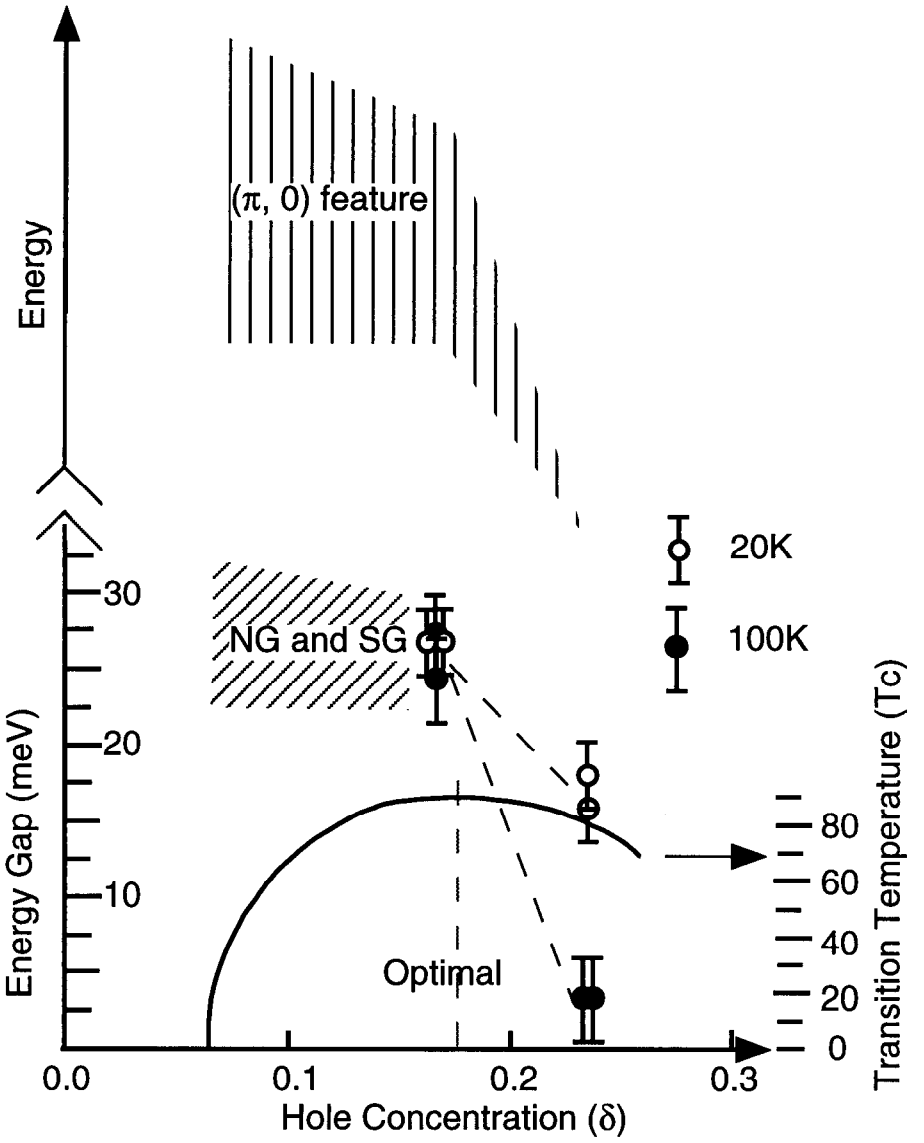

Figure 4.3: Phase diagram for the doping dependence of the energy gaps. The trend of doping dependence of the NG and the SG in the UD regime is from Ref. 15 and Ref. 16.

Chapter 5

Gap versus T_c

5.1 Data and Discussion

The superconducting state of a metal is characterized by an energy gap in the spectrum of electronic excitations. BCS-Eliashberg mean field theory [1] has been used successfully for decades in describing the superconducting state gap, Δ, in conventional superconductors such as Al or Nb. The typical mean-field theory result that the superconducting transition temperature, T_c, is proportional to Δ has been abundantly confirmed for conventional superconductors. Here we report data from angle-resolved photoemission spectroscopy showing that this proportionality is violated in underdoped samples of the high temperature superconductor (HTSC) $Bi_2Sr_2Ca_{1-x}Dy_xCu_2O_{8+\delta}$, implying a novel transition into the superconducting state.

A large variety of experimental measurements in underdoped HTSC have shown evidence for a suppression in the intensity of low energy excitations above T_c, including NMR [2], resistivity [3, 4], specific heat [5], and c-axis optical conductivity [6]. The relation, if any, between the superconducting state gap and the pseudogap or normal state gap is still an open question. Measurements on slightly overdoped BSCCO below T_c are consistent with a d-wave gap [7] and show no normal state gap to within our resolution. The present results on underdoped BSCCO samples with a wide range of transition temperatures show the same strong angular dependence of the superconducting state gap, but, in addition, they show a *normal state* gap with

similar magnitude and angular dependence in agreement with other recent ARPES work [8, 9, 10]. The normal state gap persists to temperatures well above T_c. These observations can be related to our finding that the SC gap fails to scale with T_c as expected from mean field theory. We discuss below how models with phase fluctuations in the order parameter predict pairing in the NS of underdoped HTSC up to a characteristic temperature T_{MF}, giving the two gaps a common origin and accounting for the non-mean field gap size versus T_c dependence. In these models, T_c is the temperature for phase coherence between pairs rather than the onset of pairing.

Raw data on underdoped BSCCO of two different oxygen dopings are plotted in Fig. 5.1 for temperatures well above and well below T_c. The five k-space positions were chosen by taking five cuts in the Brillouin zone along the Fermi surface. It was evident that the leading edge positions changed monotonically with angle, and that the NS and SC positions were similar. Characteristically narrow peaks appeared in the superconducting state. They are especially clear away from the $(0.4\pi, 0.4\pi)$ Fermi surface crossing. The observation of the narrow peaks indicates the broad NS lineshape is intrinsic to the doping level and not primarily the effect of disorder or impurity scattering since the scattering would also be expected to broaden features below T_c as well. Also, we note a strong and systematic increase in the low temperature height of the peaks with doping in the UD regime.

The leading edge midpoints of the EDC's in Fig. 5.1 are plotted vs. $0.5 \mid cosk_x a - cosk_y a \mid$ in Fig. 5.2. On this plot the $d_{x^2-y^2}$ gap prediction is a straight line that passes through the origin. The error bars are a combination of uncertainty in the leading edge midpoint position and the uncertainty in E_f (± 1 meV). The data agree reasonably well with the strong anisotropy of the d-wave gap, but in some cases the measured values show a flattening near the d-wave node position. One explanation is the dirty d-wave scenario [11, 12] where impurity scattering broadens the point node into a region of finite width. Systematic impurity doping studies using ARPES would be useful to clarify this point. Another contribution to the flattening is the finite k resolution combined with strong energy dispersion in the node direction [13].

The superconducting (13K) and normal state (75K) leading edge shift versus k curves for the T_c=46K sample agree very well, suggesting the two gaps are intimately

related. In the T_c=78K sample, the anisotropy of the gap is similar above and below T_c, but the magnitude shows a marked reduction at 100K and 150K. These observations raise two questions: does the gap change continuously through T_c and does the gap close at some higher temperature? To clarify these issues, more detailed temperature dependence measurements are shown in Fig. 5.3. The leading edge midpoint energies on the FS for the maximum and minimum gap are plotted for an UD T_c=85K sample. Measuring the temperature dependence of the gap with ARPES requires caution because thermal broadening and lineshape changes may affect the leading edge positions. To partially cancel these effects, we take the gap to be the difference between the leading edge midpoints at the two **k**-space locations. This gives a gap of 28±2 meV (~20% larger than a thin film of the same T_c) that changes smoothly above and below T_c, supporting the idea of a single gap function evolving with temperature. The gap becomes consistent with zero around 225K.

Next, we focus on the superconducting state gap Δ_{sc} as a function of T_c (Fig. 5.4) using the maximum difference between the leading edge midpoints on the underlying FS. For these measurements, this internally referenced gap shows the same trend as the leading edge midpoint near $(\pi, 0)$ (the d-wave gap maximum) versus T_c since the FS crossing near $(0.4\pi, 0.4\pi)$ shows a gap consistent with zero. The nine samples measured fall into three T_c groupings (all underdoped) representing three thin-film crystal growth and annealing runs. In spite of substantial error bars, it is clear that the familiar BCS mean fieled result of $\Delta_{sc} \propto T_c$ is violated (for example, Δ_{sc}=2.14kT_c for a weak coupling $d_{x^2-y^2}$ [14]). Instead Δ_{sc} stays constant or increases slightly as T_c is reduced.

For a comparison with phase diagrams, Fig. 5.4 shows a Δ_{sc} vs. doping δ (hole concentration per planar Cu) for the same underdoped samples, with each T_c converted to δ using the empirical relation $\frac{T_c}{T_{c,max}}$=1- $82.6(\delta - 0.16)^2$ [15]. Once again, the predicted BCS weak coupling d-wave result, Δ_{sc}=2.14kT_c (Fig. 5.4, dashed line), shows no resemblance to the observed doping dependence. By contrast, as T_c decreases on the overdoped side, the gap falls rapidly (although it may not be in qualitative agreement with the mean field calculation because of the *ad hoc* leading edge midpoint criterion for the gap). The failure of the mean field theory prediction for Δ_{sc} as a

function of T_c (or doping) in the underdoped region is our main result; it indicates that Δ_{sc} and T_c represent two distinct energy scales for underdoped BSCCO.

The non-mean field $\Delta_{sc} \propto T_c$ behavior is naturally related to the similarity of Δ above and below T_c in models with phase fluctuations in the complex superconducting state order parameter [16,17]. Paired electrons, and therefore a gap, exist below a mean field temperature T_{MF} that is proportional to Δ. The zero-resistance T_c is the temperature at which long range phase coherence is established. T_{MF} and T_c are the same in BCS theory since fluctuations are not considered, but T_c may be lower than T_{MF} in UD cuprates where phase stiffness is expected to be small. Photoemission is insensitive to phase, so it measure a gap below T_{MF}. The phase stiffness is proportional to the superfluid density n_s. Thus, if the phase stiffness energy scale instead of the gap determines T_c, then T_c should decrease as the doping is lowered, quite apart from any changes in Δ and T_{MF}, in agreement with the data in Fig. 5.4. In this model, Δ is determined by the same pairing interaction in the superconducting and normal states. Muon spin relaxation (μSR) measurements support the idea that T_c is determined by n_s. A universal curve with $T_c \propto n_s$ from μSR has been reported for a large number of underdoped cuprates [18]. Also, magnetoresistance measurements of 60K YBCO show a Lorentz-force independent contribution persisting to 200K [19] that may be consistent with phase fluctuations in the order parameter.

Various extensions to Anderson's original RVB idea [20] give a possible microscopic justification in terms of spin-charge separation for the phase fluctuation model, including the two energy scales (kT_c and Δ) and a distinct pseudogap regime. Spin charge separation provides a means of producing pairing of excitations without superconductivity. The fermionic spin excitation (spinons) pair into singlets at a temperature T_s greater than T_c for UD cuprates, where T_s is proportional to the gap. T_s is similar to T_{MF} and may represent a crossover instead of a true phase transition. Also, T_s decreases with increasing δ in agreement with the trend of the upper line in Fig. 5.4. The pairing was predicted to be d-wave, another area of agreement with the data. Because of the apparent flattening of the normal state gap near the d-wave node position, the data could also be consistent with recent work predicting the pseudogap regime to be a mixture of d-wave spinon pairing and pockets of spinon FS. In either

case, the charge excitations (holons) Bose condense at T_c, so once again $T_c \propto n_s$, the two dimensional Bose condensation result. T_c is also the temperature at which phase coherence between the singlets appears. These models are in agreement with the ARPES data in the doping dependence of the gap and in the existence of d-wave pairing well above T_c for underdoped samples.

In summary, the increase in the superconducting state gap with decreasing T_c violates the BCS mean-field theory prediction and suggests the existence of an energy scale for pairing that is separate from and higher than kT_c. This energy scale accounts for the pseudogap above T_c. As measured by ARPES, the normal state gap is highly anisotropic and it is similar in magnitude and **k** dependence to the superconducting state gap, supporting the idea of a common underlying pairing interaction.

5.2 References

1. J.R. Schrieffer, *Theory of Superconductivity* (Benjamin, New York, 1964)
2. M. Takigawa, A.P. Reyes, P.C. Hammel, J.D. Thompson, R.H. Heffner, Z. Fisk, and K.C. Ott, *Phys. Rev. B* **43**, 247 (1991)
3. T. Ito, K. Takenaka, and S. Uchida, *Phys. Rev. Lett.* **70**, 3995 (1993)
4. B. Buchner, P. Steiner, J. Karpinski, E. Kaldis, and P. Wachter, *Phys. Rev. Lett.* **70**, 2012 (1993)
5. J.W. Loram, K.A. Mirza, J.R. Cooper, and W.Y. Liang, *Phys. Rev. Lett.* **71**, 1740 (1994)
6. C.C. Homes, T. Timusk, R. Liang, D.A. Bonn, and W.N. Hardy, *Phys. Rev. Lett.* **71**, 1645 (1993)
7. Z.-X. Shen *et al.*, *Phys. Rev. Lett.* **70**, 1553 (1993)
8. A.G. Loeser *et al.*, *Science* **273**, 325 (1996)
9. D.S. Marshall *et al.*, *Phys. Rev. Lett.* **76**, 4841 (1996)

10. H. Ding *et al.*, *Nature* **382**, 51 (1996)

11. L.S. Borkowski and P.J. Hirschfeld, *Phys. Rev. B* **49**, 15404 (1994)

12. R. Fehrenbacher and M.R. Norman, *Phys. Rev. B* **50**, 3495 (1994)

13. R. Fehrenbacher (unpublished)

14. H. Won and K. Maki, *Phys. Rev. B* **49**, 1397 (1994)

15. M.R. Presland *et al.*, *Physica C* **176**, 95 (1991); W.A. Groen, D.M. de Leeuw, and L.F. Feiner, *ibid.* **165**, 55 (1990)

16. V.J. Emery and S.A. Kivelson, *Nature* **374**, 434 (1995)

17. S. Doniach and M. Inui, *Phys. Rev. B*, **41**, 6668 (1990)

18. Y.J. Uemura *et al.*, *Phys. Rev. Lett.* **66**, 2665 (1991)

19. J.M. Harris *et al.*, *Phys. Rev. Lett.*, **75**, 1391 (1995)

20. P.W. Anderson, *Science* **235**, 1196 (1987)

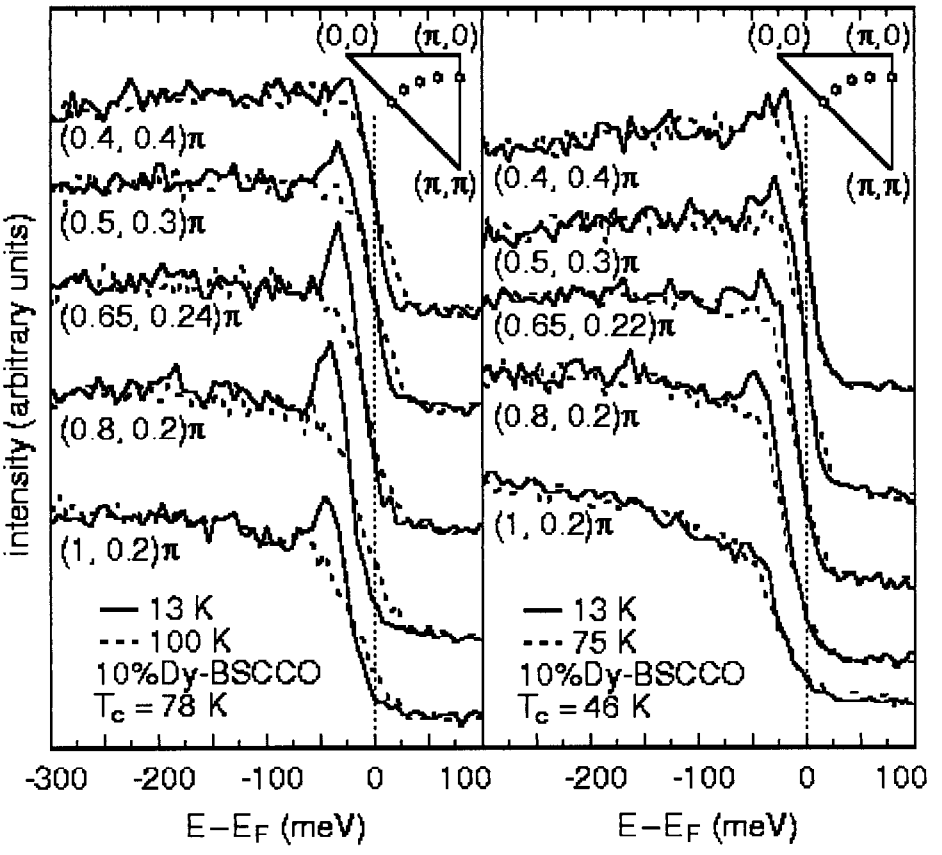

Figure 5.1: ARPES spectra near the Fermi energy for underdoped, single crystal thin films of Bi_2 Sr_2 Ca_{1-x} Dy_x Cu_2 $O_{8+\delta}$ in the superconducting and normal states. **k**-space positions were selected on the underlying FS to facilitate measuring the energy gap. The systematic shift of leading edge position with **k** shows an anisotropic energy gap.

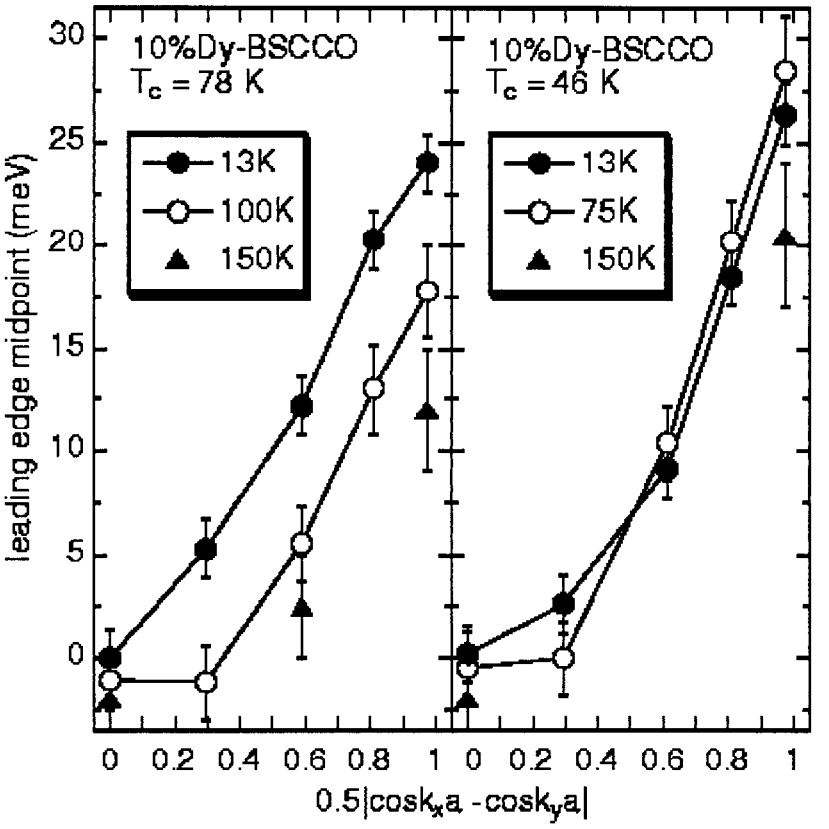

Figure 5.2: Leading edge midpoint shifts from E_f, indicative of an anisotropic energy gap, in the superconducting and normal states of Bi_2 Sr_2 Ca_{1-x} Dy_x Cu_2 $O_{8+\delta}$ extracted from the ARPES spectra of Fig. 5.1. The abscissa, $0.5 \mid cosk_x a - cosk_y a \mid$, was selected for comparison to a $d_{x^2-y^2}$ gap, which would be a straight line on this plot. The dirty d-wave scenario predicts flattening near the origin.

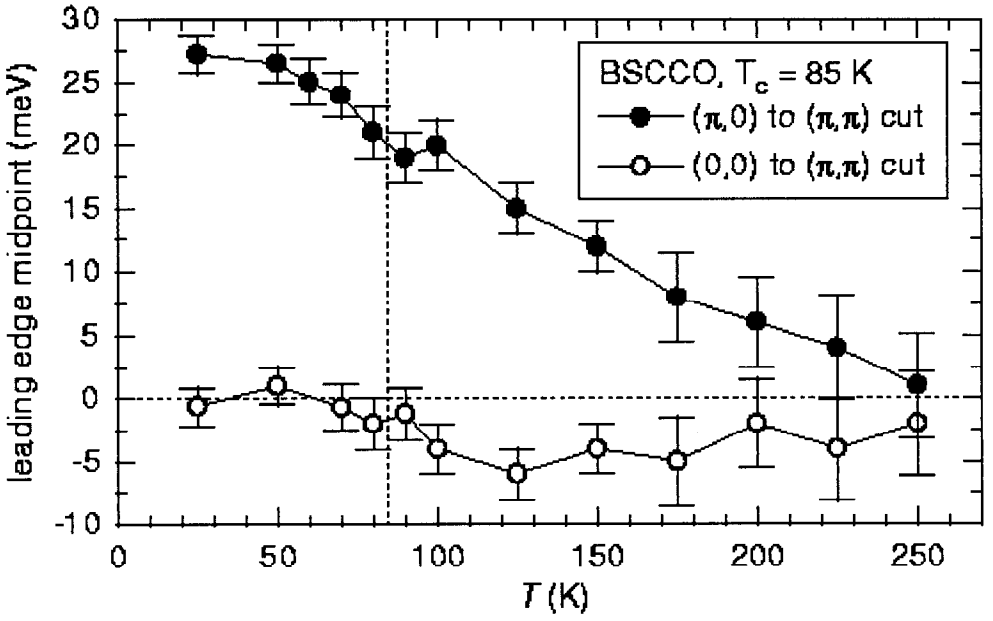

Figure 5.3: The temperature dependence of the leading edge midpoints for spectra taken at FS crossings near $(\pi, 0.2\pi)$ and $(0.4\pi, 0.4\pi)$ of an underdoped BSCCO single crystal. The difference between the two represents an energy gap that decreases continuously from 28±2 at 25K to near zero at 225K.

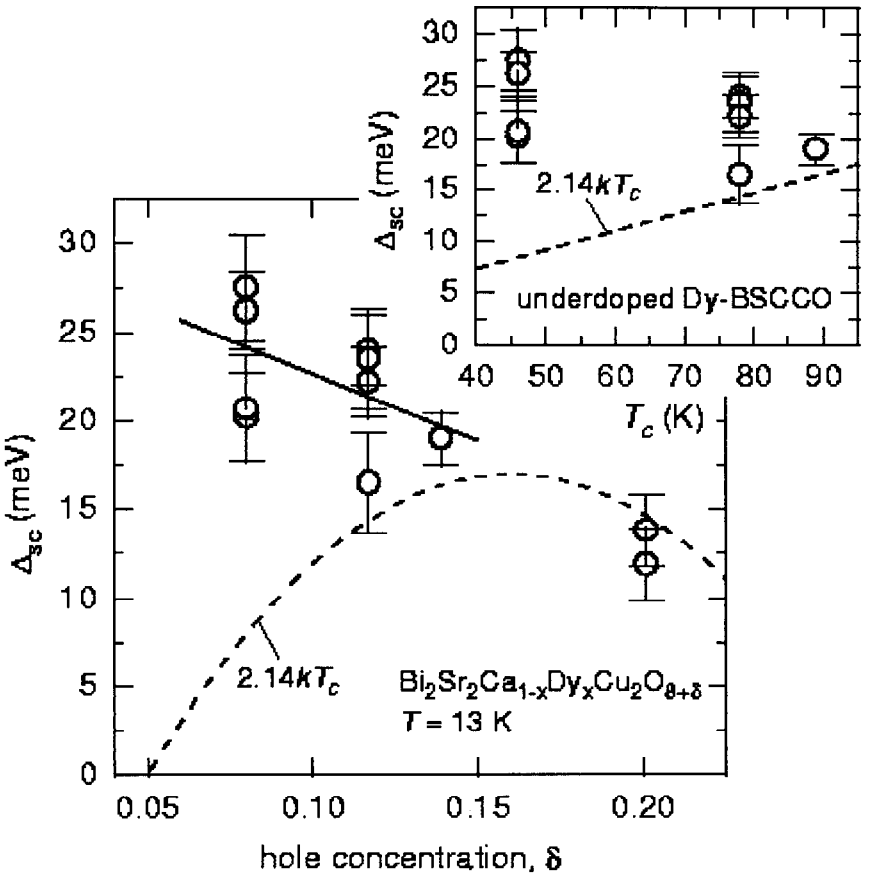

Figure 5.4: Inset: The superconducting state gap Δ_{sc} from leading edge shifts measured at 13K on Bi_2 Sr_2 Ca_{1-x} Dy_x Cu_2 $O_{8+\delta}$ plotted vs. T_c. The nine samples measured came from three growth and annealing runs, and therefore fall into three T_c groups. The dashed line is the standard BCS mean-field d-wave prediction with Δ_{sc}=2.14kT_c, shown to highlight the non-mean field trend of the data. Main Panel: Δ_{sc} vs doping δ, with δ inferred from $\frac{T_c}{T_{c,max}}$. The energy scale from T_c (2.14kT_c, dashed line) shows very different behavior from the linear fit to the Δ_{sc} data points (straight line) from the underdoped samples. By contrast, the gap values for overdoped samples decrease in the conventional way.

Chapter 6

Single Plane BSCCO

6.1 Data and Discussion

A central issue in the physics of high T_c superconductivity is the role of coupling between the two dimensional copper-oxygen planes in producing superconductivity. The T_c of these materials tends to increase with the number of layers per unit cell. It is currently an open question whether the superconducting state order parameter symmetry will be the same in one-layer and the more strongly coupled two-layer compounds. Angle resolved photoemission spectroscopy (ARPES) has the potential to resolve this issue since it is able to measure directly the anisotropy of the superconducting state gap (the magnitude of the order parameter). In the two-plane material, Bi2212, the gap was found by ARPES to be highly anisotropic, consistent with a $d_{x^2-y^2}$ order parameter [1, 2]. We report measurements of the one plane material, Bi2201, that show a similarly large anisotropy with a smaller overall gap magnitude.

In underdoped Bi2212, ARPES measurements have shown that the anisotropic gap persists well above T_c [3, 4], consistent with many other experiments that have shown a pseudogap or spin gap in the normal state of the cuprate supeconductors [5]. Current evidence for the normal state gap in one-plane materials is much weaker than in two-plane materials, and its existence is controversial [6]. Our results show a clear normal-state gap up to high temperatures in optimally doped and underdoped Bi2201, but not in overdoped Bi2201.

Single crystals of $Bi_{2+x}Sr_{2-(x+y)}La_yCuO_{6+\delta}$ were grown using a floating zone method. X-ray scattering confirms that the crystals are single phase Bi2201, and electron probe microanalysis was used to measure the atomic ratios of the cations. Substitution of trivalent La or Bi for divalent Sr reduces the hole concentration in the CuO_2 planes. The effect of La doping goes beyond changing the carrier density [7], however, and raises the maximum T_c from 10K to 30K. A roughly parabolic dependence of T_c on $(x + y)$ has been observed [8]. Our optimally doped crystals (T_c = 29K) come from substituting La = 0.35 for Sr. With no La substitution, Bi/Sr ratios of 2.3/1.7 and 2.1/1.9 give the underdoped samples with $T_c < 4$K and the overdoped samples with T_c = 8K respectively. The transition temperatures were taken at the zero resistance values and confirmed by SQUID magnetization measurements. The transition widths are less than 2K. The resistivity curves give linear-T behavior for the optimally doped samples [8], positive curvature for the overdoped samples typical of other overdoped cuprates, and linear-T dependence for the underdoped samples with an upturn at low T.

Fermi surface (FS) crossing were determined from at least 5 **k**-space cuts in one octant of each Bi2201 sample. Two cuts along high symmetry lines are plotted for three samples with different doping levels in Fig. 6.1. The data consist of energy distribution curves (EDC's) taken in the *normal state* at fixed **k**, determined by the angles between the sample normal and the analyzer. A number of nearly equivalent criteria can be applied to finding the positions of the FS crossings along the **k**-space cuts, such as identifying the point where the peak intensity decreases by $\frac{1}{2}$ in going from occupied to unoccupied states, or where the leading edge midpoint of the spectral weight comes closest to E_f. The latter (leading edge midpoint position) is useful because it is also a measure of the gap in the excitation spectrum where it fails to reach E_f [1]. The measured Fermi surface in our samples is similar to previous work on overdoped Bi2201 [9] showing a large hole pocket centered at (π, π). We find that over a wide range of doping, there is little change in the FS and no indication of a FS topology change.

The cuts in Fig. 6.1 are along the (0,0) to (π, π) [ΓY cut] and $(\pi, 0)$ to (π, π) [$\bar{M}$Y cut]. The ΓY cuts (left panels) show the largest energy dispersions and clear FS

crossings in the vicinity of $(0.4\pi, 0.4\pi)$. (We plot ΓY instead of ΓX because there is less complication from superstructure effect.) The $\bar{M}$Y cuts (right panels) show much less dispersion, but FS crossings can still be seen near $(\pi, 0.25\pi)$. The most striking change with doping occurs in the lineshape. As the hole doping increases, the lineshape becomes much narrower, indicating the imaginary part of the excitation's self-energy has dramatically decreased. Only the overdoped Bi2201 sample approaches Fermi-liquid-like behavior with well defined quasiparticle excitations. The linewidth at $(\pi, 0)$ is especially sensitive to doping, as shown in the rightmost panel. The underdoped sample barely has a peak at all, while the overdoped sample has a large peak that is nearly resolution limited. Disorder may play a role in the trend of these normal state spectra, assuming Matthiessen's rule holds, since the residual resistivity increases from the overdoped to the underdoped crystals. The residual resistivity ratio (forming $\frac{R(300)K}{R(0)K}$ by extrapolating to 0K) is 3.7 for the overdoped case, 2.4 for optimal, and 2.0 for the underdoped. However, the similarity to the trend of linewidth in Bi2212 suggests that doping is the primary cause of the linewidth change. In Bi2212, the linewidths of underdoped samples are very broad, but sharp, resolution limited peaks still appear below T_c, indicating impurity scattering is not dominant in these systems [4].

We next turn to the important issue of the superconducting state gap. As mentioned above, the shift in the leading edge midpoint may be used to characterize an excitation gap. In the overdoped case no gap is observable within our resolution. This can be seen from the spectra on the FS taken from the ΓY and $\bar{M}$Y cuts (Fig. 6.2). The leading edges of both overdoped spectra coincide. Since the BCS gap for T_c=8K is only 1.5meV, it is not surprising that the gap is too small to be seen within our error bars of $\pm$2 meV. In the optimally doped samples, however, we observe a clear and reproducible gap of 10$\pm$2 meV, in rough agreement with point contact tunneling measurements on ceramic samples of similar composition [10]. The gap is anisotropic, with a maximum along the $\bar{M}$Y cut [*i.e.*, near $(\pi, 0)$] and a minimum consistent with 0 on the ΓY cut 45° away. Comparing these two extrema (Fig. 6.2) shows the shift in the leading edge position quite clearly. Furthermore, we have reproduced the same gap value within the error bars on 3 other samples. Interestingly, the gap persists into

the normal state with no noticeable diminution. In the underdoped sample, the leading edges are not as sharp, but a reproducible gap of 7±3 meV maximum magnitude is still evident.

The measured Bi2201 superconducting state lineshape differs from that of Bi2212 because it lacks the peak and dip feature. In Bi2212 the sharp peak is at ~40 meV binding energy, followed by a dip that extends to ~90 meV [11]. If the features scale in energy with the gap [12], the the factor of 3 decrease for Bi2201 would make them difficult to resolve. It is also possible that impurity scattering plays a role in obscuring any lineshape change. Instead of a sharp peak and dip, our spectra show a moderate linewidth narrowing below T_c (Fig. 6.2).

To explore the gap anisotropy, we took a number of k-space cuts between the ΓY and $\bar{M}$Y cuts of Fig. 6.1 on the same samples. The leading edge shifts for two optimally doped Bi2201 samples are plotted against $0.5 \mid cosk_x a - cosk_y a \mid$ both below and well above T_c in Fig. 6.3. On this plot, a $d_{x^2-y^2}$ gap would be a straight line through the origin. The curves show considerable flattening near the origin compared to the pristine d-wave gap, suggestive of either the effect of interlayer tunneling matrix elements [13, 14] or pair breaking due to impurities [15].

A central purpose of the present study was to determine whether the superconducting state gap anisotropy persists as the CuO_2 planes are increasingly isolated from each other. Our observation of a strongly anisotropic gap in Bi2201 indicates that it does, since Bi2201 has a large separation between CuO_2 planes (12.3Å compared to 3.3Å for Bi2212), a huge c-axis resistivity(ρ=30Ω at 50K [8]), and nonmetallic intervening Bi-O layers. A theoretical model that may be relevant to our findings is the interlayer tunneling (ILT) model [13], since it addresses the effect of interplanar coupling on the gap magnitude and anisotropy. In the ILT model, the *sign* of the order parameter is determined by the in-plane pairing kernel, which acts as a symmetry breaking field in the space of order parameter symmetries [16, 14]. However, the anisotropy in *gap magnitude* is dominated by the effect of interlayer matrix elements [13, 14] when T_c is high. Thus, small s-wave or d-wave in-plane pairing kernels in the presence of strong interlayer coupling would give nearly identical results in ARPES gap magnitude measurements. Weakening the interlayer coupling more clearly reveals

the intrinsic single-plane gap. The highly anisotropic gap in Bi2201 is consistent with an underlying $d_{x^2-y^2}$ symmetry, perhaps with some residual interlayer pair tunneling.

Our results mesh well with the tricrystal experiments of Tsuei *et al.* carried out on the single plane cuprate Tl2201. The half-integer flux quanta observed in the superconducting state indicate a sign change in the order parameter [17]. Thus, the intrinsic interaction in a single plane favors d-wave pairing, while the overall increase in gap magnitude from Bi2201 to Bi2212 by a factor of 3 may indicate that interlayer coupling enhances the gap [13, 14, 16]. Even in Bi2201 the gap magnitude greatly exceed the BCS prediction of 4.4 meV for T_c - 29K (the leading edge midpoint shift tends to underestimate the gap).

It is important to consider whether disorder and impurities cause the gap to be smaller in Bi2201 than in Bi2212. The residual resistivity ratio (RRR) is 2.4 for optimally doped Bi2201, a rather low value that indicates substantial impurity scattering. However, some thin films of Dy-doped Bi2212 have even smaller RRR's, and they show no reduction in gap magnitude [4]. Thus, the lower gap magnitude in Bi2201 is most likely intrinsic.

The measurements of a normal state gap in Bi2201 (Figs. 6.2 and 6.3) show that the pseudogap can exist in a one plane material. A pairing enhancement based on interlayer superexchange $J_\perp$, suggested for bilayer materials [6, 18], will be absent in Bi2201 because of the large distance between CuO_2 planes and the geometric frustration induced by staggering the Cu sites along the c-axis. As in the case of Bi2212 [3], the similarity in gap anisotropy and magnitude above and below T_c suggests that the two gaps are related and that pairing occurs well above T_c. Further evidence for this point of view has come from low temperature gap measurements in Bi2212. The gap fails to decrease with T_c as T_c is decreased by underdoping [4]. The persistence of the gap in the underdoped Bi2201 sample shows the same anomalous pattern; the gap in underdoped samples represents a different energy scale from kT_c. Theoretical interpretations of separate energy scales for the gap and kT_c have included the idea that pairs form at relatively high temperatures but do not become phase coherent until T_c [19]. Microscopic theories based on spin-charge separation have separate pairings for spin and charge excitations [20], with spinon pairing occurring in general

at higher temperature than holon pairing.

The gap measurements on Bi2201 and Bi2212 as a function of doping show a striking contrast between the effect of lowering T_c by underdoping and lowering T_c by weakening the interplanar coupling. The gap (and thus the pairing strength) is relatively insensitive to underdoping but drops roughly proportionally to the maximum T_c in going from a bilayer to a single layer material.

While no detailed theory exists for the lineshape evolution with doping, the change from a narrow peak to a broad continuum with decreasing hole doping suggests non-Fermi liquid behavior and a breakdown of the quasiparticle picture. Recently, it was proposed that the peak width is due to the strong coupling of electrons to collective excitations with $\mathbf{q}$ peaked at (π, π) [21]. The width has also been attributed to the decay of the hole into a spinon and holon [22], with the hole lifetime decreasing on the underdoped side. The rightmost panel of Fig. 6.1 shows the lineshape trend clearly and is insensitive to finite $\mathbf{k}$ resolution because the dispersion is small near $(\pi, 0)$.

In summary, ARPES measurements on the gap and electronic structure of the one-plane compound Bi2201 open a new window on the occurrence of superconductivity in a relatively low T_c member of the cuprate family. These observations constrain theories by showing that in a system with very weakly coupled planes, there is a strongly anisotropic superconducting gap and also a pseudogap above T_c.

6.2 References

1. Z.-X. Shen *et al.*, *Phys. Rev. Lett.* **70**, 1553 (1993)
2. H. Ding *et al.*, *Phys. Rev. B* **54**, R9678 (1996)
3. D.S. Marshall *et al.*, *Phys. Rev. Lett.* **76**, 4841 (1996); A.G. Loeser *et al.*, *Science* **273**, 325 (1996), H. Ding *et al.*, *Nature* **382**, 51 (1996)
4. J.M. Harris *et al.*, *Phys. Rev. B* **54**, R15665 (1996)
5. For example, see N.P. Ong, *Science* **273**, 321 (1996); B. Batlogg and V.J. Emery, *Nature* **382**, 20 (1996); B.G. Levi, *Phys. Today* **49**, No.6, 19 (1996) and references therein.
6. A.J. Millis and H. Monien, *Phys. Rev. Lett.* **70**, 2810 (1993)
7. H. Nameki *et al.*, *Physica C* **234C**, 255 (1994)
8. R. Yoshizaki *et al.*, *Physica C*, **224C**, 121 (1994)
9. D.M. King *et al.*, *Phys. Rev. Lett.* **73**, 3298 (1994)
10. N. Hudáková *et al.*, *Physica C* **218B**, 217 (1996)
11. D.S. Dessau *et al.*, *Phys. Rev. Lett.* **66**, 2160 (1991)
12. C.M. Varma and P.B. Littlewood, *Phys. Rev. B* **46**, 405 (1992)
13. S. Chakravarty, A. Sudbø, P.W. Anderson, and S. Strong, *Science* **261**, 337 (1993)
14. L. Yin, S. Chakravarty, and P.W. Anderson, to be published
15. L.S. Borkowski and P.J. Hirschfield, *Phys. Rev. B* **49**, 15404 (1994)
16. A. Sudbøand S.P. Strong, *Phys. Rev. B* **51**, 1338 (1995)
17. C.C. Tsuei *et al.*, *Science* **271**, 329 (1996)

18. M.U. Ubbens and P.A. Lee, *Phys. Rev. B* **50**, 438 (1994); B.L. Altshuler, L.B. Ioffe, and A.J. Millis, *Phys. Rev. B* **53**, 415 (1996)

19. V.J. Emery and S.A. Kivelson, *Nature* **374**, 434 (1995); S. Doniach and M. Inui, *Phys. Rev. B* **41**, 6668 (1990)

20. P.W. Anderson and S.P. Strong, *Chin. J. of Phys.* **34**, 159 (1996); P.W. Anderson, *J. Phys. Cond. Matt.* **8**, 10083 (1996); X.-G. Wen and P.A. Lee, *Phys. Rev. Lett.* **76**, 503 (1996); V.J. Emery, S.A. Kivelson, and O. Zachar, cond-mat/9610094; H. Fukuyama, *Physica (Amsterdam)* **263C**, 35 (1996)

21. Z.-X. Shen and J.R. Schrieffer, *Phys. Rev. Lett.* **78**, 1771 (1997)

22. R.B. Laughlin cond-matt/9608005

23. Michihito Muroi and Robert Street, *Physica C* **248**, 290

24. Jun Kondo, *J. Phys. Soc. Japan* **58**, 2884

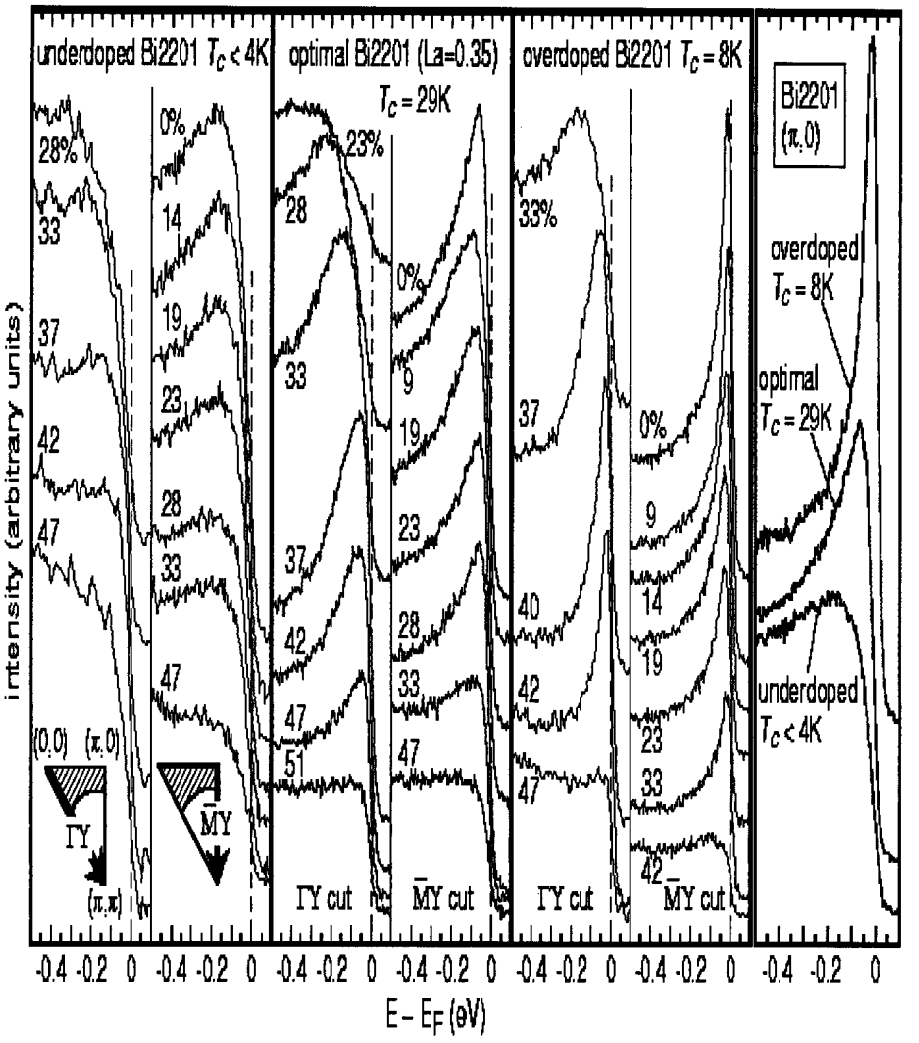

Figure 6.1: Normal state ARPES spectra for underdoped (T_c¡4K), optimally doped (T_c=29K), and overdoped (T_c=8K) Bi2201, measured at T = 100, 60 and 60K respectively. The left panels for each doping show spectra along the ΓY **k**-space cut while the right panels show the $\bar{M}$Y cut. The rightmost panel shows strong change in linewidth with doping.

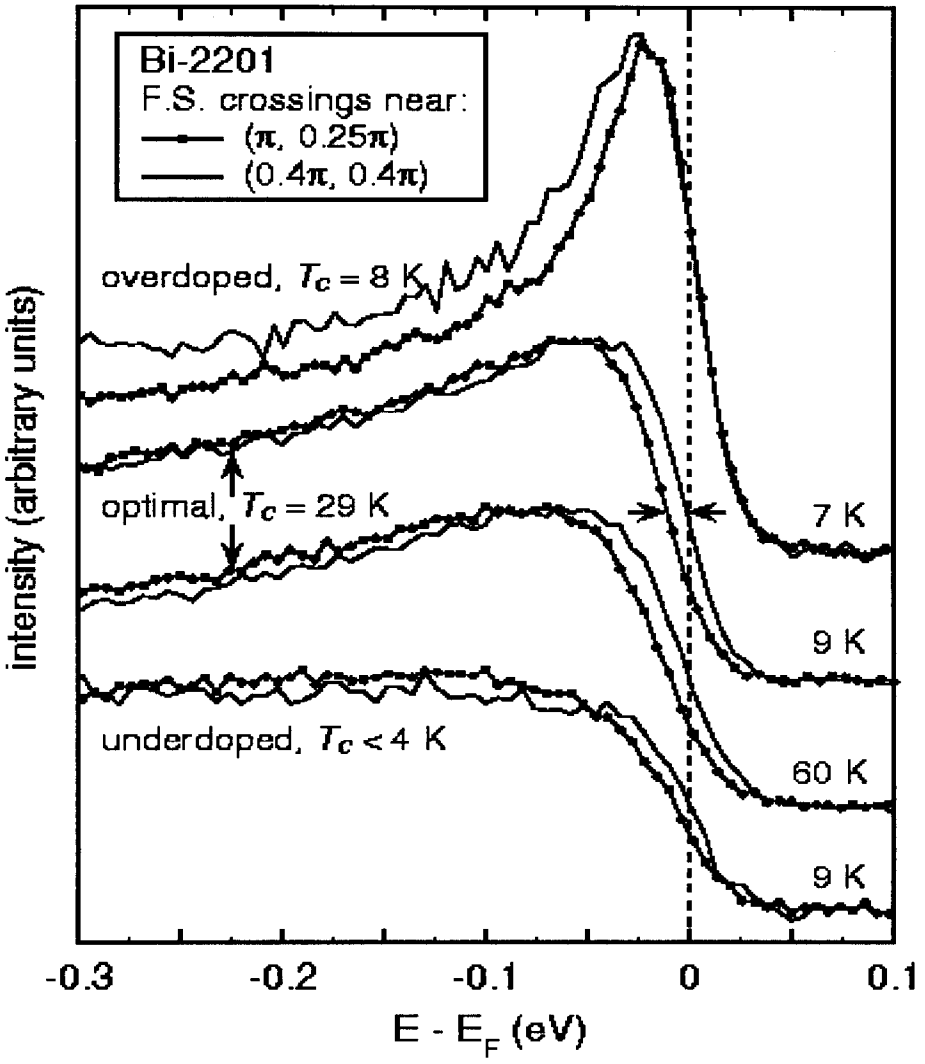

Figure 6.2: ARPES spectra at FS crossings for the maximum [near $(\pi, 0.25\pi)$ and minimum near $(0.4\pi, 0.4\pi)$] gaps for the crystals in Fig. 6.1. Shifts in the leading edge midpoints indicate an anisotropic gap, as in the 10 $\pm$ 2 meV shift between the arrows for the T_c = 29K samples at T 9K. The spectra are normalized to give the leading edges equal height in order to show the shifts between them.

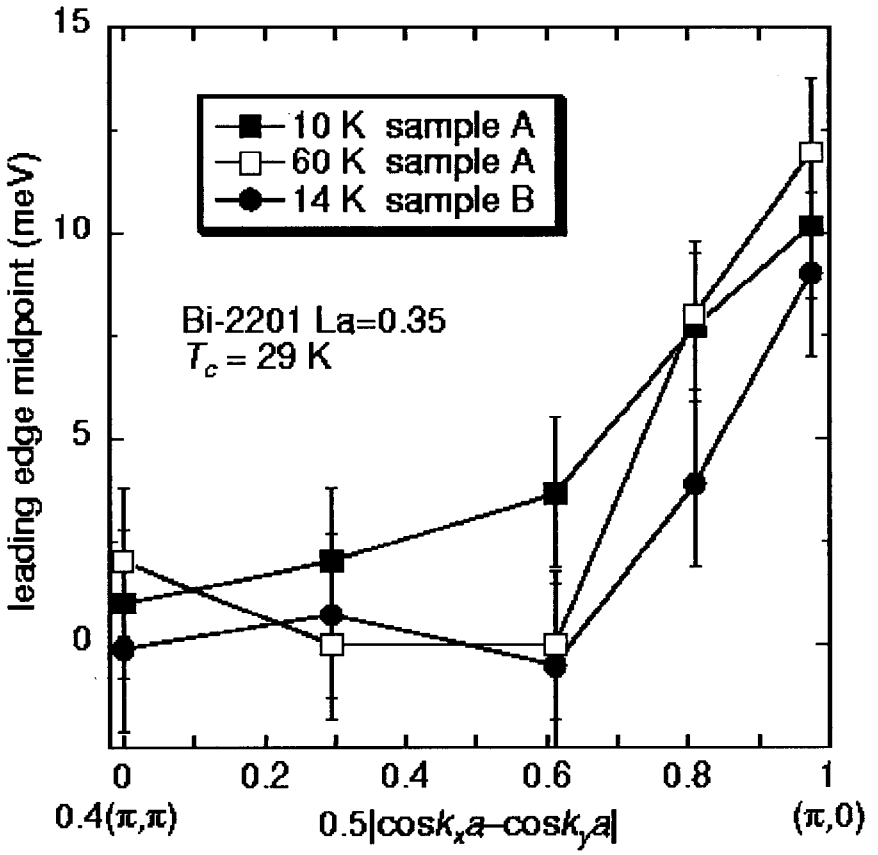

Figure 6.3: Leading edge midpoint shifts from E_f for samples A and B, indicative of an anisotropic energy gap in the superconducting and normal states of optimally doped Bi2201. A $d_{x^2-y^2}$ gap is a straight line intercepting the origin of the plot.

Chapter 7

Spectral Weight Transfer

7.1 Data and Discussion

In a conventional superconductor, T_c is regulated by the superconducting energy gap Δ, which is related to the characteristic phonon energy [1] The central physics can be described with a mean-field approach, as in the theory of Bardeen, Cooper, and Schrieffer (BCS) [2]. In this paradigm only excitations near Δ out of the available Fermi energy E_f are modified by superconductivity. The phase-space constraint imposed by these two drastically different energy scales, a few thousandths of an electron volt for Δ and a few electron volts for E_f, limits an electron with momentum **k** to mix only with electrons with momenta near **k** and -**k** through the coherence factors [1].

We report angle resolved photoemission spectroscopy (ARPES) data from optimally doped $Bi_2Sr_2CaCu_2O_{8+\delta}$ single crystals that suggests a different paradigm in high T_c superconductors. As the temperature is lowered from above T_c to well below T_c, the single particle excitation spectra show changes that strongly depend on **k**. At certain momenta, the change extends up to an energy close to 300 meV, or $40kT_c$, much larger than the BCS value near $2kT_c$. Furthermore, spectral weight is transferred from very high energy at momentum **k** to a much lower energy at another momentum **k'** that is far from either **k** or -**k**. Along the (1,0) direction, the momentum-dependent spectral weight transfer seems to broadly peak near $|\mathbf{Q}| \sim 0.45\pi$. This **Q**

and the previously found collective excitations of similar energy scale but with a different momentum transfer $\mathbf{Q}'$ broadly peaked near (π,π) [3] are intriguingly close to the charge and spin order periodicities that are required if the fluctuating charge stripes are present.

Special attention is paid during the experiment to ensure the proper normalization of the data. The spectra above and below T_c were first normalized to the integrated signal intensity above E_f that came from scattered electrons excited by higher order light and was roughly proportional to the angle-integrated spectral weight. For a given pair at each momentum, the spectra were further rescaled so that the high binding energy tails were also matched, consistent with the general expectation that the data above and below T_c should be the same at these energies. The latter procedure, which is needed because of subtle effects such as changes in sample position as a result of thermal expansion of the cryostat, involves only minor rescaling. The physics discussed here remains the same with or without the application of the second procedure.

In the normal state, a broad feature in the ARPES data along (0,0) to $(\pi,0)$ (Fig. 7.1) was observed to disperse from -300 meV near $(0.36\pi,0)$ to almost the Fermi level near $(\pi,0)$. The dispersion is rapid from $(0.36\pi,0)$ to $(0.64\pi,0)$ but slow from $(0.64\pi,0)$ to $(\pi,0)$ [5]. In the superconducting state (Fig. 7.1), a sharp peak emerges from the broad normal state feature with a dip at higher energy, although the dip is weaker than typically seen [6]. The most important observation emphasized here is the strong temperature induced $\mathbf{k}$ and E dependent spectral weight transfer. Although the overall spectral weight appears to gain slightly near $(\pi,0)$, spectral weight is lost upon the superconducting transition at momenta $(0.36\pi,0)$ and $(0.55\pi,0)$. Furthermore, the spectral weight loss extends up to a remarkably high energy of 300 meV at $(0.36\pi,0)$. However, the slight gain of spectral weight from $(0.73\pi,0)$ to $(\pi,0)$ remains concentrated at the low binding energy portion.

Fig. 7.2 plots the frequency integrated spectral weight difference above and below T_c as a function of $\mathbf{k}$. The quantity, A_{sc}-A_{normal}, where A is the $\mathbf{k}$ resolved single particle spectral weight, when normalized to the normal state value A_{normal}, gives the difference of the occupation probabilities in the two states, $\frac{n_{\mathbf{k}}(s)-n_{\mathbf{k}}}{n_{\mathbf{k}}}$ [here $n_{\mathbf{k}}$ and $n_{\mathbf{k}}(s)$

represent the occupation probabilities of the normal and superconducting states, respectively]. The data make clear that spectral weight is transferred from one $\mathbf{k}$ to another $\mathbf{k}'$. The gain in spectral weight for one $\mathbf{k}$ and loss at another $\mathbf{k}'$ is consistent with the sum rule requiring that the $\mathbf{k}$-integrated spectral weight, which is proportional to the particle number, be conserved [7]. The detailed balance of $\mathbf{k}$-integrated spectral weight requires considerations of other factors, such as photoionization cross section and phase space volume. It appears that the spectral weight is transferred by a $\mathbf{Q}\sim(0.45\pi, 0)$ for the following reasons. Among the high symmetry directions we have investigated - (0,0) to $(\pi, 0)$, $(\pi, 0)$ to (π, π), and $(0, 0)$ to (π, π) (Fig. 7.2, inset) - the $\mathbf{k}$-dependent spectral weight transfer is strongest along the (0,0) to $(\pi, 0)$ direction. Along (0,0) to (π, π), $\frac{A_{sc}-A_{normal}}{A_{normal}}$ gives a negative minimum near $(0.4\pi, 0)$ and smaller positive values from $(0.7\pi, 0)$ to $(\pi, 0)$. Considering that the spectral weight should be conserved within the first Brillouin zone, the most reasonable $|\mathbf{Q}|$ should connect the minimum at $(0.4\pi, 0)$ to the middle of $(0.7\pi, 0)$ and $(\pi, 0)$, yielding a value of $\frac{0.7\pi+\pi}{2} - 0.4\pi = 0.45\pi$. Within this scheme, the uncertainty in $|\mathbf{Q}|$ stems more from the maximum $\frac{A_{sc}-A_{normal}}{A_{normal}}$, as it is very broad. Indeed, the small amount of the spectral weight gain is close to to the experimental uncertainty. Despite these uncertainties of finer details, the general feature of the $\mathbf{k}$-dependent spectral weight transfer as a function of temperature is apparent in the raw data (Fig. 7.1). This finding deviates strongly from the BCS paradigm.

According to the BCS theory for non-mediated superconductors [1, 8] (Fig. 7.3), for electrons in the Fermi sea, only a small shell of excitations up to the characteristic phonon energy $h\nu_{phonon}$ away from the Fermi energy is possible (h is Planck's constant, ν is the phonon frequency). For two electrons with momenta $\mathbf{k}_1$ and $\mathbf{k}_2$, an exchange of a virtual phonon will yield electrons with momenta $\mathbf{k}'_1$ and $\mathbf{k}'_2$. The total momentum, $\mathbf{k}_1+\mathbf{k}_2 = \mathbf{k}'_1+\mathbf{k}'_2 = \mathbf{K}$ is conserved, requiring only that the shaded phase space region in Fig. 7.3B is available for this interaction. Because the typical value of $\frac{h\nu_{phonon}}{E_f}$ is about 10^{-2} to 10^{-3}, the phase space spanned by $\Delta\mathbf{k}$ is small, except when $\mathbf{K} = 0$. Thus, the pairing interaction in a superconducting condensate is dominated by electrons with opposite momentum, $\mathbf{k}_1 = -\mathbf{k}_2$. In a similar fashion, only the electron excitations within a shell of Δ will be modified. Depending on the electron-phonon

coupling constant, Δ can be even smaller than $h\nu_{phonon}$. In a single particle function measured by ARPES, one should only see an upward shift of the electron energy from its normal state value $\epsilon_{\mathbf{k}}$ to $\sqrt{\epsilon_{\mathbf{k}}^2 + \Delta^2}$. This energy renormalization is significant only when $\epsilon_{\mathbf{k}}$ is smaller and comparable to Δ $\sim 2kT_c$ (Fig. 7.3A). The shaded area in Fig. 7.3C depicts the change in occupation probability from that in the normal state ($n_{\mathbf{k}}$) to that in the superconducting state ($n_{\mathbf{k}}(s)$). In the superconducting state, the occupation probability is modified according to the superconducting coherence factor

$$\nu_{\mathbf{k}} = \frac{1}{2}\sqrt{1 - \frac{\epsilon_{\mathbf{k}}}{\sqrt{\epsilon_{\mathbf{k}}^2 + \Delta^2}}} \tag{7.1}$$

which stems from the quasiparticle in the superconducting state being a mixture of an electron and a hole. This factor should always be smaller than 1 for occupied states along (0,0) to $(\pi, 0)$.

The energy scale of 300 meV, or $40kT_c$, is much higher than the expected BCS value of $2kT_c$. In the strong coupling BCS-Eliashberg theory [1], one may see very week temperature-dependent changes due to phonons whose energies are higher than Δ. Although changes up to very high energies have been observed in cuprates by other techniques, they are evidently related to the dispersion (Fig. 7.1), ruling out the phonons as a possible explanation. Because the change extends up the entire dispersion of the bandwidth$\sim E_f$, which is regulated by the exchange coupling constant [9, 10], there is no hierarchy of energy scales in the system. Instead of having only a small energy window Δ out of E_f being available for pairing interactions, the whole bandwidth of scale E_f is available (Fig. 7.3D,E). This expanded window would probably mean that, instead of only the small fractions of electrons near E_f, all electrons are involved in the pairing interaction [11]. A corollary of the above observation would be that T_c may be limited by factors other than the strength of the pairing interaction. This idea is consistent with a growing indication that the superconducting transition may not be described by a mean-field theory like BCS [12], especially for the underdoped cuprate superconductors. Within the context of ARPES data, the lack of scaling of Δ with T_c [13] and the existence of the pseudogap in the normal state [14] are consistent with these views.

In addition to the high energy scale involved, perhaps more striking is the anomalous **k**-dependent spectral weight transfer above and below T_c. The occupation probability below T_c goes above the normal state value from $(0.7\pi, 0)$ to $(\pi, 0)$ (Fig. 7.3F), violating the BCS picture (Fig. 7.3C), requiring it to be smaller than the normal state value. This probability appears to come from the **k**-space region that is **Q** away. Furthermore, the result depicted in Fig. 7.3D implies that the anomalous excess spectral weight at **k**′ actually comes from much higher energy at another **k**, although the spectral weight at each **k** shifts toward higher energy as the sample is cooled below T_c. Given such a large value of $|\mathbf{Q}|$, the **k**-dependent spectral weight transfer is not caused by the mixing of states with momenta close to **k** and -**k**.

There are several possible non-BCS interpretations of the data. The observed **q** structure can be readily explained if the system has collective excitations, which have real space periodicities corresponding to **Q**, that are enhanced or developed at lower temperature. The question is the origin of these excitations, which is obviously not the Bi-O superstructure, which has a very different **q** value. An earlier observation indicated that the system has other collective excitations with $\mathbf{Q}' \sim (\pi, \pi)$ [3]. It is intriguing that **Q** and **Q**′ are close to the expected momenta of charge and spin ordering in the charge stripes that were first observed in the neutron scattering from $La_{1.48}Nd_{0.4}Sr_{0.12}CuO_4$ [15]. The stripe model envisages the doped holes segregating into domain walls (stripes) that separate antiferromagnetic regions with a phase slip of π across a domain wall (antiphase domains). The model requires the existence of a charge order peak at $\mathbf{q} = (\pm 2x, 0)2\pi$ or $(0, \pm 2x)2\pi$ and a spin ordered peak at $\mathbf{q}' = (\pi, \pi \pm x\pi)$ or $(\pi \pm x\pi, \pi)$ with x being the doping level. The neutron peak at **q**′ seen in $La_{1.48}Nd_{0.4}Sr_{0.12}CuO_4$ is of elastic nature, making the identification of the stripe correlation unambiguous. However, earlier neutron experiments from $La_{2-x}Sr_xCuO_4$ samples of lower doping have also identified inelastic peaks near the same **q**′ [16]. It has been argued that the inelastic peaks are caused by dynamic stripe correlations [15]. A recent doping dependent study of $La_{2-x}Sr_xCuO_4$ found that **q**′ stops deviating further from (π, π) when x is increased to near $\frac{1}{8}$ [17]. The presence of stripe correlation has also been predicted theoretically [18, 19]. Recently, it was found that the spacing between the (1,0) domain walls, which increases with doping

for $x < \frac{1}{8}$, saturates with x near $\frac{1}{8}$, and the situation becomes more complicated for $x > \frac{1}{8}$ [20]. Taking the nominal number of $\delta \sim 0.18$ near optimal doping [21], we use the saturated value of $x = \frac{1}{8}$ and $\mathbf{q}$= $(\pm 0.5\pi, 0)$ or $(0, \pm 0.5\pi)$ and $\mathbf{q}'$=$(\pi, \pi \pm 0.12\pi)$ or $(\pi \pm 0.12\pi, \pi)$. These momenta are intriguingly close to the observed $\mathbf{Q}\sim$ $(0.45\pi, 0)$ and $\mathbf{Q}'\sim$ (π, π).

Within the context of the above stripe interpretation, our data have important implications. First, the effect is observed in a sample with a very high T_c, unlike $La_{1.48}Nd_{0.4}Sr_{0.12}CuO_4$ case, where T_c is strongly suppressed [15]. Therefore, the stripe correlations coexist with high T_c superconductivity. The stripe correlations are short lived, as reflected in the broadness of the $\mathbf{q}$ structure. Further, because the spectral weight transferred by $\mathbf{Q}$ comes from high to low energies (Fig. 7.1), the scattering process is energy-dependent, again suggesting the dynamic nature of the stripes. This picture is consistent with a theoretical model proposed by Emery, Kivelson, and Zachar connecting the presence of fluctuating stripes and high-T_c superconductivity [11]. Second, the data provide complementary information about the stripe correlation. To date, the most important experimental evidence for stripes correlation stems from neutron scattering experiments, which are most sensitive to spin order. The information about the charge order stems indirectly from the nuclear superlattice peaks seen in neutron scattering [15], X-ray scattering [22], and extended X-ray absorption fine structure experiments [23]. The photoemission data provide more direct information for the valence-charge distribution. Further, the observed change up to 300 meV, which is an energy scale controlled by J [9, 10], suggests that the stripe phenomenon is related to the strong antiferromagnetic interactions. This result is consistent with several theoretical studies using many body models [11, 18, 19, 20]. Third, the stripe interpretation implies that the spectral weight transfer between data recorded at 20K and those recorded at 100K may not be a direct product of superconductivity. The spectral change above and below T_c may merely facilitate the identification of the stripe correlations that are gradually enhanced at lower temperatures. Having identified the stripes, ARPES may be used to study the issue of whether the stripes facilitate or compete with superconductivity.

The above interpretation is the most plausible explanation of our data, but more

experiments are needed to further check this interpretation. The most obvious check will be the results from underdoped samples, but this will be a challenging experiment because the surfaces of underdoped samples are very reactive, making it hard to get reliable temperature-dependent data with sufficient statistics to see subtle effects in Fig. 7.1, even in extremely good vacuum. Finally, we need to test our data against other theoretical models. For example, the change at $(0.36\pi, 0)$ and $(0.55\pi, 0)$ may alternatively be interpreted as a shift of the broad feature, as discussed for boson pairs [24].

The possible presence of stripes may shed light on the long-standing problem regarding the photoemission lineshape [25]. Given the stunningly sharp peak seen below T_c, the extremely broad feature in the normal state reflects a completely incoherent motion. The anomalously strong scattering may be directly related to the material's propensity to have a microscopically inhomogeneous charge distribution because they are manifestations of the same underlying interactions. This propensity of inhomogeneity is also in concert with the spectral lineshape in the superconducting state. Below T_c, the spectra may be broken into two parts, representing the two corresponding electronic components. The first is the sharp peak that represents the superfluid density [26]; the second is a higher energy portion of the spectra that is as broad as those of the normal state. Both components appear to be important for superconductivity because T_c scales with the first in the underdoped regime [13] and the pairing strength correlates with the second in the overdoped regime [3, 27]. Within the context of a recent theory [11], the first component arises from the carriers of the hole rich region, and the second arises from those in the hole poor region. This assignment is consistent with the first component scaling with doping and the second component being similar to spectra from an antiferromagnetic insulator [28] and providing pairing interactions that peak near (π, π) [3]. The growth of the first component at the expense of the low energy portion of the second component (Fig. 7.1) suggests that electrons change their allegiance to the two components dynamically. The coexistence of stripes and and superconductivity helps to visualize the two component picture. However, the phenomenology itself does not require the electronic components to form regular arrays. Thus, the next experimental challenge will be to

investigate whether stripes are merely windows that reveal the secret of the underlying interactions or are the intermediate steps leading to the high T_c. Independent of its outcome, the physical picture that has emerged here calls for a far reaching revision of our idea of metals and superconductors.

7.2 References

1. J.R. Schrieffer, *The Theory of Superconductivity* (Addison-Wesley, New York, 1988)

2. J. Bardeen, L.N. Cooper, and J.R. Schrieffer, *Phys. Rev.* **106**, 162 (1957); *ibid.* **108**, 1175 (1957)

3. Z.-X. Shen and J.R. Schrieffer, *Phys. Rev. Lett.* **78**, 1771 (1997)

4. At this photon energy,, the data approximate the momentum resolved single particle spectral weight function $A(\mathbf{k},\omega)$. Our high quality single crystals were grown by the traveling-floating-zone method. Some of these crystals were used as reference samples for systematic doping studies using Fe, Zn, and Ni [G.D. Gu *et al.*, *J. Crystal Growth* **130**, 325 (1993); *ibid.* **137**, 472 (1994); D.-S. Jeon *et al.*, *Physica C* **253**, 102 (1995)]. The data presented here were obtained from a sample with T_c = 88K, near optimal in the $Bi_2Sr_2CaCu_2O_{8+\delta}$ system. The results were reproduced in three samples from the same growth batch by Gu and colleagues. The spectra from these samples show a systematic set of subtle but important differences from other samples that we have used before [D.B. Mitzi *et al.*, *Phys. Rev. B* **41**, 6564 (1990)].

5. D.S. Dessau *et al.*, *Phys. Rev. Lett.* **71**, 2781 (1993)

6. D.S. Dessau *et al.*, *Phys. Rev. Lett.* **66**, 2160 (1991); Y. Hwu *et al.*, *Phys. Rev. Lett.* **67**, 2573 (1991); M. Norman *et al.*, *Phys. Rev. Lett.* **79**, 3506 (1997)

7. M. Randeria *et al.*, *Phys. Rev. Lett.* **74**, 4951 (1995)

8. H. Ibach and H. Luth, *Solid State Physics* (Springer, New York, 1995)

9. For an overview, see R.B. Laughlin, *J. Phys. Chem. Solids* **56**, 1627 (1995); A. Moreo *et al.*, *ibid.*, 1645; R. Preuss *et al.*, *ibid.*, 1659; Y. Otta *et al.*, *ibid.*, 1741

10. R.B. Laughlin, *Phys. Rev. Lett.* **79**, 1726 (1997)

11. V.J. Emery, S.A. Kivelson, and O. Zachar, *Phys. Rev. B* **56**, 6120 (1997); *Physica C* **282-287**, 174 (1997)

12. B.G. Levi, *Phys. Today* **49**, no.6, 17 (1996)

13. J.M. Harris *et al.*, *Phys. Rev. B* **54**, R15665 (1996)

14. D.S. Marshall *et al.*, *Phys. Rev. Lett.* **76**, 4841 (1996); A.G. Loeser *et al.*, *Science* **273**, 325 (1996); H. Ding *et al.*, *Nature* **382**, 51 (1996)

15. J.M. Tranquada *et al.*, *Nature* **375**, 561 (1995)

16. S.W. Cheong *et al.*, *Phys. Rev. Lett.* **67**, 1791 (1991); T.E. Mason *et al.*, *ibid.* **68**, 1414 (1992); T.R. Thurston *et al.*, *Phys. Rev. B* **46**, 9128 (1992)

17. K. Yamada, private communication

18. H.J. Schultz, *J. Phys. (Paris)*, **50**, 2833 (1989)

19. D. Poilblanc and T.M. Rice, *Phys. Rev. B* **39**, 9749 (1989); J. Zaanen and O. Gunnarson, *ibid.* **40**, 7391 (1989); S.A. Kivelson and V.J. Emery, *Physica C* **235-240**, 189 (1994)

20. S.R. White and D.J. Scalapino, cond/mat9801274

21. W.A. Groen, D.M. de Leeuw, and L.F. Feiner, *Physica C* **165**, 55 (1990)

22. M.V. Zimmermann, private communication

23. A. Bianconi *et al.*, *Phys. Rev. Lett.* **76**, 3412 (1996)

24. X.-G. Wen and P.A. Lee, cond/mat9709108

25. G.A. Sawatzky, *Nature* **382**, 480 (1989); P.W. Anderson *Phys. Rev. Lett.* **67**, 2569 (1991)

26. Although ARPES only measure the single particle spectral function, this connection is empirically justified because its strength correlated with T_c [27] and T_c scales with superfluid density [29] in the underdoped regime.

27. P.J. White *et al.*, *Phys. Rev. B* **54**, R15669 (1996)

28. B.O. Wells *et al.*, *Phys. Rev. Lett.* **74**, 964 (1995)

29. Y.J. Uemura in *Proceedings of the CCAST Symposium on High-T_c Superconductivity and C_{60} Family*, Beijing, 1994; S. Feng and H.C. Ren, Eds. (Gordon and Breach, New York, 1995), pp 113-142

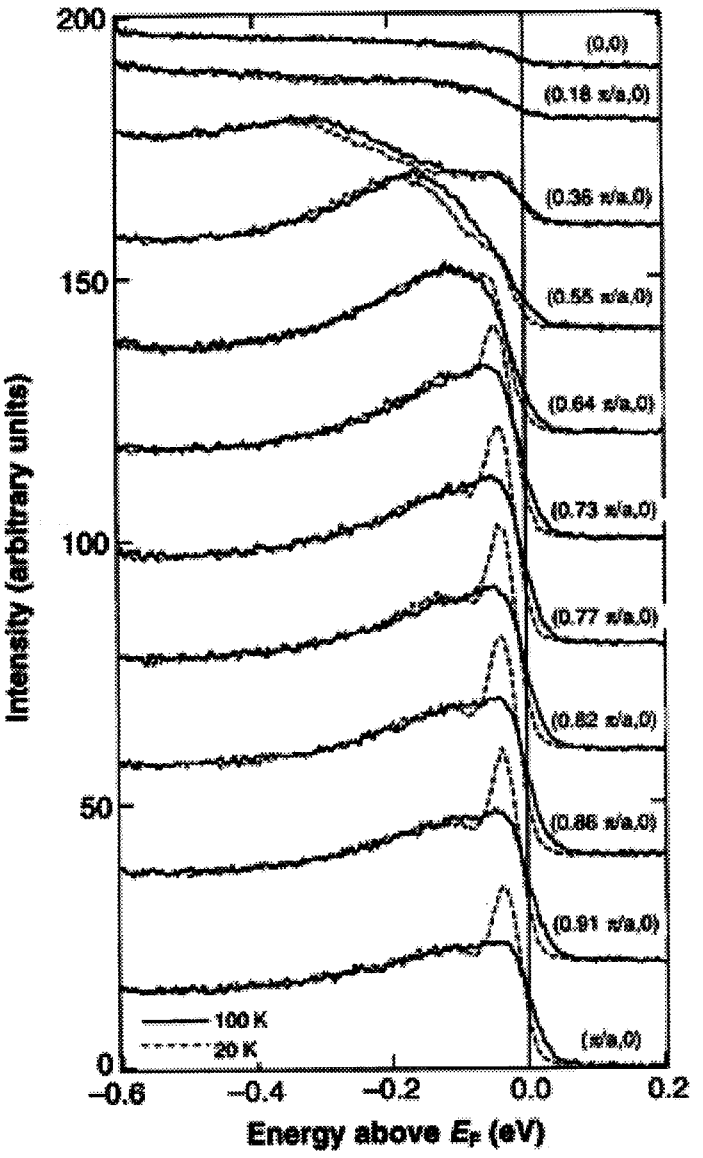

Figure 7.1: Angle-resolved photoemission data along (0,0) to $(\pi, 0)$ from a Bi2212 single crystal with $T_c = 88K$. The solid line gives data at 100K, and the dashed line gives data at 20K. The momenta are expressed in units of $\frac{1}{a}$, with a being the lattice constant.

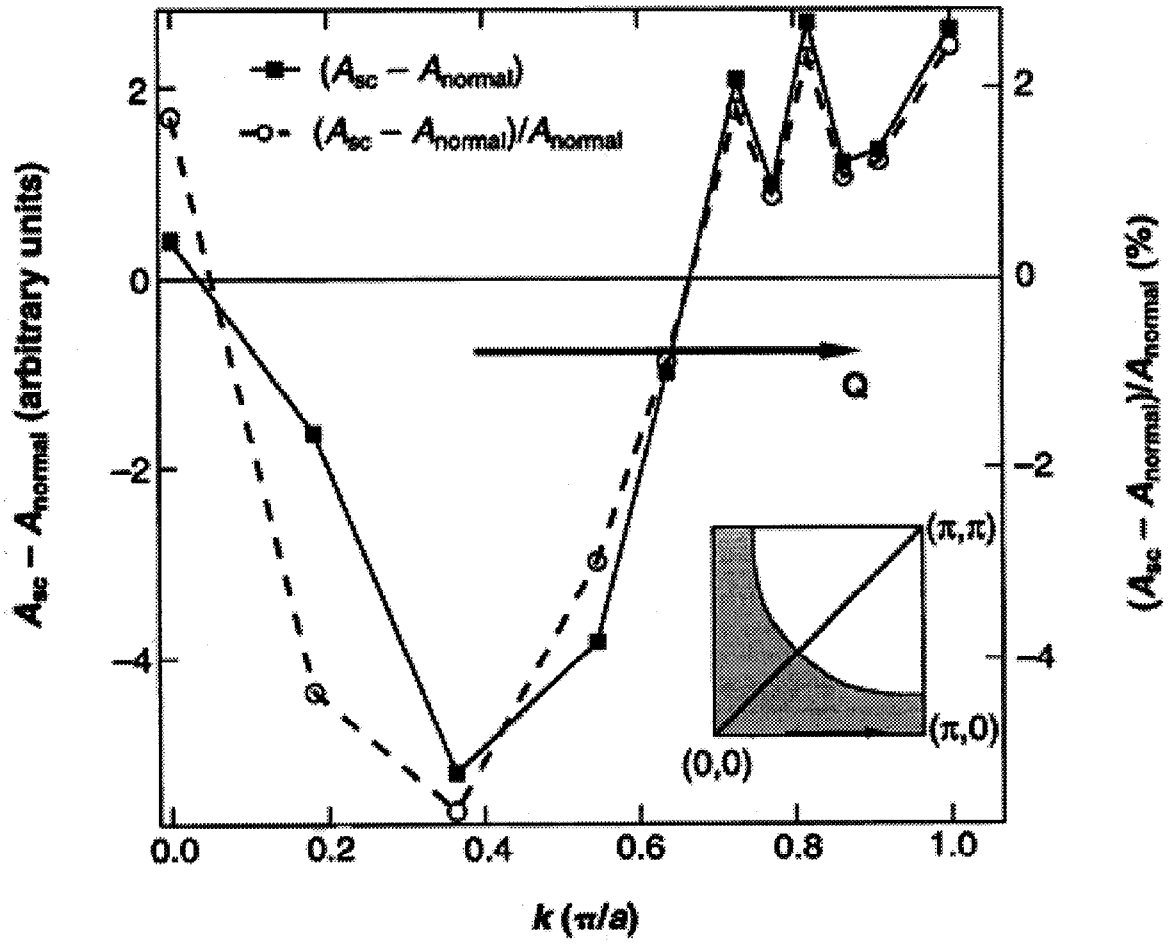

Figure 7.2: Momentum dependent spectral weight change along (0,0) to (π, π). The data show that the spectral intensity is transferred from one momentum to another, with a transferring vector **Q** broadly peaked between 0.4π and 0.5π. (Inset) The expected Fermi surface. The shaded area depicts the occupied states.

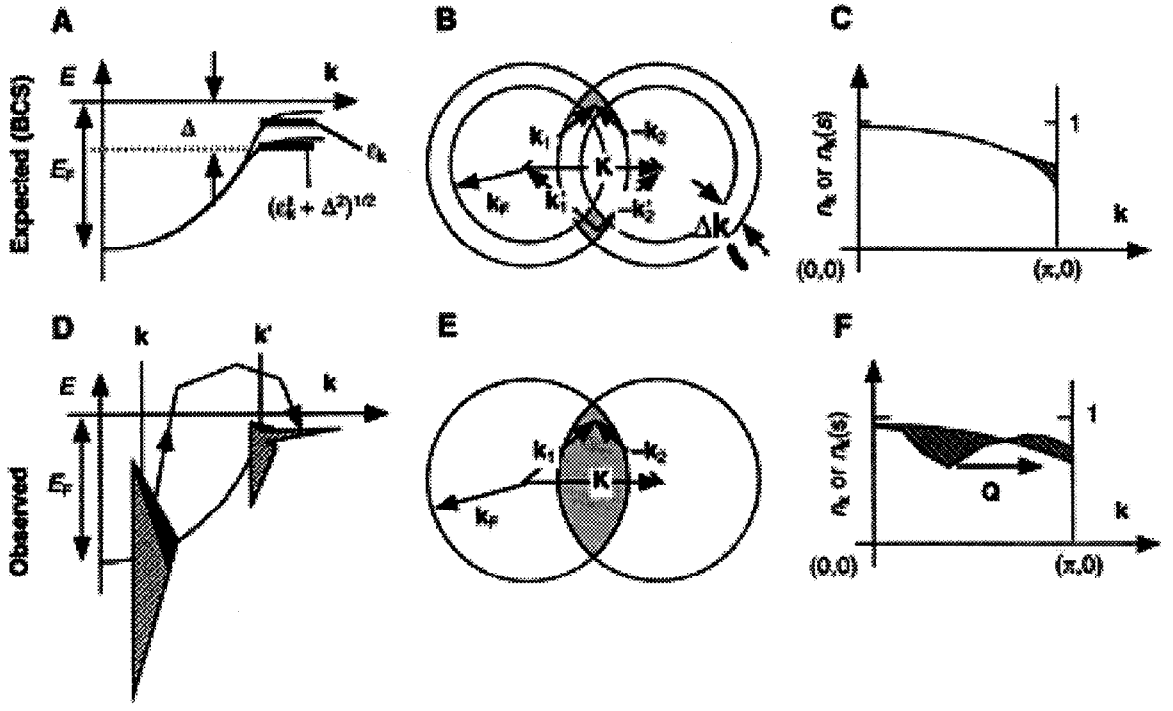

Figure 7.3: Schematic comparison between (a through c) BCS theory and (D through F) the observed result. (**A**) Quasiparticle band diagram and expected energy position at $\epsilon_{\mathbf{k}}$ and $\sqrt{\epsilon_{\mathbf{k}}^2 + \Delta^2}$ above and below T_c, respectively. (**B**) Allowed phase space (shaded area) for pairing interaction of electrons $\mathbf{k}_1$ and $\mathbf{k}_2$. (**C**) Occupation probability. The shaded area is the reduction below T_c. (**D**) Spectral weight transfer from $\mathbf{k}$ at higher energy to various $\mathbf{k}'$ at lower energy, in contrast to (A). (**E**) The relaxed phase space constraint (shaded area). (**F**) Measured occupation probabilities, which is the frequency integrated spectral weight. The shaded area is the difference above and below T_c.

Chapter 8

Photoemission Studies on Zn-BSCCO

8.1 Introduction

Impurity doping has been a very effective tool to probe the properties of cuprate superconductors. In particular, Zn substitution of Cu in the CuO_2 planes is known to suppress T_c [1] - [6]. An extensive amount of experiments has been conducted to understand the effect of Zn doping, including specific heat, microwave, NMR, μSR, optical, neutron, and tunnelling experiments [7] - [20]. Transport and microwave experiments indicate that Zn is a very strong scatterer, resulting in a strong increase in the residual resistivity in the plane [3] [4] [12]. A similar conclusion was drawn from μSR experiments, which also found that Zn suppresses the superfluid density [15]. Specific heat, transport, and optical experiments indicate that Zn doping alters the residual density of states and affects the low energy charge dynamics [10] - [13] [21]. NMR and neutron experiments generally show that Zn introduces low lying excitations in the spin channel [16] - [19] and dramatically affects the dynamical spin fluctuations. In particular, the NMR experiments show that Zn induces local magnetic moments in the normal state that do not otherwise show local moment behavior.

More recently, Zn doping was also found to enhance the T_c suppression and other anomalies near $\frac{1}{8}$ doping in $La_{2-x}Sr_xCuO_4$ (LSCO), $YBa_2Cu_3O_7$ (YBCO), and Y

doped $Bi_2Sr_2CaCu_2O_{8+\delta}$ (Bi2212) [22]. This latter result has been speculated to be due to the charge stripe instability [22], similar to a possible interpretation of neutron data from LSCO. In addition, a neutron scattering experiment has shown two aspects of Zn doping. First, it found that Zn shortened the correlation length of the static spin density wave [20]. Second, it found that the Zn shifted the spectral weight to lower energy, a fact consistent with the idea that Zn serves to stabilize a short range order incommensurate spin density wave state which might otherwise be purely dynamic [16] [20].

This issue of microscopic phase separation is of current interest. Based on incommensurate neutron scattering data from LSCO (recently also observed in YBCO [23]), it has been proposed that the cuprates develop stripes at low temperature in certain doping regimes [19] [20]. Here the stripes refer to microscopically phase separated insulating and metallic regions forming spin and charge ordered one-dimensional structures [24] - [30]. While the interpretation of neutron data is plausible, the experimental evidence for charge ordering remains elusive at present. Except for the case of Nd doped LSCO, no evidence of charge ordering has been detected. Zn doped Bi2212 may be a good system for an angle resolved photoelectron spectroscopy (ARPES) investigation of this issue. First, Zn doping is found to enhance the T_c suppression and other anomalies near $\frac{1}{8}$ doping in LSCO [22], YBCO [23], and Y doped Bi2212 [31]. The $\frac{1}{8}$ anomaly is thought to be associated with the stripe instability [19]. Second, from what we will show later, Zn impurities dramatically alter the electronic structure along the $(0,0)$ to (π,π) line. This data can be rationalized by the fact that Zn induces an antiferromagnetic region around it and enhances the local charge inhomogeneity.

By using ARPES, we will explore these aspects in detail. Over the last decade ARPES has played an important role in advancing our understanding of the low energy single particle excitations in these novel superconductors, starting with the observation of band like features [32]. Most notably, ARPES facilitated the observation of the d-wave superconducting gap structure as well as the normal state pseudogap [33] [34] [35] [36]. Several groups have attempted to study the impurity doping effects of the electronic structure using ARPES. Quitmann *et al.* [37] have performed

room temperature ARPES of Ni and Co doped Bi2212 to address the changes of the electronic structure in the normal state but not the changes in the superconducting state. Our experiments on Bi2212 will address both the normal and superconducting states. Gu *et al.* [38] have attempted to study Zn and Co doped YBCO for which the superconducting property of the CuO_2 planes is complicated by the surface chain signal [39]; Bi2212 lacks the surface chain complication of YBCO.

8.2 Experimental

Single crystals of $Bi_2Sr_2Ca(Cu_{1-x}Zn_x)_2O_{8+\delta}$ (Zn doped Bi2212, x=0.006,0.01) were prepared using a traveling solvent floating zone method [40] [41]. These crystals were characterized according to T_c and the Zn concentration, which was determined by electron probe microanalysis (EPMA). The crystals were grown under the nominal condition to produce optimal doping, with T_c of the Zn doped samples ranging from 83K to 78K. The transition widths vary from 3-5K according to susceptibility measurements, indicating the high quality of these crystals. The single phase of the samples was verified by X-ray scattering. X-ray rocking curves indicate that the crystalline quality of the Zn doped Bi2212 is comparable to that of the pure Bi2212; the presence of stacking faults was checked by taking the rocking curves of the $(0,0,\ell)$ X-ray diffraction peaks and the results were comparable between pure Bi2212 and our Zn doped Bi2212 [40]. In addition, Laue back scattered X-ray diffraction was done for alignment purposes and no difference was detected between the standard and the Zn doped sample. In this paper, data from 3 samples of pure Bi2212 are presented with $T_c \approx 91$K, 89K and 88K. The former two reveal themselves to be typical samples of high quality, but the last one with a critical temperature of 88K exhibits behavior between the ones closer to optimal doping and the ones doped with Zn. Therefore, we conjectured that the 88K sample had some unknown impurities. Attempts were made to determine the stoichiometry more precisely via EPMA, but owing to the number of species in the compound and the low concentration of the impurity, this was difficult with conventional means. While this may seem strange to include, it is nevertheless presented to make a connection to our previously published results [42]

and to provide continuity of our work. This paper is also an homage to the previously neglected subtleties on our part associated with this kind of doping in Bi2212. Therefore, we elucidate our old results in light of our new findings.

Data in Figs. 8.1, 8.2, 8.3, 8.4, 8.5 were recorded with a Vacuum Science Workshop analyzer attached to beamline 5-3 of the Stanford Synchrotron Radiation Laboratory (SSRL). The total energy resolution was typically 35meV and the angular resolution was $\pm 1°$. The nominal chamber pressure during the measurement was 2-3x10^{-11} torr and the photon energy used was 22.4eV. At this photon energy an ARPES spectrum mimics the spectral function, A($\mathbf{k}$,ω) [43], weighted by the appropriate factors, such as matrix elements, the Fermi function, etc. The ARPES spectra in the remaining data were recorded with a Scienta analyzer attached to beamline 10 of the Advanced Light Source (ALS). The total energy resolution was typically 15meV and the angular resolution was $\pm 0.15°$ with the spectrometer operating in angle mode. The nominal chamber pressure was 6x10^{-11} torr and the photon energy used was 25eV. Spectra from SSRL were taken within 10-12 hours of cleaving so as to minimize aging effects as previously reported [33] [44]. Spectra from ALS were taken within a shorter time to compensate for additional aging caused by the higher photon flux. With the SSRL apparatus, we can only take selected $\mathbf{k}$ points in order to have spectra with low enough statistical noise to identify subtle changes in the lineshape. With the ALS apparatus we can take about 40 spectra at the same time with 0.15°-0.3° spacing. The flatness of the surfaces of the pure and Zn doped samples was verified by laser reflection patterns after the samples were cleaved *in situ*. Fermi levels were determined by a gold reference sample in electrical contact to the samples.

8.3 Electronic Structure Evolution

In this section we report detailed results of ARPES on the nature of the Zn doping effect on the electronic structure of the Zn doped Bi2212 system. We found significant changes in the electronic structure near the Fermi level with a small amount of Zn doping. Along the (0,0) to (π, π) direction, Zn doping essentially wipes out the otherwise well defined spectral peak [45] in samples with T_c as high as 83K. This

behavior contrasts strongly to the case where scattering impurities are located off the CuO_2 plane as well as to the case of an underdoped CuO_2 plane. Zn doping also causes systematic changes in data near $(\pi, 0)$, which is close to the anti-node region of the d-wave pairing state. Indeed, the superconducting gap is decreased as one would expect from pair breaking considerations. At the same time, the dip seems almost gone in Zn doped Bi2212. This suggests an interesting evolution of the $(\pi, 0)$ superconducting spectrum as the traditionally two distinct features (the broad incoherent peak and the sharp spectral peak) seem to evolve simultaneously with Zn doping.

8.3.1 Experimental Observation

Fig. 8.1 presents ARPES data at selected **k**-space points along (0,0) to (π, π) for pure, Zn doped, Dy doped and underdoped samples. Two sets of data from the pure and the Zn doped samples are shown to illustrate the reproducibility. These points were chosen for their proximity to the Fermi surface and were spaced sufficiently in momentum to reveal the behavior of the Fermi level crossing. For data from pure sample in Fig. 8.1a-b, we see a relatively sharp feature disperse across E_f in the expected way. As the peak gets closer to the Fermi level, it apparently narrows in width and, at some point, loses intensity until it ultimately vanishes. This observation is consistent with previous work [32] [34] [35] [36], and much of the peak width is attributable to angular and energy resolutions. This general behavior is qualitatively what one expects of a quasiparticle. For data from the Zn doped samples from Fig. 8.1c-d, the dramatic difference is readily apparent. The spectral peak is wiped out with no sharp feature seen at the expected crossing or before it [46]. (We note in Fig. 8.1d that the peak is not recovered upon cooling.) For comparison, Fig. 8.1e-f reproduces our results from two underdoped samples in similar **k**-space locations [34]. The underdoping in these samples (T_c near 65K for both) was achieved either by removing oxygen or by substituting 10% Ca by Dy. In both cases the feature along ΓY remains fairly sharp; this contrasts strongly with data from the Zn doped samples in Fig. 8.1c-d. For the 10% Dy doped sample there is the additional effect of

scattering by Dy impurities, whose concentration is much higher than that of the Zn impurities. It is clear that the Zn impurities in the CuO_2 plane did far more damage to the quasiparticle peak than the more highly concentrated Dy impurities, which are located in the Ca plane sandwiched by the CuO_2 planes.

Fig. 8.2 shows the $(\pi, 0)$ spectra of the pure and the Zn doped samples and reproduces previously published results on overdoped and underdoped samples for comparison. Unlike the ΓY line as shown in Fig. 8.1, the normal state spectra of the pure and Zn doped samples are similar in this region of **k**-space. Both samples show very sharp peaks in the superconducting state. The fact that one can see such a sharp peak below T_c in Zn doped samples gave us confidence on the intrinsic nature of the very broad feature in Fig. 8.1c-d. It is possible that a disordered surface can produce the effect seen in Fig. 8.1c-d, however the coexistence of a disordered surface and the sharp feature seen in the data at $(\pi, 0)$ is unlikely.

There are several subtle but important differences between the $(\pi, 0)$ superconducting spectra for the pure and Zn doped samples. Readily apparent is the fact that there is virtually no dip at the higher binding energy side of the sharp peak in the Zn doped samples, whereas the dip is clearly visible in the pure sample as found before [47] [48]. The superconducting quasiparticle peak is also broader in the Zn doped sample, implying a stronger scattering rate. In the Zn free sample, the peak width is resolution limited. While the spectral weight of the Zn free sample is balanced above and below T_c, the spectral weight of the Zn doped sample is increased at lower temperature because of the sharp peak's development. Two changes in the spectra contribute to this imbalance: the dip no longer exists and the peak is significantly broadened, even though it has the same relative maximum. The sum rule of $A(\mathbf{k}, \omega)$ requires spectral weight to come from other locations in energy and/or momentum space. We will address this point later.

Another significant observation in Fig. 8.2a is that the sharp peak in the Zn doped sample shifts to lower binding energy as compared to that of the Zn free sample. This can be interpreted as the size of the superconducting gap being suppressed in the Zn doped sample. In the literature, the size of the energy gap in photoemission is often characterized by the position of the leading edge midpoint in the spectra recorded

at the underlying Fermi surface [33] [34] [35] [36]. In this case, because the peak is appreciably broadened in the Zn doped sample, the leading edge analysis is not ideal. We use the quasiparticle peak position as a way to characterize the gap. Here, we use the $(\pi, 0)$ peak even though it is not exactly at the Fermi crossing. However, since the band dispersion is very flat in this region, we can use it to track the relative change in the gap size.

The relative changes of the peak in Fig. 8.2a suggest the superconducting gap is suppressed in the Zn doped samples. Note the difference in the rate of Δ suppression and T_c suppression as a function of Zn doping. It is clear that the gap is severely suppressed in the Zn doped samples, given the modest T_c decrease at this doping level. This was consistent with an earlier conclusion that T_c and gap are not directly related energy scales [24]. A possible scenario is that T_c is not limited by pairing strength but by phase fluctuation effects [49] [50] [51]. It is also worth noting that the normal state spectrum at $(\pi, 0)$ of the Zn doped sample is cut off by the Fermi function, ruling out the existence of the normal state pseudogap. This is not the case for Zn free Bi2212 in Fig. 8.2a. This finding can be interpreted as Zn doping suppressing the pseudogap or creating low lying excitations inside the gap as reported by other experiments [17] [18].

Summarizing data from Figs. 8.1 and 8.2, we observed correlated changes of the electronic structure as a function of Zn doping: the strong suppression of the quasiparticle along the ΓY line; the suppression of the superconducting gap; the broadening of the superconducting peak and the suppression of the dip near $(\pi, 0)$.

8.3.2 Discussion of Electronic Structure Evolution Results

The experimental data presented raise several interesting points about impurity doping in the cuprates. The first and foremost has to do with whether the conduction mechanism can be described by quasiparticle dynamics. The dramatic differences in the ARPES data of Fig. 8.1c-d with a small amount of Zn doping is unexpected from the doping dependence studies of other materials. Photoemission is a signal averaging experiment and is usually quite insensitive to a small amount of doping change,

unlike the case here. In transition metal oxides one usually sees only subtle changes with doping variation up to 10-20% [52]. In ordinary metals like Cu or Al the spectra do not change with a very small amount of impurities. This is not the case for Zn doping; the spectra change dramatically. The fact that the change in the Zn spectra in the normal state was consistent with the change in the superconducting state gave us confidence on the intrinsic nature of this effect (again we note that the very sharp peak below T_c at $(\pi, 0)$ shows it was not due to a contaminated surface). The magnitude of the change with a relatively small amount of Zn suggests the system may be very close to a certain instability, and the effect of the Zn impurity is amplified by this intrinsic instability. In Zn free samples the sharp, dispersive feature along the ΓY direction resembles what one would expect from quasiparticles with well defined $\mathbf{k}$, although the feature is still too broad for this description. On the other hand, Zn doped Bi2212 showed that there is no quasiparticle with well defined $\mathbf{k}$ at all in this direction. Given the modest change of T_c, the change seen in Fig. 8.1c-d is quite remarkable. It suggests that normal state quasiparticles with well defined momenta are not essential for superconductivity. The observed change of the low energy electronic structure in Fig. 8.1c-d is consistent with reports from other experiments. NMR, specific heat, microwave, optics, and transport experiments indicate that Zn doping alters the residual density of states [10] - [13] [21] and affects the low energy and spin dynamics [15] - [19]. The $\mathbf{k}$-resolved information from ARPES is new.

To emphasize the peculiar effect of only a tiny amount of Zn (0.6%, average concentration), we wish to examine what one would expect from simple considerations. Naively, one would think that Zn doping causes scattering in the CuO_2 plane, and this would cause an angular averaging effect; this is similar to the scattering of an incident electron with wavenumber $\mathbf{k}$ by an impurity and mixing with the scattered spherical wave, which is made of a range of $\mathbf{k}$. To mimic this process we averaged the spectra from the six angles in Fig. 8.1a and still obtained a reasonably sharp peak (uppermost curve of Fig. 8.1a). As parallel cuts are similar in the nearby regions, inclusion of these cuts in the averaging process would give a similar effect to what we have done here. The averaged data still had a sharper structure than those in Fig. 8.1c-d. Considering the Zn doping is only 0.6%, the scattering effect would be much less than

the averaging process as we have done here even if Zn acts as a scatterer. Therefore, the notion of Zn being a simple scatterer seems insufficient to explain the effect seen in Fig. 8.1c-d. An alternate hypothesis is required. It may be that the Zn impurities induce some collective effects like the ones suggested by neutron experiments. One collective effect is that Zn impurities induce long range antiferromagnetic order that co-exists with the spin-Peierls transition seen in in $Cu_{1-x}Zn_xGeO_3$ [53] [54] [55].

Another is that the Zn impurities may pin the dynamical stripes [16] [19]. We will now explore whether this idea provides a self consistent explanation to our data. Specifically, we want to see whether the data are compatible with the idea that Zn impurities pin the dynamical stripes. There are two reasons for us to consider this possibility. The first has to do with transport experiments at $\frac{1}{8}$ doping [22]. It has been strongly suggested that the T_c suppression and other transport anomalies at $\frac{1}{8}$ doping are related to the stripe instability [19]. The work on Zn-Y doped Bi2212 is particularly relevant to our discussion here [31]. In Zn doped cases (2-3%), it is found that the electrical resistivity and thermoelectric power exhibit less metallic behavior than usual near a doping level of $\frac{1}{8}$. At the same time, T_c's for samples near a doping level of $\frac{1}{8}$ are also anomalously suppressed. These results suggest that the Zn doped Bi2212 system has certain similarity to the LSCO system where data are interpreted as possible evidence that Zn pins the dynamical stripes. The second reason concerns results from neutron experiments. Recent neutron scattering data from Zn doped LSCO indicate that Zn doping shifts the spectral weight of the incommensurate peaks at $(\pi, \pi \pm \delta\pi)$ to lower frequencies [16]. As the incommensurate peaks are interpreted as scattering from dynamical stripes [19], the downward shift of spectral weight has been interpreted as stablization of the dynamic stripes [16]. On the other hand, it is also found that Zn broadened the incommensurate neutron peak, which indicates that Zn doping disrupts the long range order and shortens the correlation length. Hence, it appears that a random distribution of Zn impurities shortens the long range correlation but stabilizes the short range correlation which would otherwise be more dynamic [19].

Now, we wish to draw upon the phenomenological similarities between the ARPES data for LSCO and Bi2212 along (0,0) to (π, π). Empirically, ARPES features along

(0,0) to (π,π) are always sharp, even in underdoped materials (Fig. 8.1e-f). This is also the case for YBCO and Bi2212 systems [39] [56] [57] [58] as well as the insulating $Sr_2CuO_2Cl_2$ and $Ca_2CuO_2Cl_2$ [59]. The only cuprate that violates this empirical rule is the LSCO system. The data from LSCO system show strong resemblances to that of the Zn doped system here [60]. In the LSCO case spectra along the (0,0) to (π,π) direction are found to be extremely broad, while one can still see well defined peaks near $(\pi,0)$ for highly doped cases - a fact that shows that the extremely broad feature along the (0,0) to (π,π) direction is not due to a bad surface. With the increase of Sr doping, the change of the spectra along (0,0) to (π,π) is not monotonic. For $x<0.05$, one sees a broad dispersive feature that behaves like the feature seen in the insulating $Sr_2CuO_2Cl_2$. For $0.05<x<0.15$, one hardly sees any dispersive feature at all. For $x>0.2$ one again sees a dispersive feature that shows a clear Fermi level crossing. Hence, the broadness of the feature along (0,0) to (π,π) is not simply due to the random disorder of the Sr impurities as the Sr content increases monotonically. There is another likely contribution to the broadness of the features, and the contribution might be connected to the intrinsic electronic inhomogeneity. Based on neutron experiments, the evidence for stripe correlation is strongest in the LSCO system and is most visible in the doping range near $\frac{1}{8}$ [19]. Given the similarity of the data from Zn doped Bi2212 and from LSCO, one may wonder whether the destruction of the spectral peak along (0,0) to (π,π) in the Zn samples is also related to the electronic inhomogeneity. This issue is also related to the recent transport measurement on Zn-Y doped Bi2212 [31].

Extensive numerical calculations using Hubbard or t-J models have been carried out on small cluster samples [61]. The systematics of the spectral lineshapes seen in Bi2212, YBCO, $Sr_2CuO_2Cl_2$, $Nd_{2-x}Ce_xCuO_4$, as well as the doping dependence, can very well be accounted for by these calculations. However, the spectral behavior of Zn doped Bi2212 and LSCO cannot be explained by these calculations even qualitatively. All calculations produce a sharp structure along (0,0) to (π,π), even when additional parameters such as t' and t'' are included [62]. On the other hand, an exact diagonalization of the spectral function shows that an introduction of attractive forces along the $(\pi,0)$ or $(0,\pi)$ directions strongly suppresses the quasiparticle-pole strength along

(0,0) to (π,π) direction [63]. These forces were introduced to simulate the effects of stripes on the electronic structure, although the origin of stripes is unclear. In another calculation on the t-J model, it is found that a Zn vacancy pins the domain wall, similar to the case where a Zn vacancy bounds a hole of $d_{x^2-y^2}$ symmetry [64]. Summarizing the above discussion, it appears that the scenario of electronic phase separation can provide a self consistent accounting of the data. However, the above interpretation is not unique, and the phase separated regions do not necessarily have 1D order.

Alternatively, the interpretation of the data may come from a more phenomenological viewpoint. Zn does have an effect on the electronic properties of the cuprates. One particular result is that Zn induces local moments on neighboring Cu sites [8] [65]. This glassy array of antiferromagnetic droplets will probably become more ordered as the temperature is lowered [66]. This will affect the electronic structure, and it is possible that the phenomena here are just manifestations of that fact. At the same time, quasiparticles at $(\frac{\pi}{2},\frac{\pi}{2})$ may suffer significant scattering, resulting in the washed out features we see here. The spectral lineshape changes at $(\pi,0)$ are not surprising as Zn has an effect on the superfluid density, n_s. According to Nachumi *et al.* [67], the Zn impurity acts as a dead center for n_s. This pocket of no superfluid extends over an area of $\pi\xi^2$, where ξ is the in-plane coherence length. This also says that the volume available for superconductivity is reduced, and this ought to be reflected as a decrease in n_s. Comparing the relative strength of the $(\pi,0)$ peak with and without Zn, it is hard to say that the data points towards this conclusion. Furthermore, one should compare samples with the same δ, and that has been a hard parameter to control in the growth of Bi2212. It should be noted that while we have included this for the sake of discussion, the role of Zn in forming local moments in underdoped cuprates is still an open issue [68].

The next issue concerns the spectral lineshape of the photoemission experiments. The systematic changes in ARPES data with Zn doping provide a new perspective on several long standing problems about the unusual photoemission lineshape observed in high T_c superconductors. These problems can best be illustrated by the spectral

lineshape change at $(\pi, 0)$ above and below T_c, as shown in Fig. 8.2. As the temperature is lowered below T_c, a sharp quasiparticle peak emerges at the low energy edge of the broad normal state feature accompanied by a dip structure at higher energy. In Zn doped Bi2212 the dip is gone, but the peak persists and even gains intensity as it is broadened but with roughly similar height. It is often assumed that the sharp peak develops below T_c because of an increase in quasiparticle lifetime, which is independently measured in other experiments [69] [70]. The traditional interpretation of the peak and dip structure is associated with the electronic pairing mechanism [72]. In this case, the peak is the superconducting quasiparticle at gap energy Δ (for the case when the normal state quasiparticle peak is at the Fermi level) and the dip is caused by the suppression of the spectral weight between the energy Δ and 3Δ as the electronic medium itself is gapped. More recently, a phenomenological self-energy was proposed to explain the peak and the dip in a very similar spirit [73]. In both of these cases, the dip and the peak go hand in hand because they are manifestations of the same self-energy change.

The data from Zn doped Bi2212 add to a list of puzzles associated with the above interpretation as Zn doping kills the dip without diminishing the intensity of the peak so that the peak and dip do not necessarily follow each other. The other puzzles are represented by the following examples. First, the expectation of spectral weight suppression between Δ and 3Δ is based on a very general argument compatible with any electronic pairing mechanism so that the dip will appear as long as the electronic excitation spectrum opens a gap. This expectation is in strong contrast to the fact that one does not see a dip structure in the pseudogap state of the underdoped samples where the electronic excitation spectrum opens a gap [35]. It is also very strange that the sharp peak emerges only below T_c in the underdoped samples although the spectrum is gapped well above T_c, as if the single particle spectral function is sensitive to the superconducting order. Further, the intensity of the sharp peak shows a monotonic correlation with doping and, thus, the superfluid density. These empirical observations are not compatible with the conventional wisdom that the single particle spectral function should not be sensitive to the superconducting condensate. In fact, we believe this puzzle is a very important clue and its understanding will lead to a

deeper insight into these materials. Second, the sharp peak and the broad feature at higher binding energy side of the dip seem to behave independently [74]. Fig. 8.2 shows the $(\pi, 0)$ spectra in the superconducting state with different doping. It is clear that the energy of the superconducting peak hardly changes, but the broad feature and the shape of the dip change significantly. Third, the photoemission spectra obtained in the normal state of the doped superconductor show a striking resemblance to that of the insulator, albeit the energy position of the broad feature near $(\pi, 0)$ evolves with different doping. Finally, we have to consider the fact that the peak and dip structures are not seen in YBCO. Despite the chain complication, we can still get the consistent result about the Fermi surface, the d-wave gap, and the sharp peak at X $(\pi, 0)$ in YBCO [39]. However, the dip structure is not seen even in measurements where the sample is cleaved and kept at 10K continuously. The above puzzles suggest that we may need to re-evaluate the problem in a very different way, as the conventional wisdom cannot explain the data.

8.4 Temperature Dependence

In this section we report the temperature induced ARPES spectral change in Zn doped Bi2212. As with the spectra themselves, the temperature induced change varies with doping. With the increase of Zn impurities in the samples, we see a strong temperature dependence in the data. Furthermore, the temperature induced spectral change extends to very high energy in Zn doped samples. Empirically, the temperature dependence of the overdoped metal is much weaker than that of the undoped insulator [75]. In the later case, the temperature dependence persists up to an energy scale of about an electron volt. Since the carrier density is not changed with Zn substitution of Cu, the enhanced temperature dependence is consistent with the idea that Zn creates antiferromagnetic regions around it which exhibit stronger temperature dependence.

If Zn enhances the tendency of microscopic phase separation, the next question is whether the phase separation takes the form of 1D stripes as transport experiments seem to suggest [31]. The key difficulty lies in the fact that the traditional tools

(*e.g.* X-ray or electron scattering) are sensitive to all electrons in the system, while the charge ordering, if present, occurs for electrons close to the Fermi level. This 'large background' signal from other electrons makes the detection of any charge density wave very difficult. Angle resolved photoemission may provide an opportunity to address this important and current issue as one can view ARPES as a kind of photoelectron diffraction experiment. Since the ARPES data near E_f probe only the last valence electron, it is naturally more sensitive to charge inhomogeneities as it discriminates against the background signal from other electrons. Further, the relatively low kinetic energy of these photoelectrons make them more sensitive to any charge density modulation than the high energy electrons and X-rays used in typical experiments. The complication, of course, is that these photoemitted valence electrons will be multiply scattered by other electrons (including the core electron) - a complex process itself is the source of information and, thus, cannot be avoided. This will reduce the sensitivity and increase the difficulty in the data analysis. Nonetheless, ARPES may still have higher sensitivity as it has the energy selectivity so one can probe specific orbitals.

Motivated by this consideration, we have made attempts to use ARPES to investigate the issue of charge stripes in cuprates. If charge stripes develop at low temperatures, as indirectly suggested by neutron scattering experiments, it may diffract the photoelectrons and cause a **k**-dependent change in integrated spectral weight, n(**k**). In an earlier report [42], we presented data that suggested a **q** dependent spectral weight shift, and we have attributed that to the stripe instability because the **Q** value so determined is quite close to what one expects from charge stripes. We have also observed the enhanced effect of the **q** dependent spectral weight shift in the Zn doped samples. This latter aspect of the data, however, exhibits strong scatter and cannot be made unambiguous. Therefore, we have also detailed the uncertainties associated with our interpretation of the **q** shift of the spectral weight and its connection with charge stripes. In this context, we have also discussed the claim that the spectral weight to be temperature independent [76]. We disagree with this premise and we show the prior data and claims of the same authors actually pointed to the contrary. We believe there are systematic changes of the spectra with temperature

which depend on the doping and impurity concentration in the sample. On the other hand, the connection between the temperature dependence in the ARPES data and the stripe picture is not as straightforward as we have suggested [42], largely due to experimental uncertainties such as sample aging. Despite this, our recent work on Bi2212 systems has found a straight Fermi surface segment that strongly resembles the Fermi surface of the stripe phase in $La_{1.28}Nd_{0.6}Sr_{0.12}CuO_4$ [77]. This suggests that the charge stripe feature does exist in Bi2212, although the stripes are weaker as one can see the presence of quasiparticle like features near the d-wave node line. The quasiparticle state is strongly suppressed in Nd-LSCO where static stripes exist.

8.4.1 Experimental Observation

Fig. 8.3 shows ARPES data from pure and Zn doped samples. Again, two sets of data from Zn doped samples (Fig. 8.3d-e) were presented to illustrate reproducibility. Samples in Fig. 8.3a-b are pure Bi2212 sample while sample in Fig. 8.3c behaves as if it contains impurities. The first qualitative observation is that the Zn doped samples show a stronger temperature dependence. This temperature dependence correlates with the change of the spectral lineshape, with the Zn doped samples having a larger steplike background relative to the broad peak. As the temperature is lowered, a sharp peak develops near $(0.8\pi, 0) - (\pi, 0)$, but without a dip structure (Fig. 8.2a). The temperature induced change persists to very high energy. This is more clearly visible in the spectral lineshape of the sample in Fig. 8.3d. When the peak moves away from E_f, the spectra for the two temperatures have different curvatures, with the 100K spectra being concave down and the 20K spectra being concave up. This behavior is beyond experimental uncertainties as we will discuss later. The enhanced temperature dependence with Zn doping is consistent with the empirical result that the temperature dependence of ARPES gets stronger as the magnetic correlations get stronger. In $Sr_2CuO_2Cl_2$ we see a much stronger temperature dependence on an energy scale of approximately 1eV [75]. $Sr_2CuO_2Cl_2$ is a Mott insulator with strong magnetic correlation. In addition, the charge ordered manganite, $Pr_{0.5}Sr_{0.5}MnO_3$ shows a temperature dependence of spectral weight up to 1.2eV [78]. To contrast,

overdoped Bi2201 (the one plane version of Bi2212) with weak magnetic correlation does not show much temperature dependence (see next paragraph). If Zn induces a local antiferromagnetic region around itself, it will presumably show a strong temperature dependence. This lends itself to the idea that Zn strengthens the tendency of microscopic phase separation.

We now move to the second aspect of the temperature dependence of the ARPES spectra from the Zn doped samples. While the spectral weight is gained near $(\pi, 0)$, it is reduced near $(0.3\pi, 0) - (0.5\pi, 0)$. At first glance, it appears there is a $\mathbf{q}$ dependent spectral weight shift [42]. The data from the two Zn doped samples are quite consistent with each other although they do differ in subtle ways. Judging from the sharpness of the feature, the sample in Fig. 8.3e is more overdoped than sample in Fig. 8.3d. As shown before, ARPES lineshapes are extremely sensitive to doping changes [35] [36]. To check whether the apparatus worked appropriately, we show in Fig. 8.4 ARPES data recorded at 20K and 100K for two Bi2201 samples taken under identical conditions as those of Bi2212 samples. As the temperature is lowered, the two sets of data match to within our error. In our experimental runs we checked the Bi2201 many times; the fact that they matched so well in all cases gave us confidence that the experimental apparatus worked properly. It is important to note that the calibration run using Bi2201 was not done across the superconducting transition so no significant lineshape change was involved and the situation was simpler.

While samples in Fig. 8.3a-b do not show any change in $n(\mathbf{k})$ with temperature, samples in Fig. 8.3c,d,e show subtle changes. Fig. 8.5 depicts the integrated spectral weight, $n(\mathbf{k}) = \int A(\omega,\mathbf{k})\, f(\omega)\, d\omega$ versus $|\mathbf{k}|$ for the samples in Fig. 8.3b,c,d. Note that the $n(\mathbf{k})$ curves have different shapes so the change cannot be simply corrected by a shift in $\mathbf{k}$ (or a tilt in angle) meaning the difference cannot be trivially attributed to angular irreproducibility with temperature. This point will be elaborated upon in detail later. Taken naively, it appears that the spectral weight is shifted from $\mathbf{k} \sim (0.3\pi, 0) - (0.5\pi, 0)$ to $(0.8\pi, 0) - (\pi, 0)$ region with a $|\mathbf{Q}|$ of about $0.4\pi - 0.5\pi$.

8.4.2 Discussion of Temperature Dependence Results

Because the **Q** value of $(0.4\pi, 0) \sim (0.5\pi, 0)$ is quite similar to what one expects from stripes, we attributed this **q** shift to the stripe instability [42]. We were further encouraged by the fact that the **q** shift is more pronounced in Zn doped samples because Zn doping presumably enhanced the $\frac{1}{8}$ anomaly. This is also consistent with the fact that the spectra along (0,0) to (π, π) direction of Zn doped samples look like that of LSCO where the evidence for stripes is the strongest [19] [22]. However, there are some important points to be addressed within that interpretation.

One important issue is whether this effect of a change in n(**k**) was due to angular misalignment on our part. It is emphatically stated that our results were reproducible and exhaustively studied. The following statements are included to emphasize resoundingly the veracity of the qualitative aspect of this observation if not the quantitative as well. For the sake of argument, it is conjectured that the variation in n(**k**) is due to some angular mismatch in going from above T_c to below T_c. To explore this possibility, we utilized an ARPES system with finer momentum (angular) resolving power than previously used. The difference is at least a factor of *seven* better than that for the typical ARPES system. The resulting data (taken in angle mode) is presented for a $Bi_2Sr_2Ca(Cu_{0.99}Zn_{0.01})_2O_{8+\delta}$ sample in Fig. 8.6. Data is presented for both an aged and a fresh sample. It is noted that no pair of hot and cold curves overlay each other, that is to say, assuming some kind of angular misalignment in cooling the apparatus, one would expect a given high temperature curve to have some match among the group of cooler curves. That is not the case. A realistic question would be if sample aging contributed to this effect. It is noted that the intentionally aged sample also has no pair of matching curves. Now, of course, thermal broadening must be taken into account as well as the fact that there is some amount of change due to the superconducting state *especially* near $(\pi, 0)$. However, the points chosen were not close to $(\pi, 0)$ and thermal broadening of this magnitude does not account for the differences seen. To investigate this even further, the spectral weight was integrated for both samples and plotted versus **k** in Fig. 8.7. The data from the fresh Zn sample reproduces the results of Fig. 8.3 and Fig. 8.5 and are consistent with our earlier results [42]. The reader can readily discern that in the very least, the shapes

of the n(**k**) do not match one another, either for the fresh or aged sample, no matter how they are translated in **k** (an action correcting for the supposed angular misalignment). Although the interpretation of the data may change in light of new findings or information, the experimental observation of this effect is without question.

An additional issue to be addressed concerns periodicity of the **Q** structure. A central premise in solid state physics is that periodicity seen in the first Brillouin zone at **q** should also be seen at **q**+**G** in the second Brillouin zone, where **G** is the usual reciprocal lattice vector. That is to say that the effect we found between $[0, \pi]$ should be realized between $[\pi, 2\pi]$ as well. This observation would confirm our estimate of $|\mathbf{Q}|$ and establish a true periodicity. However much this is desired, the experiment, nonetheless, dictates its impracticality. This would involve the sampling of more points, which would increase the likelihood of aging effects, which have been so detrimental to the experimental act. However, in an attempt to satisfy a probable and fair question on the part of the reader, we utilized our system at ALS with the higher photon flux and sampling density. Our results on a Zn doped sample are shown in Fig. 8.8 as an n(**k**) plot extending into the second Brillouin zone. What this plot shows is the suppressed spectral weight between $[\pi, 2\pi]$. This is most likely due to matrix element effects [43]. The error bars in the second zone comprise a larger percentage of the total as compared to the first zone. Taking a difference of these above and below T_c would be less informative than doing so in the first zone, and we are already pushing the experimental limitations of our apparatus. It is possible to revisit this question.

It has been recently been suggested that n(**k**) should be temperature *independent.* Further, all temperature induced changes are confined in the window of 3Δ with Δ being the superconducting gap [43]. Following that assumption, any temperature dependence ought to be attributable to experimental artifact. However, after careful consideration of some key results, we find the assertion of spectral weight conservation to be inconsistent. Fig. 8.9 reproduces data [43] published by the same authors cited in ref. 76 as a proof for the lack of temperature dependence [43]. In ref. 43, in distinct contrast to ref. 76, the same authors state that spectral weight *is* conserved for $\mathbf{k}=\mathbf{k}_f$ but *is not* conserved for $\mathbf{k}\neq\mathbf{k}_f$ (which is the region of relevance). After subtracting

out temperature dependent background, the same authors claimed a 10% change in spectral weight between T=13K and T=105K. While the reason for this inconsistency of claims by the same authors needs to be investigated, it is clear that the claim of spectral weight conservation has not been established contrary to ref. 76.

Some other points are in order concerning the issue of angular misalignment [76]. The n(**k**) curves (see Fig. 8.5 and Fig. 8.7) show shape changes with temperature that cannot be explained by a rigid angular shift, as discussed earlier. In other words, one cannot slide the two n(**k**) curves at different temperatures to match each other because they have different shapes, contrary to the example of ref. 76. As shown by the results of Fig. 8.4, the experimental setup works appropriately. The fact that the spectra at two temperatures match so well in the Bi2201 samples in all cases rule out the possibility of angle tilt of our sample manipulator as the temperature changed. Any possible angle shift can only stem from the mechanical flatness of the sample surface which is a random quantity. However, we have observed a strong correlation between the **q** shift and other electronic structure changes: the destruction of the normal state quasiparticle along the (π, π) direction, the suppression of the superconducting gap, the broadening of the superconducting peak, and the suppression of the superconducting dip near $(\pi, 0)$. While the surface flatness can introduce error, this random variable alone cannot explain the *systematic* changes observed.

To further test the issue of charge stripes in Bi2212, we need to find a better way to passivate the surface. Although Bi2212 has a very stable surface in comparison to most cuprate samples, it appears that it is not stable enough if one wants to detect very subtle effects on the scale of a few percent unless extreme care is taken with respect to vacuum quality. This is the main source of uncertainty of our previous result [42]. Rather than wrestle further with this uncertainty, perhaps an alternative methodology would serve. To test the idea of stripes, we need to study materials where the evidence for stripes from other experiments is unambiguous (this will establish what one should expect from stripes, although some theoretical ideas have already been proposed). This has been done recently in the stripe phase of $La_{1.28}Nd_{0.6}Sr_{0.12}CuO_4$ [79]. The effect is very strong so a modulation of n(**k**) with 0.5π periodicity is seen without the need to do the difference curve. More recently,

we have used an alternative approach to the problem by looking at the Fermi surface nesting feature which is strongly present in the stripe phase [79]. With a global mapping in n(**k**), we have found clear Fermi surface nesting features similar to those seen in the static charge order phase [77]. This does support the notion of the presence of stripes even in Bi2212 when one looks at the data with high frequency. However, the stripe instability is weaker in Bi2212 than in the LSCO system. In Bi2212, one can still see a quasiparticle like feature along (π, π) direction while this is totally absent in LSCO.

8.5 Summary

In conclusion, we recast the most important qualitative observation of our experiment - the destruction of the quasiparticle peak along ΓY with relatively small amounts of Zn impurities. Whatever the microscopic mechanism causing the change, be it simple impurity scattering or some random pinning of the phase separated domains, this observation is significant to the understanding of the relevance of quasiparticles in the normal state. Data in Fig. 8.1a,b,e,f may reasonably be interpreted within the context of the quasiparticle picture, a concept that is the foundation of the modern theory of solids and is extensively used to address the high T_c problem. Yet, one would be very hard pressed to call the data in Fig. 8.1c-d as reflecting quasiparticles, and superconductivity with T_c as high as 83K survived. Taken naively, the existence of conventional quasiparticles with well defined **k** does not seem to be necessary for the realization of high temperature superconductivity. We also have studied temperature dependence in the ARPES data from the $Bi_2Sr_2Ca(Cu_{1-x}Zn_x)_2O_{8+\delta}$ system. With Zn doping, we observed strong temperature dependence in the data which persists up to very high energy. This observation is consistent with the idea that Zn enhances the tendency of electronic inhomogeneity, a result consistent with NMR result [8].

We acknowledge S.A. Kellar, X.J. Zhou, and P. Bogdanov for technical help, and R.B. Laughlin, D. S. Dessau, A.J. Millis, M. Norman, B.O. Wells, S.A. Kivelson, A. Fujimori, D. J. Scalapino, H. Eisaki, N. Nagosa, and D. van der Marel for helpful discussions. ARPES experiments were performed at SSRL which is operated by the

DOE Office of Basic Energy Science, Division of Chemical Sciences. The Office's Division of Material Science provided support for this research.

8.6 References

1. A. Maeda *et al.*, *Phys. Rev. B* **41**, 4112 (1990)
2. G. Xiao *et al.*, *Phys. Rev. B* **42**, 8752 (1990)
3. T.R. Chien, Z.Z. Wang, and N.P. Ong, *Phys. Rev. Lett.* **67**, 2088 (1991)
4. Y. Fukuzumi *et al.*, *Phys. Rev. Lett.* **76**, 684 (1996)
5. R. Lal *et al.*, *Phys. Rev. B* **49**, 6382 (1994)
6. T. Kluge *et al.*, *Phys. Rev. B* **52**, R727 (1995)
7. H. Hancotte *et al.*, *Phys. Rev. B* **55**, R3410 (1997)
8. H. Alloul *et al.*, *Phys. Rev. Lett.* **67**, 3140 (1991)
9. K. Ishida *et al.*, *Physica C (Amsterdam)* **179**, 29 (1991)
10. J.W. Loram, *Physica C* **235-240**, 134 (1994)
11. J.L. Tallon *et al.*, *Phys. Rev. Lett.* **79**, 5294 (1997)
12. D.A. Bonn *et al.*, *Phys. Rev. B* **50**, 4051 (1994)
13. K. Mizuhashi *et al.*, *Phys. Rev. B* **52**, R3884 (1995)
14. S. Tajima, R. Hauff, and W.-J. Jang, *SPIE* **2696**, 24 (1996)
15. C. Bernhard *et al.*, *Phys. Rev. Lett.* **77**, 2304 (1996)
16. H. Hirota *et al.*, *Physica B* **241-243**, 817 (1997)
17. K. Kakurai *et al.*, *Phys. Rev. B* **48**, 3485 (1993)
18. Y. Sidis *et al.*, *Phys. Rev. B* **53**, 6811 (1996)
19. J.M. Tranquada, cond-matt/9709325; J.M. Tranquada *et al.*, *Nature* **375**, 561 (1995)

20. K. Yamada *et al.*, *Phys. Rev. B* **57**, 6165 (1998); T. Suzuki *et al.*, *Phys. Rev. B* **57**, R3229 (1998); H. Kimura *et al.*, preprint

21. N.L. Wang *et al.*, *Phys. Rev. B* **57**, R11081 (1998)

22. Y. Koike *et al.*, *Solid State Communication* **82**, 889 (1992); Y. Koike *et al.*, *Physica C* **282-287**, 1233 (1997); Y. Koike *et al.*, *Journal of Low Temp. Phys.* **105**, 317 (1996); M. Akoshima *et al.*, *Phys. Rev. B* **57**, 7491 (1998)

23. P. Dai, H.A. Mook, and F. Dogan, *Phys. Rev. Lett.* **80**, 1738 (1998); H.A. Mook *et al.*, *Phys. Rev. Lett.* **77**, 370 (1996)

24. V.J. Emery, S.A. Kivelson, O. Zachar, *Phys. Rev. B* **56**, 6120 (1997)

25. G. Siebold *et al.*, *Phys. Rev. B* **58**, 13506 (1998)

26. J. Zaanen and O. Gunnarson, *Phys. Rev. B* **40**, 7391 (1989)

27. H. J. Schultz, *J. Phys. (Paris)* **50**, 2833 (1989)

28. A.H. Castro Neto and F. Guinea, *Phys. Rev. Lett.* **80**, 4040 (1998)

29. Yu. A. Krotov, D.-H. Lee, and A.V. Balatsky, *Phys. Rev. B* **56**, 8367 (1997)

30. S.R. White and D.J. Scalapino, *Phys. Rev. Lett.* **80**, 1272 (1998); *ibid.* **81**, 3227 (1998)

31. M. Akoshima *et al.*, *Phys. Rev. B* **57**, 7491 (1998)

32. C.G. Olson *et al.*, *Science* **245**, 731 (1989)

33. Z.-X. Shen *et al.*, *Phys. Rev. Lett.* **70**, 1553 (1993)

34. D.S. Marshall *et al.*, *Phys. Rev. Lett.* **76**, 4841 (1995)

35. A.G. Loeser *et al.*, *Science* **273**, 325 (1996)

36. H. Ding *et al.*, *Nature* **382**, 51 (1996)

37. C. Quitmann *et al.*, *Phys. Rev. B* **53**, 6819 (1996); C. Quitmann *et al.*, *Journal of Superconductivity* **8**, 635 (1995); P. Almeras *et al.*, *Solid State Communications* **91**, 535 (1994); P. Almeras *et al.*, *Physica C* **235-240**, 957 (1994)

38. C. Gu *et al.*, *J. Phys. Chem. Solids* **54**, 1177 (1993)

39. M.C. Schabel *et al.*, *Phys. Rev. B* **55**, 2796 (1997); M.C. Schabel *et al.*, *Phys. Rev. B* **57**, 6107 (1998); M.C. Schabel *et al.*, *Phys. Rev. B* **57**, 6090 (1998)

40. R. Yoshizaki *et al.*, *J. Low Temp. Phys.* **105**, 927 (1996); D.-S. Jeon *et al.*, *Physica C* **253**, 102 (1995); L.-X. Chen, H. Ikeda, and R. Yoshizaki, *Physica C* **282-287**, 1205 (1997)

41. G.D. Gu *et al.*, *J. Crystal Growth* **137**, 472 (1994); G.D. Gu *et al.*, *J. Crystal Growth* **130**, 325 (1993); G.D. Gu *et al.*, *Physica C* **263**, 180 (1996)

42. Z.-X. Shen *et al.*, *Science* **280**, 259 (1998)

43. M. Randeria *et al.*, *Phys. Rev. Lett.* **74**, 4951 (1995)

44. H. Ding *et al.*, *Phys. Rev. Lett.* **78**, 2628 (1997)

45. In this paper we follow the conventional notation in the literature and call the broad peak seen in the normal state the quasiparticle peak. More critical analysis of the normal state data, especially the contrast between the normal and superconducting states at $(\pi, 0)$, suggests that one may not be able to meaningfully describe a quasiparticle peak in the normal state, at least for the **k**-space region away from the (0,0) to (π, π) line. (G.A. Sawatzky, private communication)

46. The low temperature data does allow the possibility of a gap, but more needs to be done before a conclusion can be drawn.

47. D.S. Dessau *et al.*, *Phys. Rev. Lett.* **66**, 2160 (1991)

48. Y. Hwu *et al.*, *Phys. Rev. Lett.* **67**, 2573 (1991)

49. V.J. Emery, S.A. Kivelson, *Nature* **374**, 4347 (1995)

50. S. Doniach, M. Inui, *Phys. Rev. B* **41**, 6668 (1990)

51. C.S. de Melo, M. Randeria, J.R. Engelbrecht, *Phys. Rev. Lett.* **71**, 3202 (1993)

52. K. Morikawa *et al.*, *Phys. Rev. B* **54**, 8446 (1996)

53. M. Hase *et al.*, *J. Magn. Magn. Mat.* **177-181**, 611 (1998)

54. K. Manabe *et al.*, *Phys. Rev. B* **58**, R575 (1998)

55. T. Sekine *et al.*, *J. Phys. Soc. Japan* **67**, 1440 (1998)

56. R. Liu *et al.*, *Phys. Rev. B* **45**, 5614 (1992); R. Liu *et al.*, *Phys. Rev. B* **46**, 11056 (1992)

57. J.M. Harris *et al.*, *Phys. Rev. B* **54**, R15665 (1996)

58. K. Gofron *et al.*, *Phys. Rev. Lett.* **73**, 3302 (1994)

59. B.O. Wells *et al.*, *Phys. Rev. Lett.* **74**, 964 (1995)

60. A. Ino *et al.*, cond-mat/9809311

61. E. Dagatto, *Rev. Mod. Phys.* **66**, no. 3, 763 (1994)

62. C. Kim, *et al.*, *Phys. Rev. Lett.* **80**, 4245 (1998)

63. T. Tokyama and S. Maekakwa, private communication

64. D. Poilblanc, D.S. Scalapino, W. Hanke, *Phys. Rev. Lett.* **72**, 884 (1994)

65. A. V. Mahajan *et al.*, *Phys. Rev. Lett.* **72**, 3100 (1994)

66. C. Pepin and P. A. Lee, *Phys. Rev. Lett.* **81**, 2779 (1998)

67. B. Nachumi *et al.*, *Phys. Rev. Lett.* **77**, 5421 (1996)

68. G. V. M. Williams and J. L. Tallon, *Phys. Rev. B* **57**, 10984 (1998); C. Bernhard *et al.*, *Phys. Rev. Lett.* **58**, R8937 (1998)

69. D.A. Bonn, *et al.*, *Phys. Rev. Lett.* **68**, 2390 (1992)

70. J.M. Harris, *et al.*, *J. Low Temp. Phys.* **105**, 877

71. J.M. Harris, *et al.*, *J. Low Temp. Phys.* **105**, 877

72. P.B. Littlewood and C. M. Varma, *Phys. Rev. B* **45**, 12636 (1992)

73. M.R. Norman and H. Ding, *Phys. Rev. B* **57**, R11089 (1998)

74. Empirically, one may naively think that the peak and dip minimum energy actually scale with each other. This is reasonable as the dip minimum energy is basically determined by the peak energy and half of the width.

75. C. Kim *et al.*, unpublished

76. J.C. Campuzano *et al.*, cond-matt/9811349

77. D. Feng *et al.*, unpublished

78. A. Chainani *et al.*, *Phys. Rev. B* **56**, R15513 (1997)

79. X.J. Zhou, P. Bogdanov, S.A. Kellar, T. Noda, H. Eisaki, S. Uchida, Z. Hussain, Z.-X. Shen, *Science* **286**, 268 (1999)

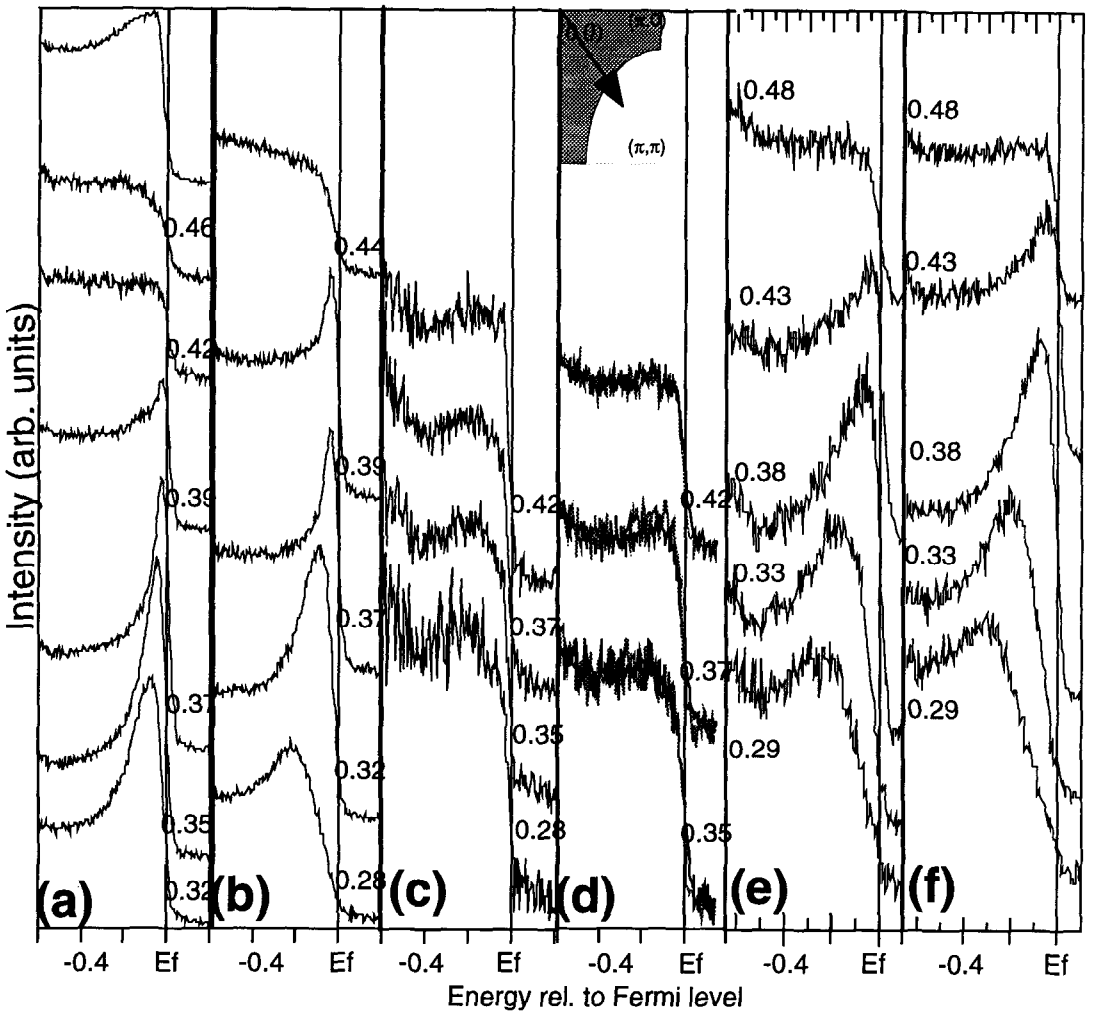

Figure 8.1: ARPES data along (0,0) to (π, π) cut for several types of $Bi_2Sr_2CaCu_2O_{8+\delta}$. The number near the spectrum indicates the k-space point. (a) and (b) are pure with T_c of 91K; (c) and (d) are Zn doped with T_c of 83K; (e) is 10% Dy doped with T_c of 65K (underdoped sample); (f) is an oxygen reduced (underdoped) with T_c of 67K. All spectra were collected at 100K under comparable conditions. For the Zn doped sample (d), spectra recorded below T_c (gray line) is the same within the experimental uncertainty. The topmost spectrum in panel (a) is the *average* of the others (see text for discussion).

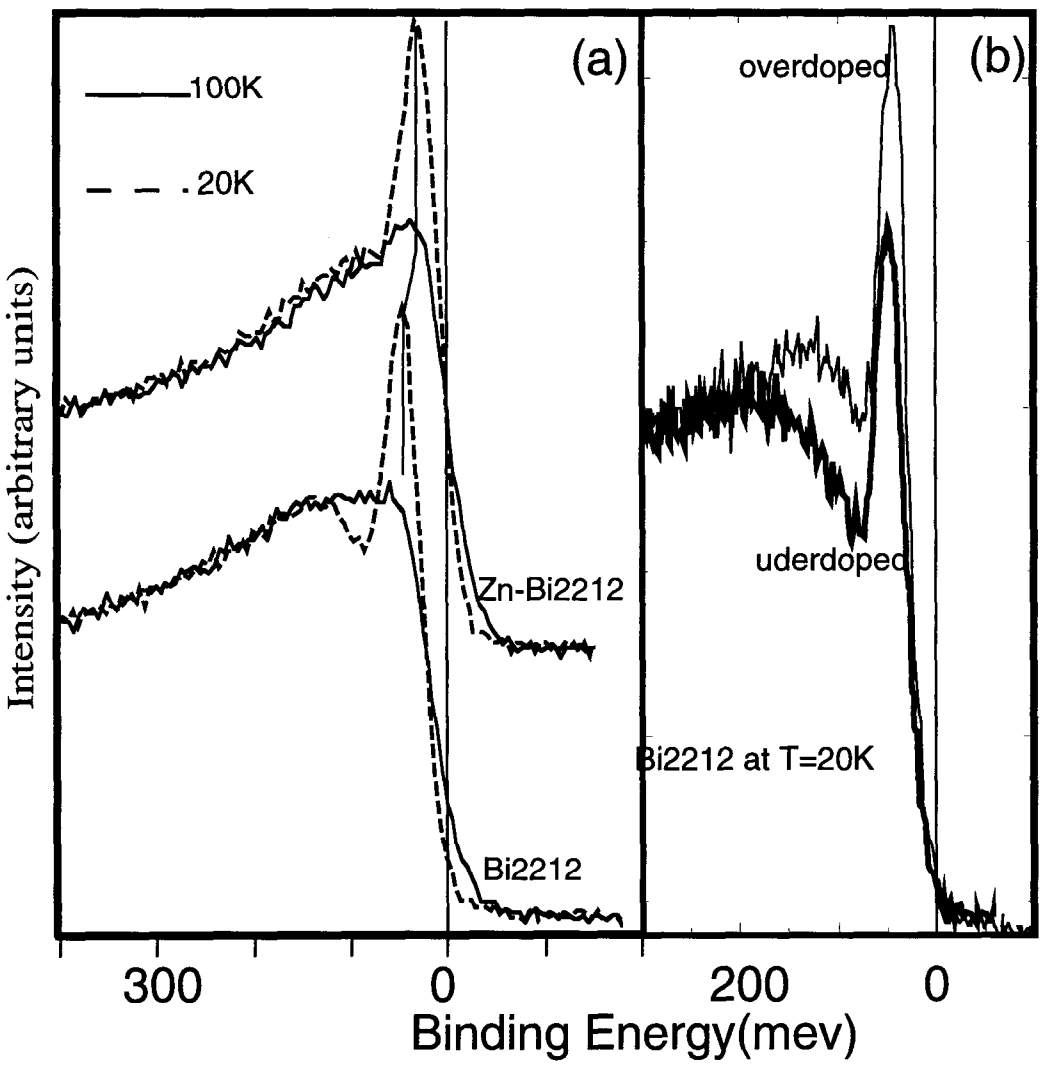

Figure 8.2: ARPES spectra of $Bi_2Sr_2CaCu_2O_{8+\delta}$ recorded at $(\pi, 0)$ for (a) pure ($T_c \approx 91K$) and Zn doped ($T_c \approx 83K$) in the normal (100K) and superconducting (20K) states and for (b) pure underdoped and overdoped in the superconducting state (20K).

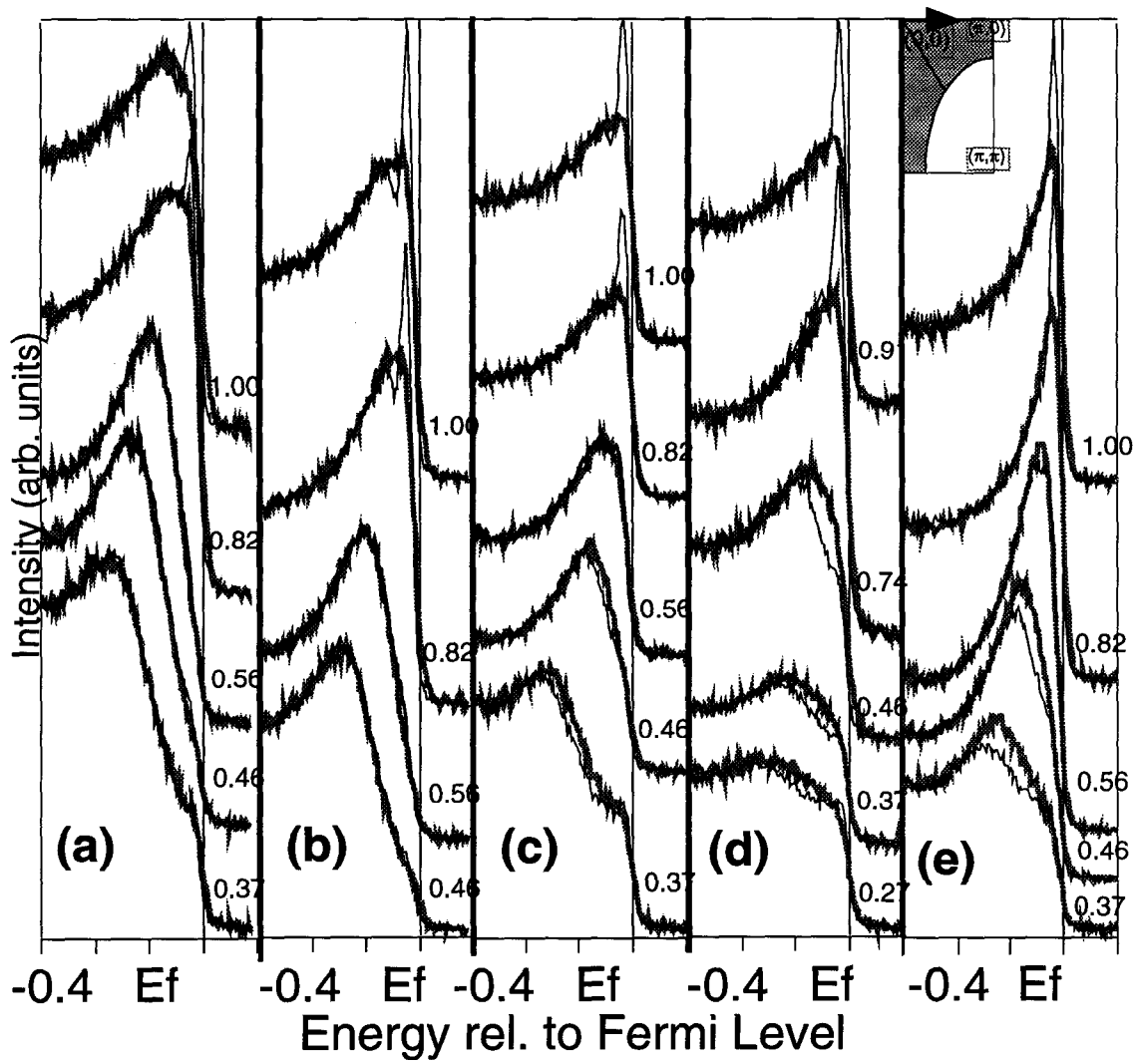

Figure 8.3: ARPES data along (0,0) to $(\pi, 0)$ cut for $Bi_2Sr_2CaCu_2O_{8+\delta}$ for (a) pure ($T_c \approx$89K); (b) pure ($T_c \approx$91K); (c) pure ($T_c \approx$88K); (d) Zn doped ($T_c \approx$78K); (e) Zn doped ($T_c \approx$83K). 100K data are represented by the gray lines while 20K data are represented by the black lines.

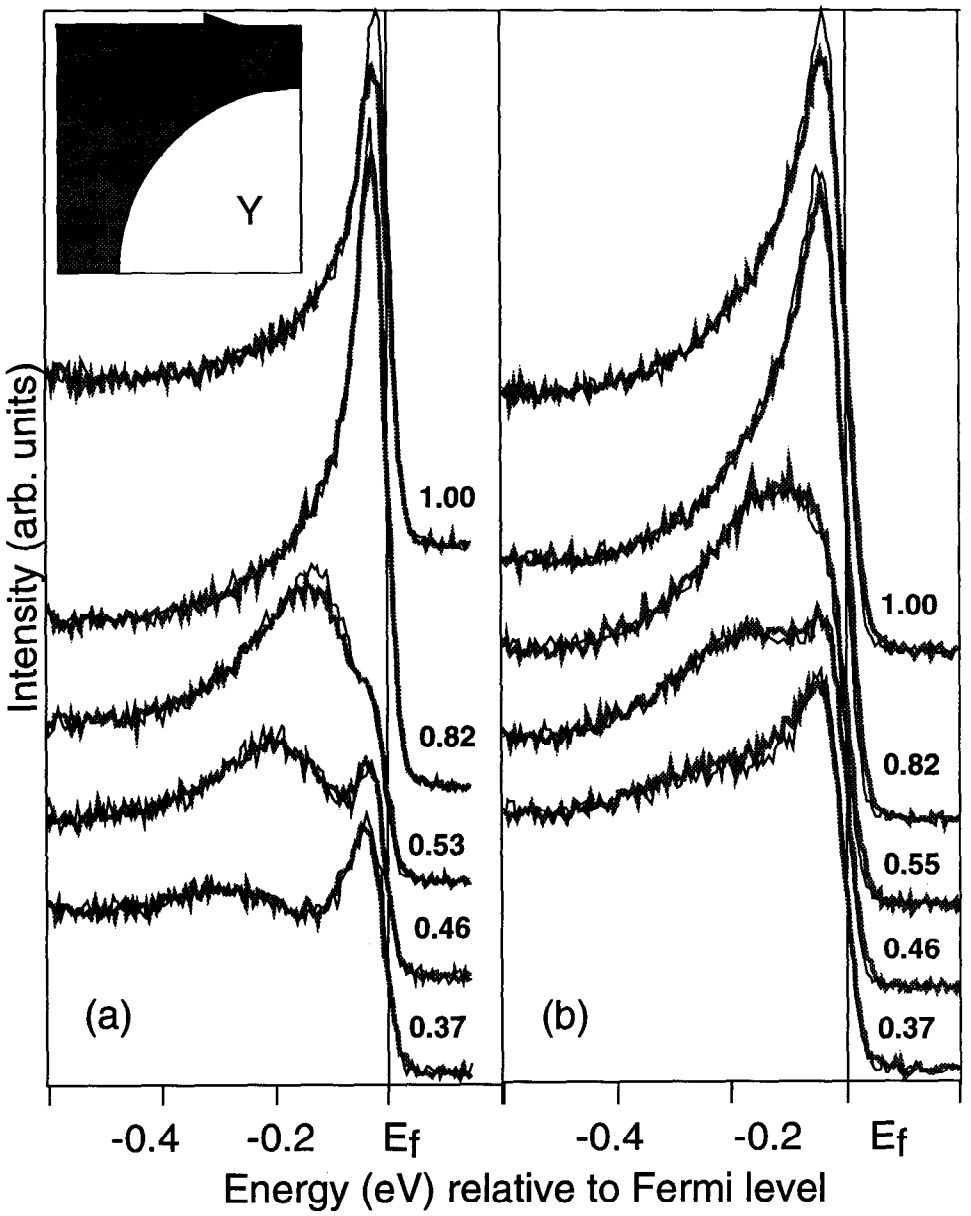

Figure 8.4: ARPES data along $\Gamma\bar{M}$ cut for two samples (a and b) of the overdoped version of the one plane compound, $Bi_2Sr_2CuO_6$, with $T_c \approx 8K$. 100K data are represented by the gray lines while 20K data are represented by the black lines.

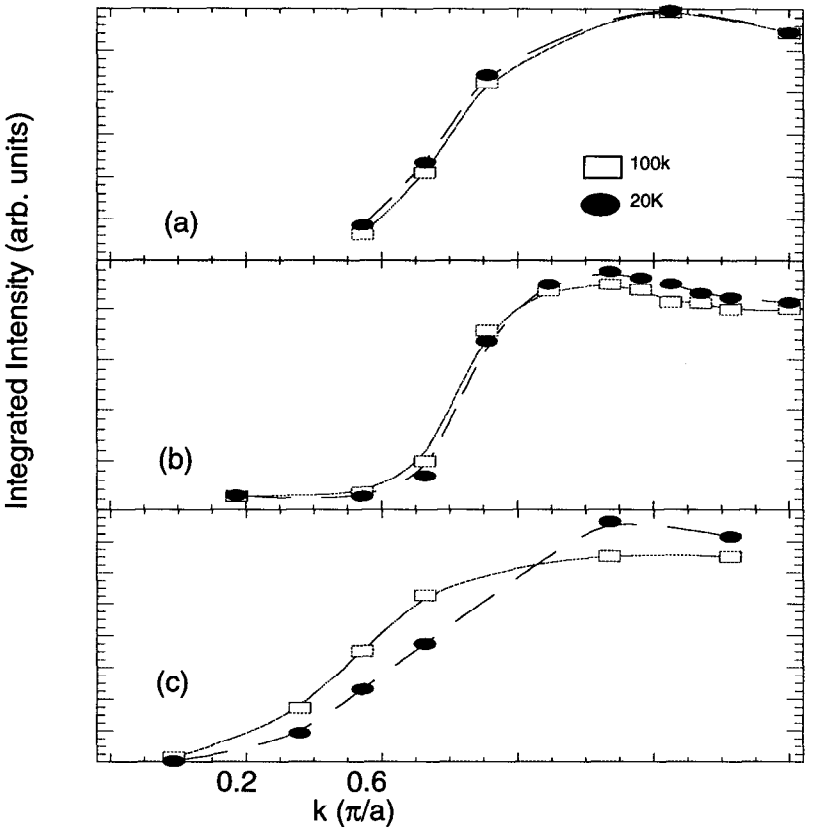

Figure 8.5: $Bi_2Sr_2CaCu_2O_{8+\delta}$ n(k) plots versus |k| for (0,0) to $(\pi, 0)$ for (a) pure ($T_c \approx$91K, Fig. 8.3b); (b) pure ($T_c \approx$88K, Fig. 8.3c); and (c) Zn doped ($T_c \approx$78K, Fig. 8.3d). Open squares represent 100K data; filled circles represent 20K data. Error bars of $\pm 1\%$ of the total are not included because of scale.

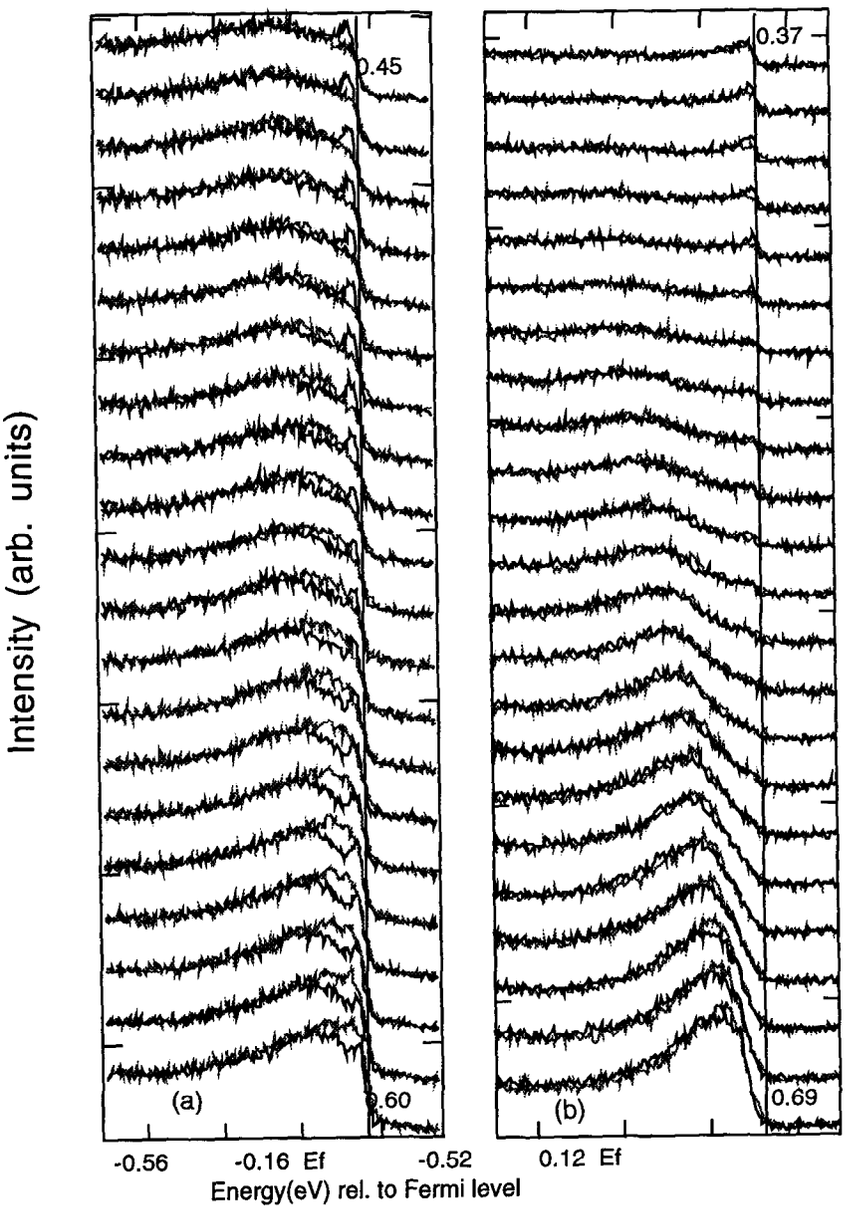

Figure 8.6: Data from $Bi_2Sr_2Ca(Cu_{0.99}Zn_{0.01})_2O_{8+\delta}$ along (0,0) to $(\pi,0)$ cut for T=100K(solid), 20K(gray) for (a) fresh sample and (b) aged sample. The k is indicated by the position along (0,0) to $(\pi,0)$ in units of $\frac{\pi}{a}$ given by the number to the right for the topmost and bottom spectra. Successive pairs of spectra are evenly spaced to show detailed evolution of the features. Data are taken in angle mode.

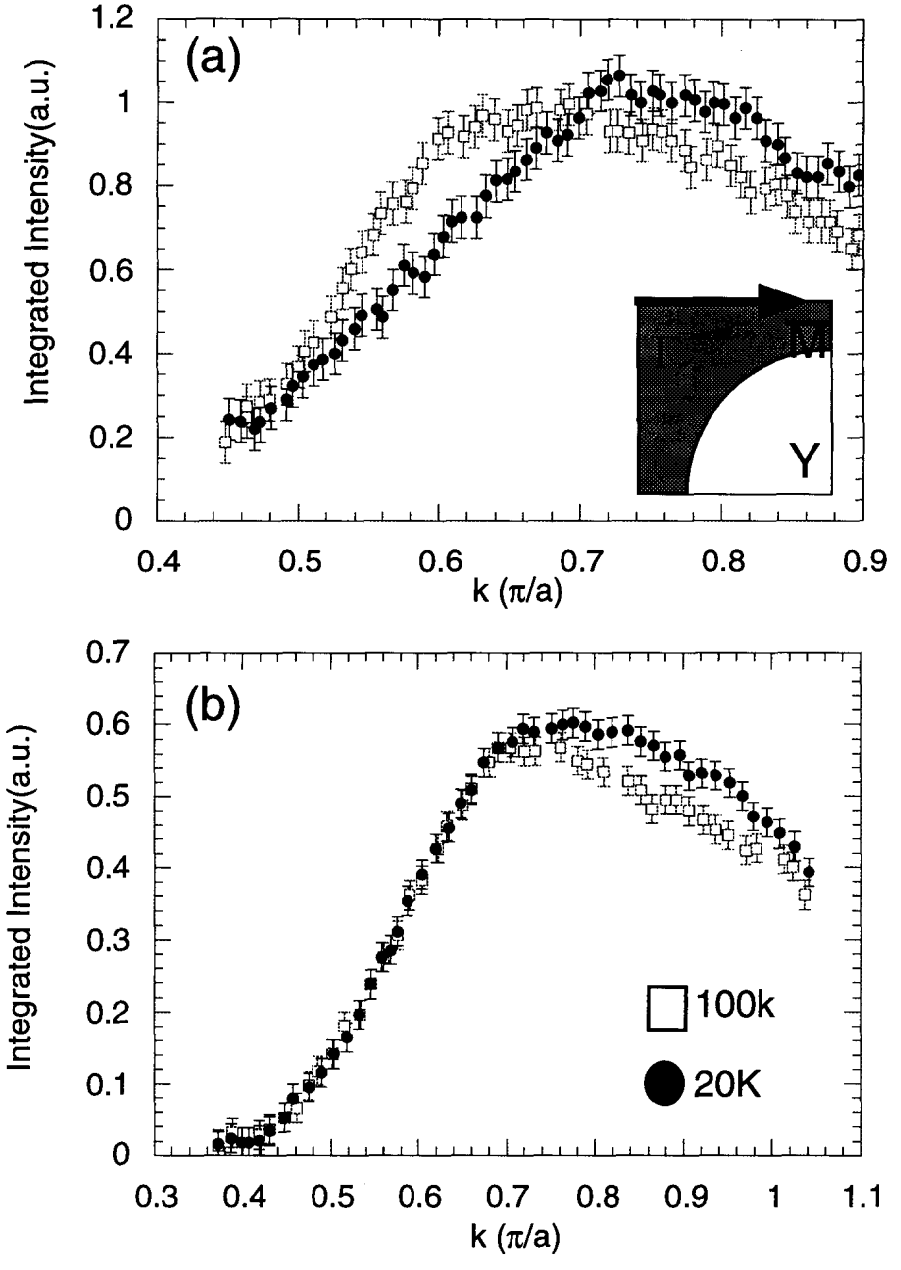

Figure 8.7: (a) n(**k**) plots along $\Gamma\bar{M}$ for fresh surface data (Fig. 8.6a). (b) n(**k**) from aged surface data (Fig. 8.6b).

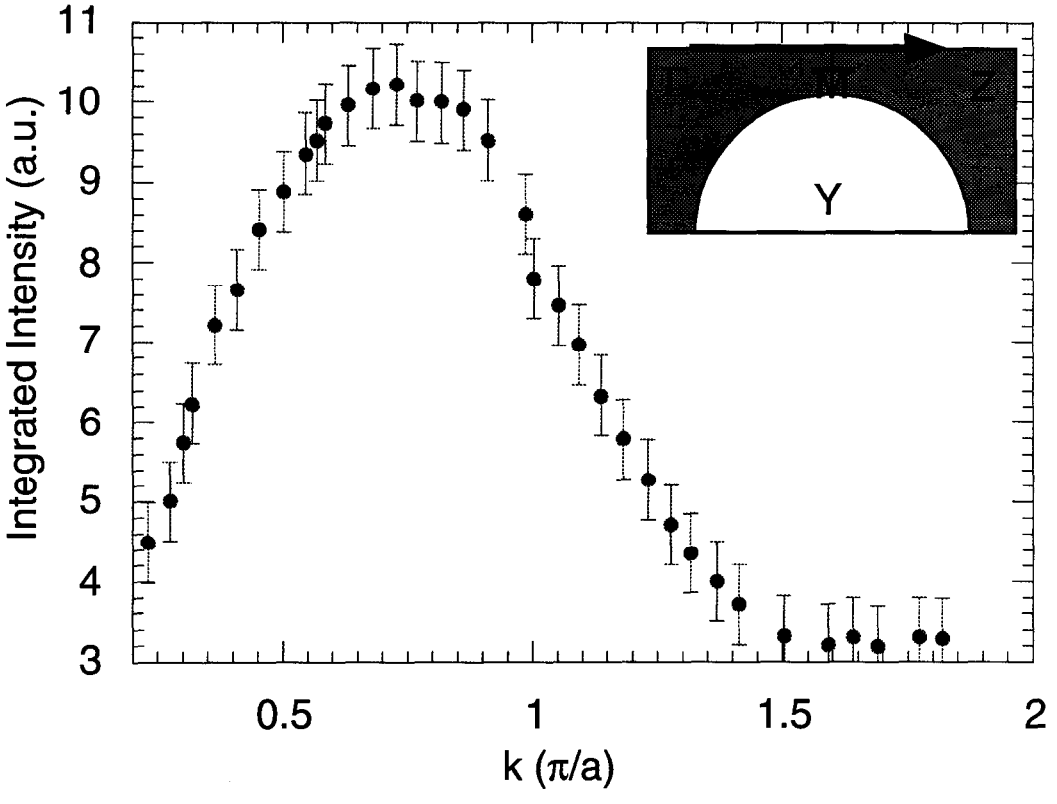

Figure 8.8: n(**k**) along $\Gamma\bar{M}$ for $Bi_2Sr_2Ca(Cu_{0.99}Zn_{0.01})_2O_{8+\delta}$ extending into the second Brillouin zone taken in the normal state (T=100K).

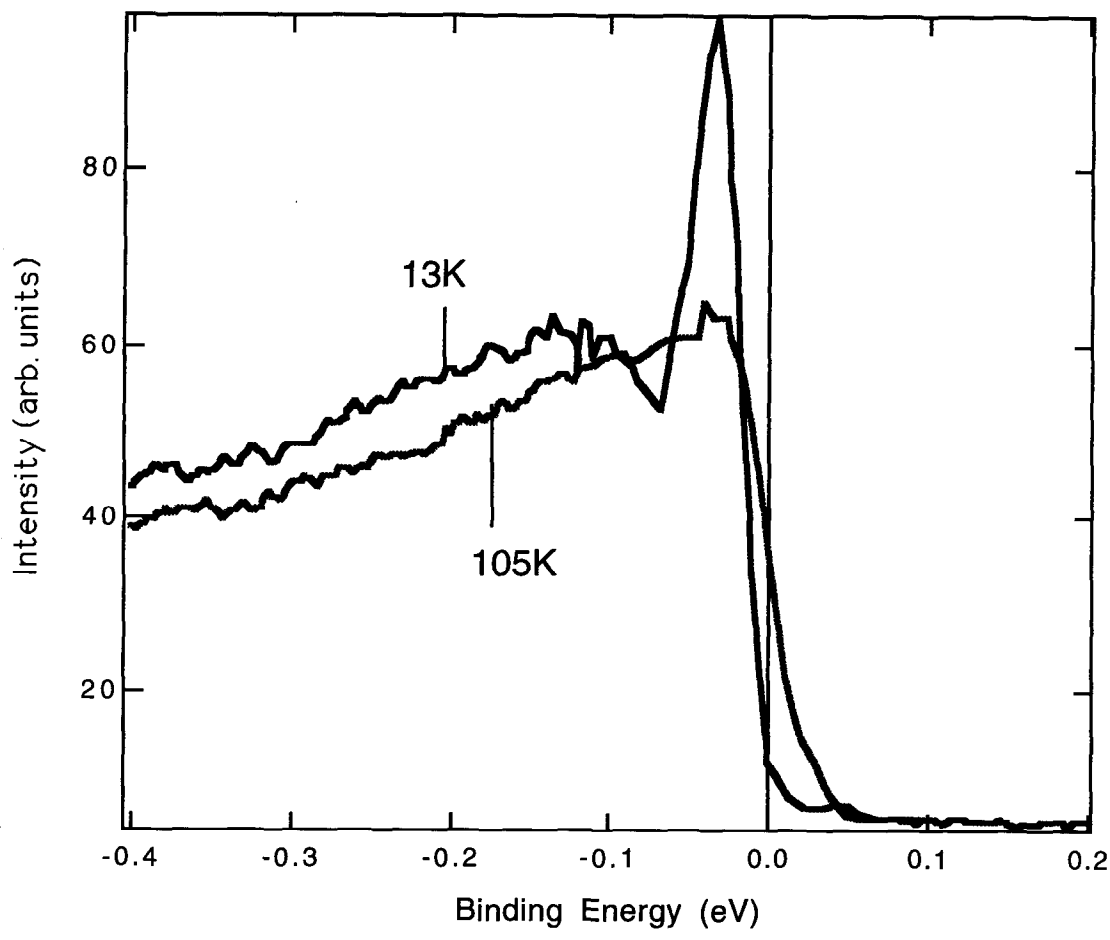

Figure 8.9: Data taken from ref. 43 showing near optimal $Bi_2Sr_2CaCu_2O_{8+\delta}$ ($T_c \approx 87$) spectra near the $\bar{M}$ point above (105K) and below T_c (13K).

Appendix A

Technical Discussion

In this appendix we will analyze the uncertainties in our experiment and address the comments of ref. 76. We discuss three issues: sample dependence, **k** uncertainty due to angle tilt, and sample aging.

The first question is sample variation. As can clearly be seen in Fig. 8.3, the spectra along $(\pi, 0)$ line show a systematic variation that is strongly correlated with changes we have reported in the preceding chapter. These changes in the spectra with impurities are much larger than the changes with temperature and, thus, are the first order effects. The differences are most obvious at relatively low angles (near $\mathbf{k}\sim(0.3\pi, 0)$-$(0.4\pi, 0)$) where one sees a broad maximum with a step like function near E_f. For the pure BSCCO type samples the maximum is well above the step like background. For the Zn doped samples the maximum is only slightly above the step. These differences are clearly related to the impurities or defects in the sample and are strongly correlated with other changes as we detailed in the preceding paper. This ratio appears to be less sensitive to doping variation as (a) and (b) have similar ratios but different doping. Empirically, we see stronger temperature dependencies in samples where the broad maximum is smaller, as in Fig. 8.3d-e. The sample that yielded the data in Fig. 8.7, which does not show as strong temperature dependence and **q** effect looks more like that of data from impure BSCCO sample in Fig. 8.3 although it has 0.6% Zn impurities. This variation of the broad peak to step like background ratio in Zn doped samples is likely caused by nonuniformity of impurity

distribution, but the details still need to be investigated. As will become clear later, the authors of ref. 76 completely overlooked the spectral variation with the number of impurities and/or defects. We disagree with this approach. In particular, we believe the authors of ref. 76 are mistaken to extend the observation of one sample with lineshape similar to our samples (see Fig. 1 of ref. 76) as a general observation.

The second question is whether the **q** shift is caused by a **k**-uncertainty due to a small angle tilt resulting from sample manipulator movement with temperature. The authors of ref. 76 showed two sets of n(**k**) profile with different temperatures and found them to match if they slide the two n(**k**) curves relative to each other. They then speculated that the **q** shift observed in our experiment is caused by the same effect.

The simplest answer can be found in Fig. 8.5 and Fig. 8.7. The key is that the n(**k**) curves at the two temperatures have different shapes, so they cannot match each other by an angular slide in contrast to the claims of ref. 76. Therefore, the angular uncertainty cannot be the primary explanation. We have other reasons to doubt the angular tilt is the main source of error in our data. The fact that the spectra at at two temperatures match so well in the Bi2201 samples in all cases rule out the possibility of angle tilt of our sample manipulator as the temperature changed. This leaves the sample surface flatness as the only possible pitfall in the following sense: since the sample position moves with temperature variation (thermal expansion and contraction), we have to reoptimize accordingly. In doing this, we may look at slightly different spots of the sample at 100K versus 20K. If the surface is not completely flat, one may have a small angle tilt as one moves to different parts of the sample. There are several problems in accepting the sample flatness being the main source of error. Primarily, sample flatness is a random variable; it is hard to believe that it would occur only in some Bi2212 samples but not any 2201 samples. Next, assuming it did exist, it would not be clear why such a presumably random agent would cause a systematic effect in the data. One would expect opposite effects in our results, but this was never seen. As an experimental procedure, we performed laser reflection tests for all samples studied and found that our samples are optically flat; we did not find any systematics that suggest our Zn doped samples are less flat. X-ray rocking curves

from Zn-Bi2212 showed peaks as sharp as those from pure Bi2212 and sharper than those from Bi2201. Finally, our samples are of $1mm^2$ size or less, which is smaller than the x-ray beam size of SSRL BLV so that our beam overfills the sample. The focal point of our analyzer is of comparable size. Therefore, the likely case is that we always look at the whole sample rather than a portion of the sample. Therefore, while momentum uncertainty may still bring error to our experiment, it cannot explain the systematics in the data.

The third problem is sample aging, which may turn out to be a more serious issue than we have previously realized [42]. The data in Fig. 8.7b has signs of sample aging as the energy integrated intensity, $\int n(\mathbf{k})\, d\mathbf{k}$, of the 20K data is higher than that of the 100K data. The data at 20K were recorded later than that at 100K so that the 20K data are from an older sample, consistent with the empirical experience that aged samples show spectral signatures similar to overdoped Bi2212. We agree with the authors of ref. 76 that the effect of sample aging is harder to rule out. A difficulty with sample aging is that they do depend not only on the sequence of experiments, they also depend on the temperature as more residual gas condenses on the sample at lower temperature. As it stands now, we cannot rule out the possibility that the sample aging has misled us to identify the **q** shift. However, we offer the following thoughts. I)All our data were recorded in a similar vacuum of (5-6x10^{-11} or better which is an order of magnitude better than 4x10^{-10}case raised by ref. 76); it is not clear why the **q** effect is more pronounced in samples with more impurities and/or defects (as internally characterized by the larger step like background in the Zn doped samples and impure BSCCO samples). We do not know whether defects or impurities can accelerate the surface aging process and thus lead to systematics in our data. We also have a feeling that the composition of the residual gas is crucial. For example, water molecules are worse than others given the same base pressure. We did not realize the seriousness of this problem and believe the sample aging may be the main source of error in connecting the **q** shift to stripes. II)We have not yet found a satisfactory mechanism that would allow us to explain away the **q** effect naturally with aging as its cause, while keeping in mind the systematic changes of the data with impurities that are not clearly explainable by the aging effect. We leave this as an

open issue for further investigation. With improved surface passivation techniques, we may be able to handle this difficult issue to provide a definitive answer. We are devising experiments to test this. We should note that the aging effect is rather subtle; this should not affect the qualitative conclusion of the preceding chapter.

Now we discuss a more technical problem. The idea of looking for periodicity, as suggested in ref. 76, is valid but not practical with the current experimental setup. In principle, the $n(\mathbf{k})$ and its variation should show periodicities reflecting the underlying crystal symmetry. Fig. 8.8 shows $n(\mathbf{k})$ curves for the first two zones. It is clear that $n(\mathbf{k})$ does not have the symmetry with respect to $(\pi, 0)$ as one would expect from the underlying crystal symmetry. This is a well known result and is the same with that of ref. 76 in a smaller $\mathbf{k}$-space window. This result is likely a consequence of matrix elements effects that are not fully understood. It is also very clear that the $n(\mathbf{k})$ in the second zone is very weak, making the temperature dependence study impractical with our current setup. The window selected in our experiment [42], $(0.3\pi, 0)$ to $(\pi, 0)$, provides the best opportunity to see anything within the limits of detection [42]. The authors of ref. 76 should be fully aware of these practical issues; it is unclear why they have stressed this point so much, and we believe the implication is misleading. As general remarks, the issues raised in ref. 76 are reasonable. The problem is that one can always make general remarks about any experiment. In this case, these general remarks are misleading as the authors of ref. 76 associate the problems with the specific experimental results without independent check.

Before closing, we need to point out that the alternative explanation for the spectral weight change is due to strong impurity scattering and the effects of coherence factors from Cooper pair formation. This possibility was not discussed in our previous paper. In this case, the $\mathbf{q}$ shift along (0,0) to $(\pi, 0)$ line is caused by a combination of coherence factor effects and strong impurity scattering. In a conventional superconductor, the coherence factors affect only states near the Fermi level. In the case of high T_c superconductors, the bandwidth is narrow and the pairing potential is strong. As a result, the whole band (or at least a significant fraction of the whole band) is affected by the coherence factors, ${u_k}^2$ and ${v_k}^2$, with the occupied part losing weight and the empty part gaining weight. Near the region of $(0.3\pi, 0)$ to $(0.5\pi, 0)$, a large

k-space region is occupied and spectral weight is lost in the superconducting state. Near the region of $(0.8\pi, 0)$ to $(\pi, 0)$, impurity scattering will mix in empty states outside the narrow stripe of occupied region along the $(0.8\pi, 0)$ to $(\pi, 0)$ line resulting in a gain of spectral weight in the event that there are more empty states than occupied states in the **k**-space window averaged by the impurity scattering. Here, we also have to assume that Zn doping suppressed T*, which is reasonable in light of other experiments [18, 17], so our measurements are above and below the pairing temperature. For sample A of Fig. 8.3, both 100K and 20K are probably below T* so no coherence factors difference come into play, and no **q** shift is observed. In this scenario, $2\pi/|\mathbf{Q}|$ is roughly the Cooper pair size. Given $|\mathbf{Q}|\sim 0.4\pi$-0.5π, one obtains a value of 20-25$\mathring{A}$, which is reasonable.

Summarizing the above discussion, it is clear that while ref. 76 raises some valuable questions, it does not provide a satisfactory answer to the data.. The foundation of ref. 76, which is that the previous work has established n(**k**) to be temperature independent, is not factual and is in contradiction to earlier claims by the same authors. Ref. 76 is deficient by having completely overlooked two crucial elements of the effect - namely the crucial changes in spectral lineshape with impurities and/or defects and the intriguing correlation with other properties. The uncertainty in **k** due to angular uncertainty is a danger, but we do not believe the systematic results in our data can be attributed mainly to this random process. Sample aging, on the other hand, is a possibility that cannot be ruled out and could be a source of error.

Appendix B

Further Discussion

Spectral weight nonconservation is an intriguing topic. A variety of studies were performed to verify this peculiar observation. Rather than offer an analysis of this phenomenon, this section is included merely to highlight the existence of this effect under conditions not included in the literature.

Fig. B.1 displays data from a Ni-doped sample of BSCCO. This data is presented to demonstrate the lack of spectral weight conservation in much the same vane as that discussed in Section 8 and Section 7.1. This sample is reminiscent of the Zn doped and dirty BSCCO samples in this regard. The spectral weight transfer as a function of **k** is quite similar to the ones shown before. Ni acts as an intraplanar impurity in much the same way as Zn. Comparable results between the two reinforces the notion that the effect seems to be intrinsic to the impurity doped samples. However, we suffer from the same uncertainty with regard to knowledge of the exact impurity doping and quantifying the exact stoichiometries of the other elements as well. BSCCO is inherently resistant to an exact determination of the species via chemical analysis due to the number of elements present and the absence of known standards.

Fig. B.2 and Fig. B.3 revisit the subject of spectral weight transfer but at higher temperatures *above* T_c. The upshot of this is that the spectral weight nonconservation takes place above the critical temperature as well. The spectra themselves are in Fig. B.2. The **Q** shift is given pictorially in Fig. B.3 with the 20-100K data for comparison. The same qualitative change in spectral weight is seen. If there is

another temperature, $T_{AFM}>T^*$, associated with stripe formation, then it would be consistent with high temperature neutron data.

As an aside, the experiment done strictly above T_c confirms something else as well. O_2 absorption is a strong function of temperature. In fact, it happens a great deal more rapidly at lower temperatures (T<100K) than higher temperature. If this effect were somehow produced by the adsorbates on the sample, one expects a remarkable difference between the low temperature set of data versus the high temperature set of data. This was not the case so it would be hard to conclude that this effect was related to sample aging alone. While these things are hard to quantify, this is a strictly qualitative observation.

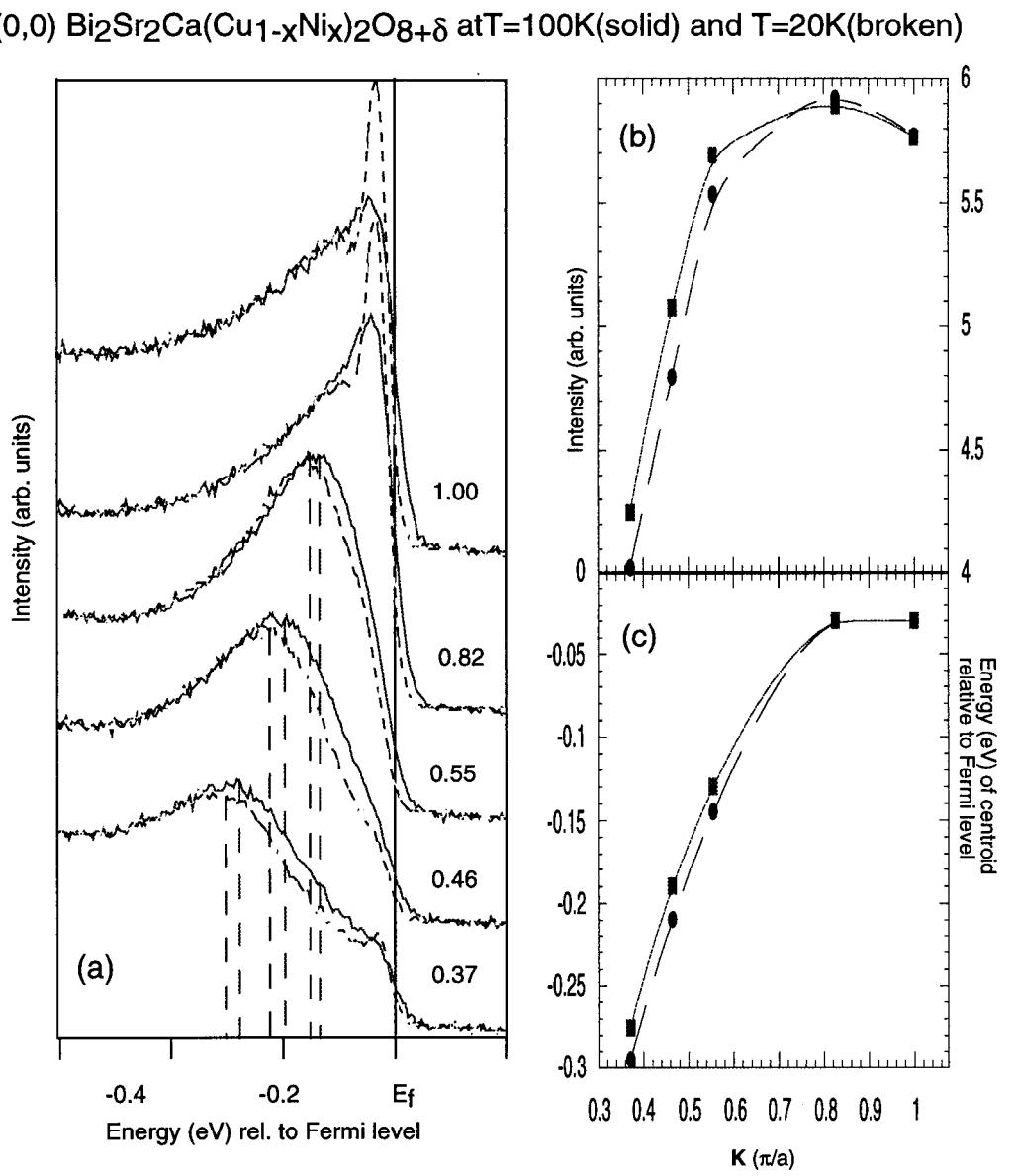

Figure B.1: Data from Ni(2%) doped BSCCO. The left panel is taken at five different **k**-space points along $\Gamma\bar{M}$ in the normal state (solid line) and superconducting state (broken line). The bottom right panel shows the position of the centroid as a function of **k** and the top right panel shows the spectral intensity versus **k**.

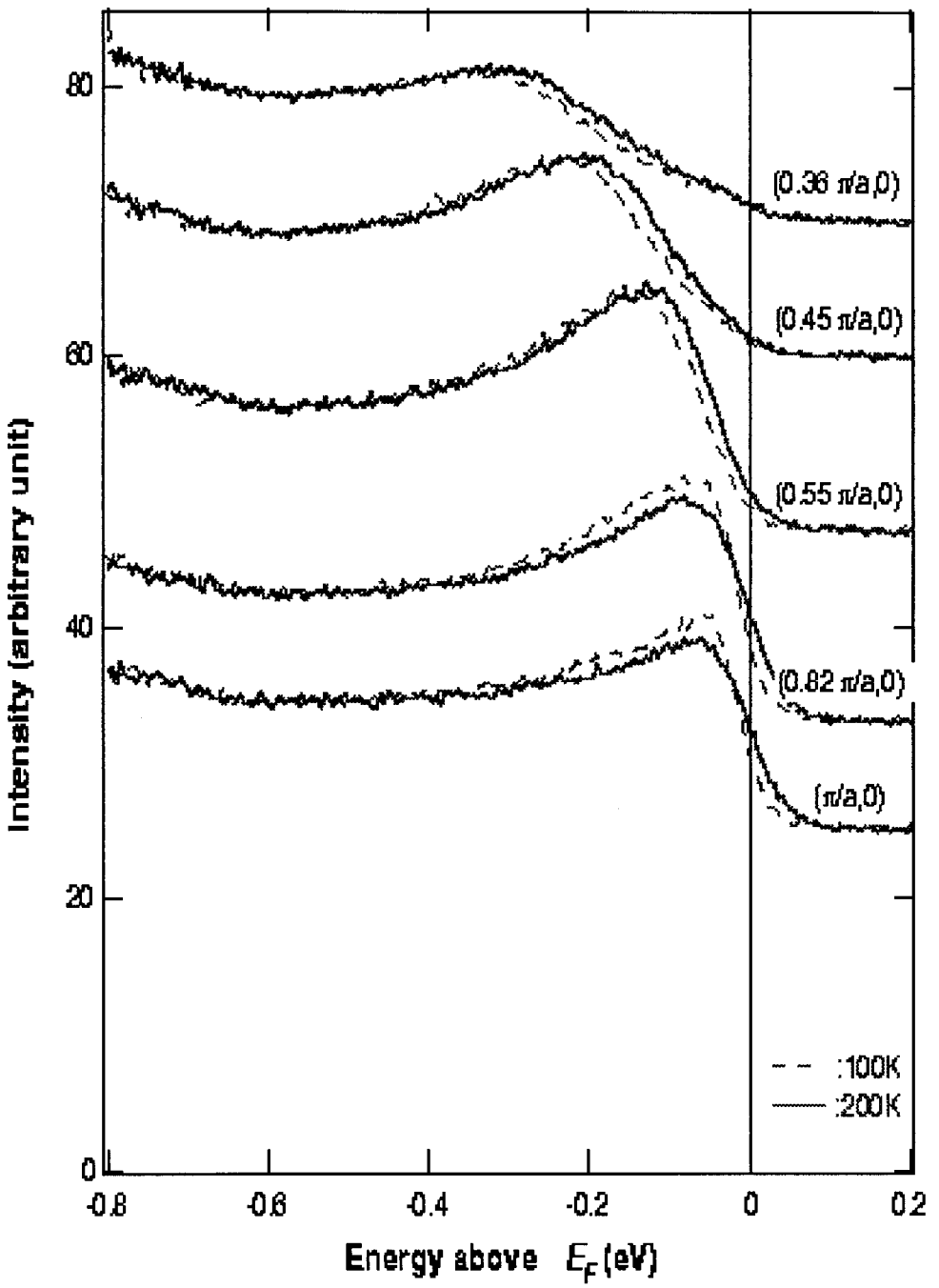

Figure B.2: Data 0.9% Zn doped BSCCO ($T_c \approx 78K$ taken along (0,0) to (π, π). The dashed line is data taken at 100K while the solid line is data taken at 200K. The systematic trend of spectral weight transfer between the two temperatures is qualitatively similar to that of Fig. 7.1. It should be noted here that if oxygen absorption is a serious problem, the result would not have reproduced for this case since oxygen absorption is temperature dependent.

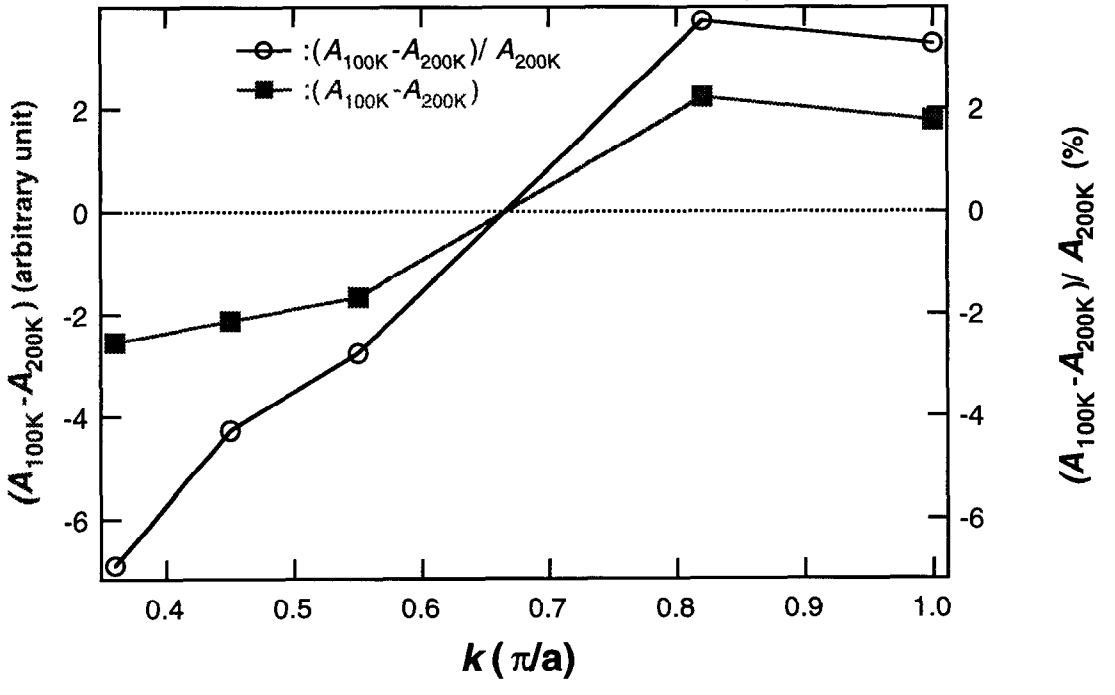

Figure B.3: Integrated spectral weight vs. k for the data in Fig. B.2 with data from Fig. 7.2. Again, the simialrity between this and Fig. 7.2 is noted. The weakened effect may be due to difference in oxygen concentration (although both are *nominally* doped) or due to differences in Zn concentration (0.6% vs. 0.9%) but that is harder to quantify according to the growers.

Appendix C

Bi2278

To make an attempt at completion, the number of CuO_2 planes was not only *reduced*, but it was also *increased.* We studied Bi2278 (samples obtained from Jim Eckstien of varian Labs and UIUC) with T_c of about 70K. The point of this was to see the persistence of the d-wave gap by increasing n. It is usual to see $T_{c,max}$ increase with n, however, from a photoemission standpoint, these samples typically do not cleave well. The samples provided for this study were grown via MBE technique.

A popular notion with multi-layered cuprate materials is that the charges do not sit uniformly throughout the layers in a given unit cell. The reason for this stems from the conductivity between the individual planes. References for this effect are [23] and [24]. These models suggest that the charges tend to accumulate on the extreme layers of the unit cell. Since PES records information from only the topmost layers, one expects a kind of overdoping effect in the spectrum, which is indeed what is observed. However, the aim of this preliminary study was only to test for the anisotropy of the gap, which is insensitive to the doping levels of the superconductor.

The data are shown in Fig. C.2 and Fig. C.1. Fig. C.2 displays the comparison of two **k**-space points where the gap is minimum $(0.34\pi, 0.34\pi)$ and maximum $(\pi, 0.2\pi)$. We find above T_c the absence of a leading edge shift, while below T_c a difference develops between the two leading edges,*i.e.*, a gap opens up. The overall lineshape is consistent with previous experience about overdoped samples. Also, the quasiparticle peak at $(\pi, 0.2\pi)$ is reproduced in these samples as well. This is another confirmation

of the robust nature of the superconducting gap in BSCCO. As said before, this is a multilayer compound. Some degree of interplanar transport is expected according to models mentioned previously. This is explored in Fig. C.1 where we fix on 3 distinct k-space points and tune the photon energy to test for dispersion in the k_z direction. The presence of dispersion seems to suggest some three dimensionality. This data was taken by M. Zhang *et al. (unpublished)* More work may elucidate this question.

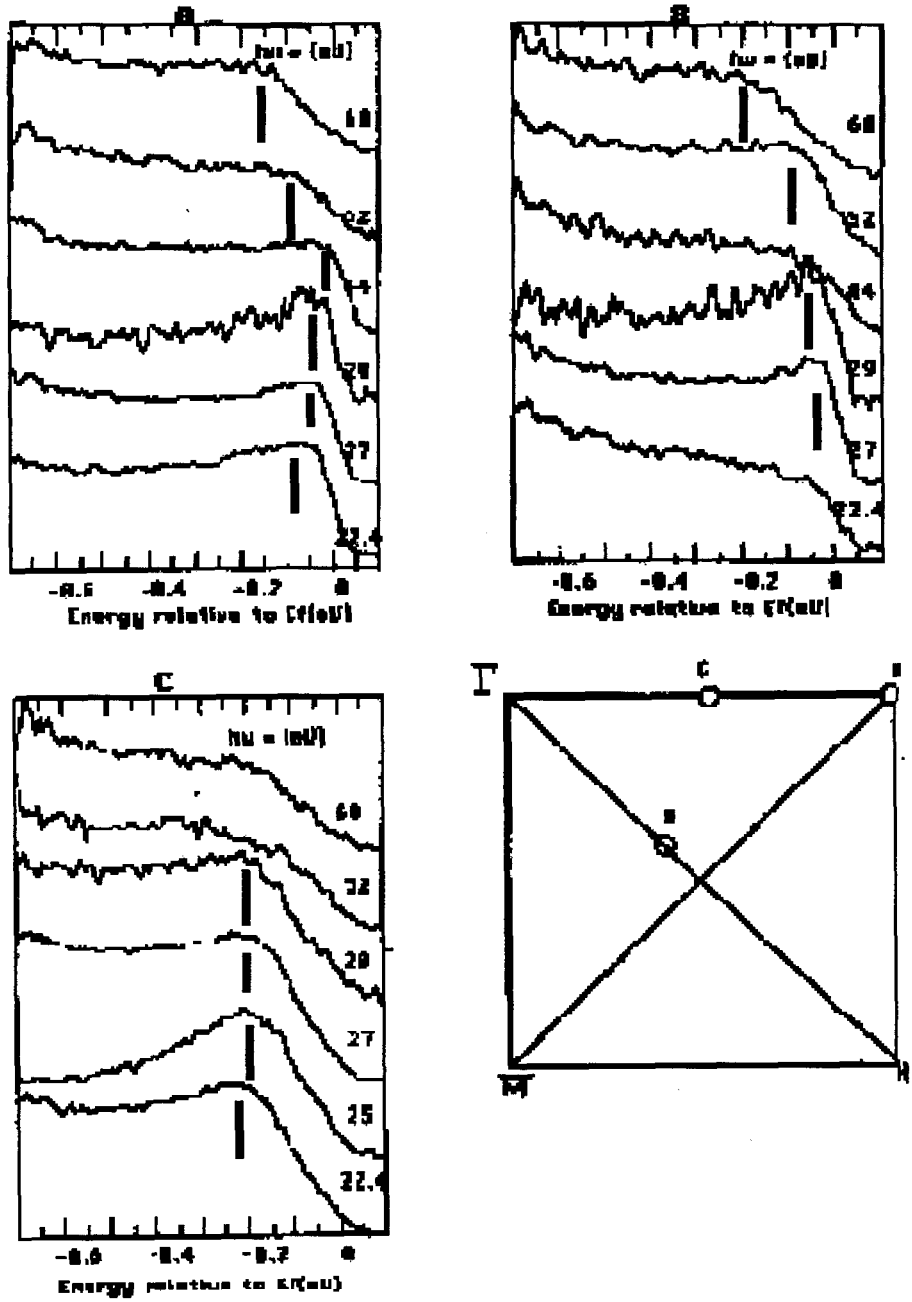

Figure C.1: 3 k-space points (indicated by the lower rt. hand panel) of 8-layer BSCCO taken at various photon energies to show the dispersion in k_z

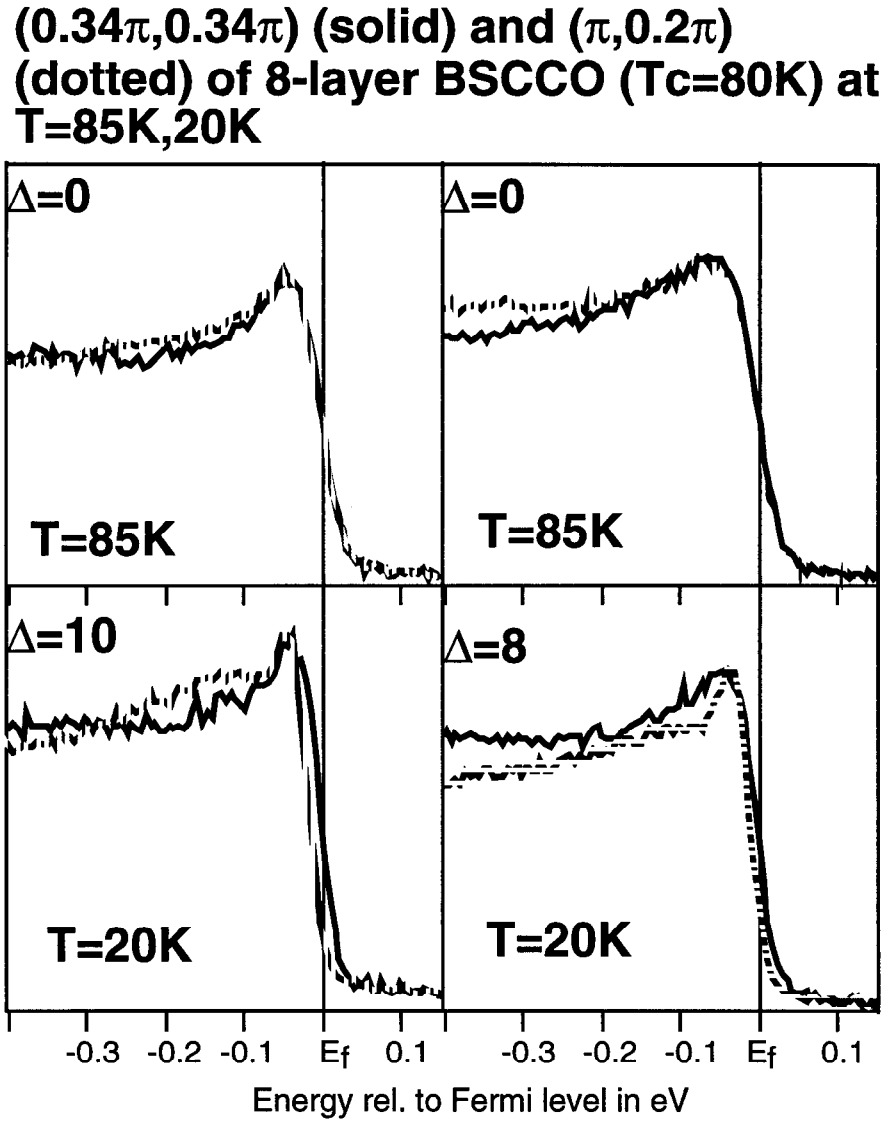

Figure C.2: 2 k-space points of Bi2278 at FS crossing to indicate the anisotropy of the superconducting gap and the lack of the normal state gap of this particular compound.

Appendix D

Other Data

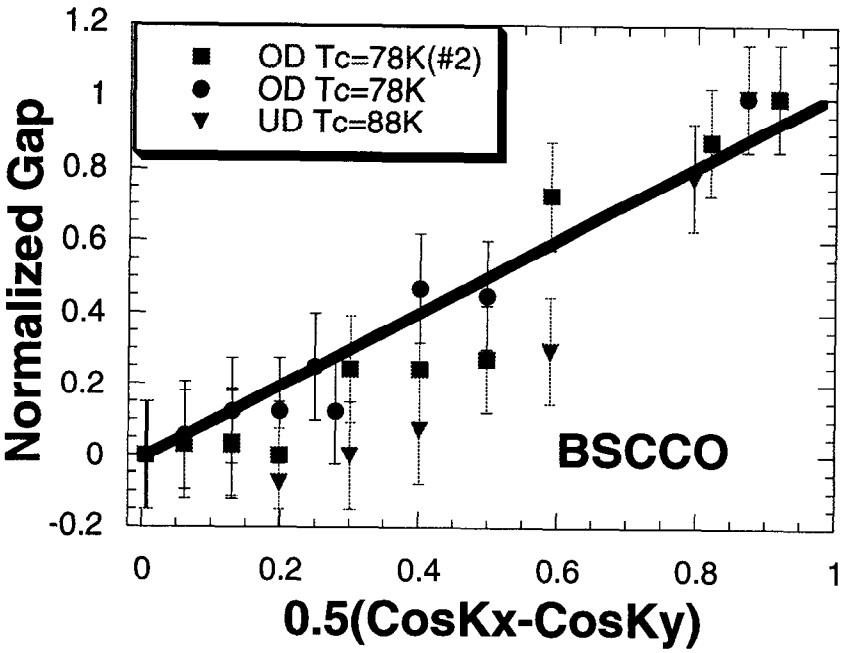

Figure D.1: Normalized gap vs. $0.5 \mid cosk_x a - cosk_y a \mid$. Data from Chapter 4 plotted to illustrate anisotropy. Data show for one run on underdoped sample (T_c=88K) and two *consecutive* runs on the same overdopedsample (T_c=78K). Data in *superconducting* state.

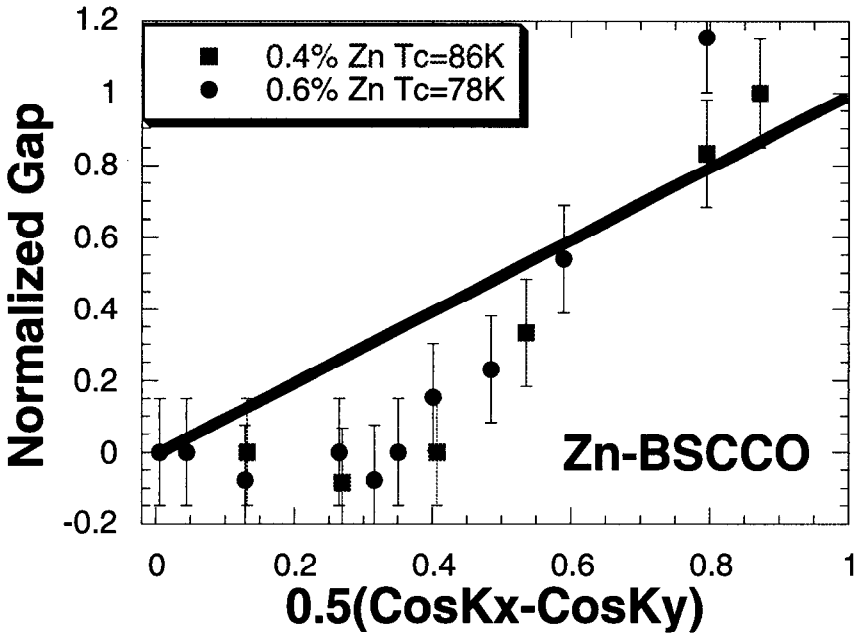

Figure D.2: Normalized gap vs. $0.5 \mid cosk_x a - cosk_y a \mid$. Zn doped BSCCO from Yoshizaki. Data in *superconducting* state.

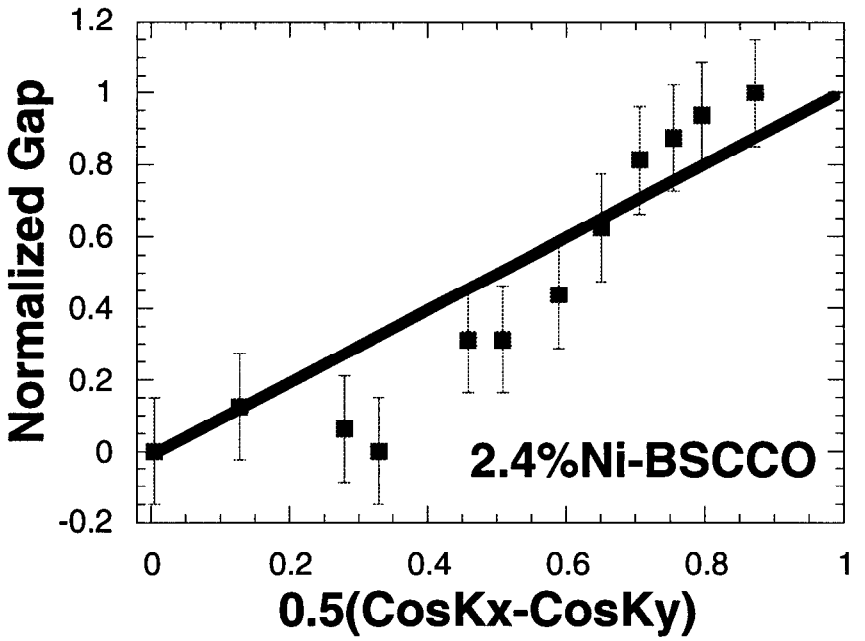

Figure D.3: Normalized gap vs. 0.5 | $cosk_x a - cosk_y a$ |. Anisotropy of superconducting gap of 2.4% Ni doped Bi2212 grown by Yoshizaki. T_c=78K.

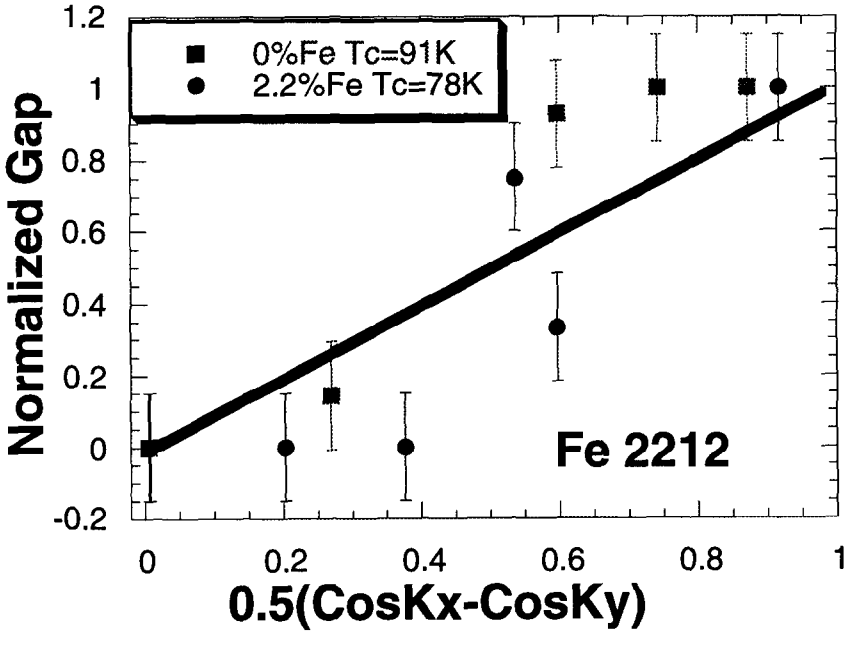

Figure D.4: Normalized gap vs. 0.5 | $cosk_x a - cosk_y a$ |. Anisotropy of 0.0% and 2.2% Fe doped BSCCO. *Care must be taken here to note that Fe is multivalent and Fe substitutes on two sites according to Mossbauer spectroscopy. This is an unresolved issue.*

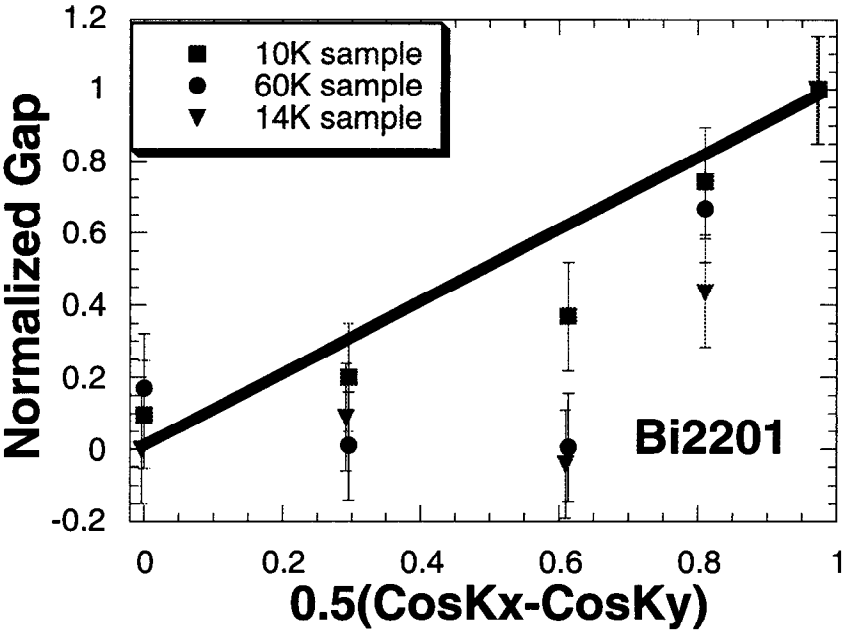

Figure D.5: Normalized gap vs. 0.5 | $cosk_x a - cosk_y a$ |. Anisotropy of Bi2201. Data same as Fig. 6.3

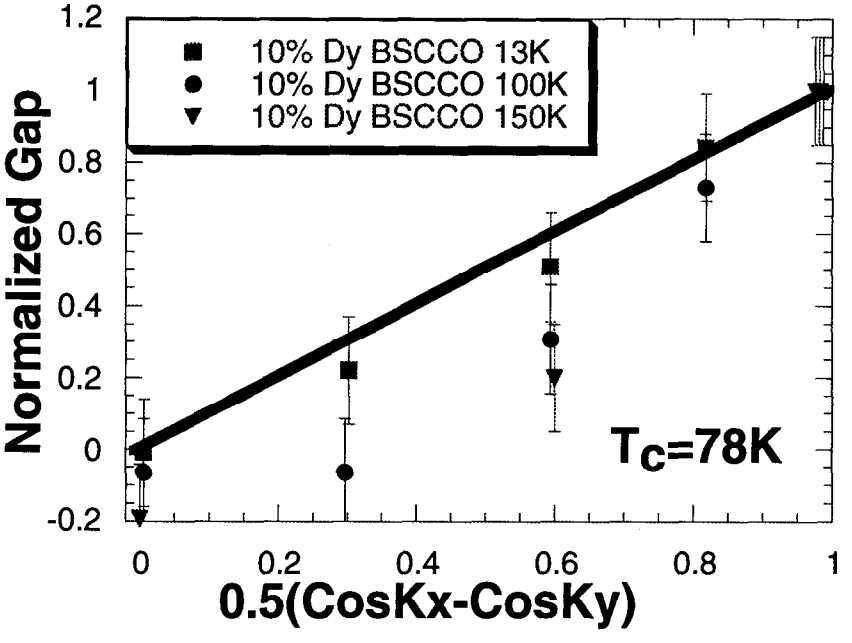

Figure D.6: Normalized gap vs. $0.5 \mid cosk_x a - cosk_y a \mid$. Data from 5 showing superconducting anisotropy. See Fig. 5.3.

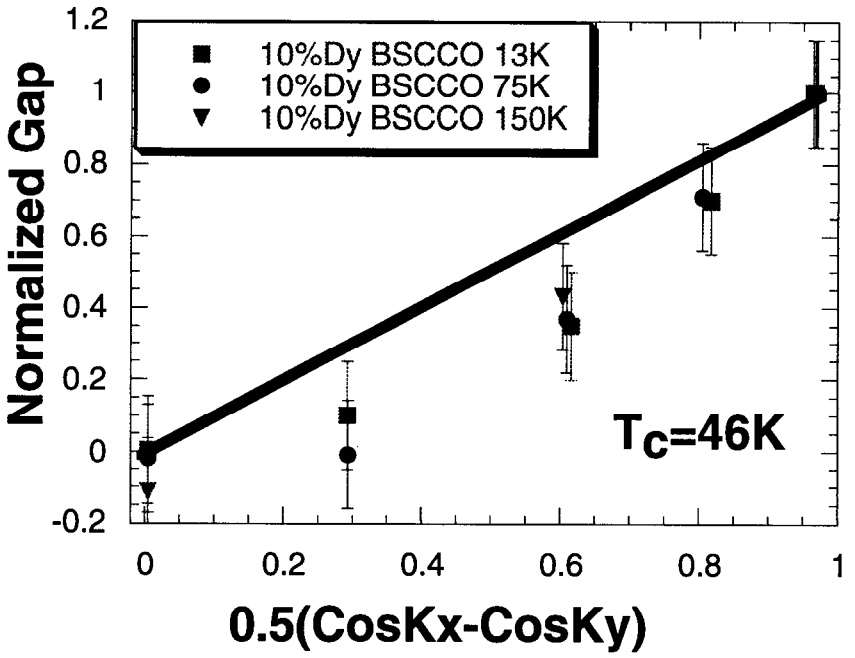

Figure D.7: Normalized gap vs. 0.5 | $cosk_x a - cosk_y a$ |. Data from 5 showing superconducting anisotropy. See Fig. 5.3.